

## **Science Concept 4: The Lunar Poles Are Special Environments That May Bear Witness to the Volatile Flux Over the Latter Part of Solar System History**

**Science Concept 4: The lunar poles are special environments that may bear witness to the volatile flux over the latter part of solar system history**

Science Goals:

- a. Determine the compositional state (elemental, isotopic, mineralogic) and compositional distribution (lateral and depth) of the volatile component in lunar polar regions.
- b. Determine the source(s) for lunar polar volatiles.
- c. Understand the transport, retention, alteration, and loss processes that operate on volatile materials at permanently shaded lunar regions.
- d. Understand the physical properties of the extremely cold (and possibly volatile rich) polar regolith.
- e. Determine what the cold polar regolith reveals about the ancient solar environment.

### **INTRODUCTION**

The presence of water and other volatiles on the Moon has important ramifications for both science and future human exploration. The specific makeup of the volatiles may shed light on planetary formation and evolution processes, which would have implications for planets orbiting our own Sun or other stars. These volatiles also undergo transportation, modification, loss, and storage processes that are not well understood but which are likely prevalent processes on many airless bodies. They may also provide a record of the solar flux over the past 2 Ga of the Sun's life, a period which is otherwise very hard to study. From a human exploration perspective, if a local source of water and other volatiles were accessible and present in sufficient quantities, future permanent human bases on the Moon would become much more feasible due to the possibility of in-situ resource utilization (ISRU). In turn, this would enable further exploration and use of the lunar environment. However, before ISRU missions can be considered the distribution and physical properties of volatiles and of the regolith in which they lie must be more fully understood.

### **Background**

A review of the current understanding of lunar polar volatiles is required in order to determine potential locations to address each Science Goal, as well as sites that would address all Science Concept 4 goals. We begin with a review of key terminology, in order to better define the scientific importance of the lunar poles. We then give brief recounts of the geology and exploration context of the lunar polar regions to further explain why these regions are "special environments" (NRC, 2007).

### **Definitions of key terms within Science Concept 4**

In order to meaningfully discuss the topics addressed in Science Concept 4 Science Goals, some general terminology must first be defined. The following subsections highlight major terms used in the NRC 2007 document and throughout this section.

### Permanently Shadowed Regions (PSRs)

Because the Moon's axis of rotation is nearly perpendicular to the plane of its orbit around the Sun (axis inclination  $\sim 1.5^\circ$ ) (Spudis *et al.*, 1998), the Sun always appears at or near the horizon in polar regions. The very small obliquity causes some high topographic features near the lunar poles to be constantly illuminated by the Sun, while some topographic depressions are permanently shaded from sunlight (and in some areas, reflected earthshine). These regions may act as 'cold traps' for volatiles migrating across the lunar surface (Fig. 4.1). Volatiles enter PSRs and then are unable to escape due to extremely low temperatures (*e.g.*, Watson *et al.*, 1961).

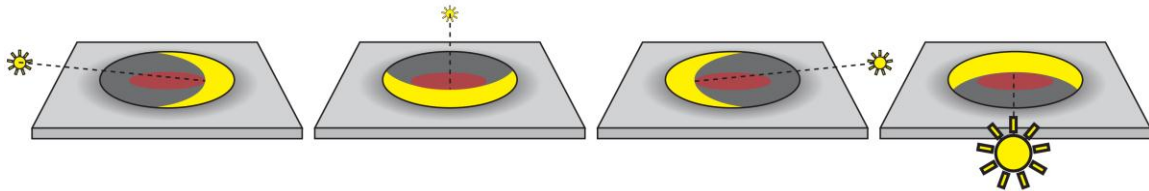


FIGURE 4.1 Schematic showing the position of the Sun low on the horizon over a lunar crater, and how the sunlit areas (yellow) never reach the Permanently Shadowed Region (PSR, red).

### Polar regions

In order to study polar environments, the extent of the polar region must be considered. As an initial constraint, the Lunar Prospector neutron spectrometer detected elevated levels of hydrogen above  $\pm 70^\circ$  latitude (Feldman *et al.*, 1998). This area includes Schrödinger basin, which is interesting geologically and exhibits large fissures that might be good traps for volatiles. This region also includes the southernmost portion of the South Pole – Aitken basin (SPA), the largest basin on the moon. SPA is also very old, and interesting in terms of both lunar geologic and volatile history. The locations of PSRs serve as an additional constraint, as they are not found at latitudes lower than  $\pm 80^\circ$  (MIT, 2011). We thus restrict our study to the latitudes of  $\pm 80^\circ$ – $90^\circ$  (Fig. 4.2).

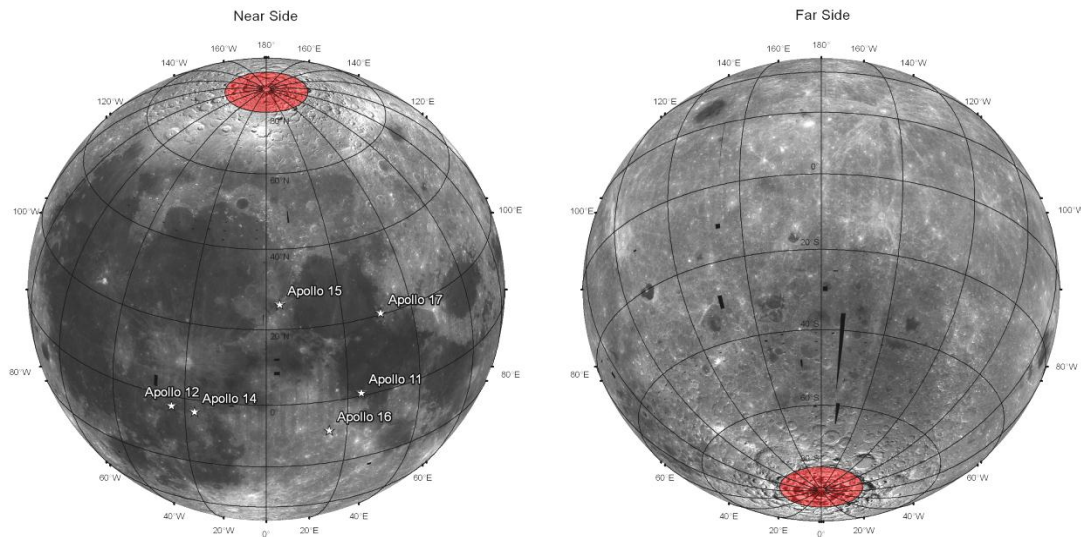


FIGURE 4.2 Extent of our study area at the lunar poles (see following sections for explanation).

The ages of polar volatiles can be constrained by the Moon's orbital and polar history. As the lunar orbit increased in radius, lunar obliquity varied up to  $77^\circ$  (Siegler *et al.*, 2011), but the current obliquity regime has been reasonably constant for the past  $\sim 2$  Ga (Siegler *et al.*, 2011a, 2011b; Ward *et al.*, 1975). In addition to obliquity variations with time, there is also a possibility that the Moon has undergone true polar

wander during its history. Grimm *et al.* (1986) examined fault abundances and orientations, but their work did not yield conclusive evidence of polar wander. Magnetic anomaly data from Apollo 16 and 17 magnetometers, however, suggests polar wandering of 90° early in lunar history (Fig. 4.3). Such extreme polar wandering could be explained by changes in the moment of inertia due to early bombardment (Runcorn *et al.*, 1980). Because of the possibility of polar wander and obliquity changes, we place a time constraint of 2 Ga on the modern lunar obliquity and polar locations. PSRs are therefore taken to be no older than 2 Ga directly at the poles, and younger still with decreasing latitude (Siegler *et al.*, 2011a). Thus, the oldest obtainable polar volatiles are likely to be no older than 2 Ga.

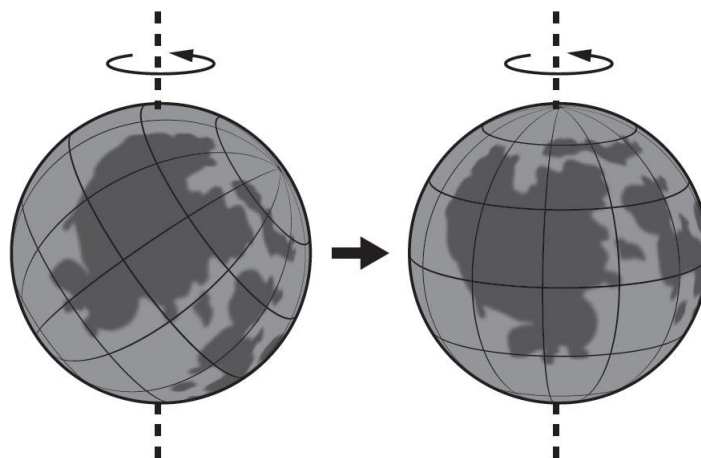


FIGURE 4.3 Depiction of polar wander, showing how the location of the axis of rotation for the Moon may have changed in relation to the surface over time. This is distinct from obliquity changes, where the axis is moving relative to the orbital plane instead of the body’s surface.

#### Volatiles

In the lunar science community, volatiles are defined as chemical elements and compounds that become unstable and vaporize, sublimate, or are otherwise mobilized at low temperatures (Table 4.1). Lunar volatile elements can be divided into two groups, vapor-mobilized and solar-wind-implanted. The latter group includes H, C, N, and the noble gases (He, Ne, Ar, Kr, Xe); study of these elements can have important implications for understanding radiation history, lunar outgassing, and solar history (Haskin *et al.*, 1991). Solar-wind-implanted volatiles are most likely to be found in permanently shadowed regions (PSRs) at the lunar poles (Haskin *et al.*, 1991) due to ‘cold trapping’, though the implantation process is globally homogeneous.

Table 4.1 Sublimation point of various substances at lunar surface pressures. Sublimation temperature values from Zhang and Paige (2010).

| Chemical Formula     | Name            | Sublimation Temperature | Sublimation Temperature | Cut off Temperature |
|----------------------|-----------------|-------------------------|-------------------------|---------------------|
|                      |                 | (K)                     | (°C)                    | (°C)                |
| N <sub>2</sub>       | Nitrogen        | 16.20                   | -257.0                  | 16                  |
| CO                   | Carbon monoxide | 18.20                   | -255.0                  |                     |
| Ar                   | Argon           | 19.50                   | -253.7                  |                     |
| CH <sub>4</sub>      | Methane         | 22.00                   | -251.2                  |                     |
| Kr                   | Krypton         | 24.50                   | -248.6                  |                     |
| Ar-6H <sub>2</sub> O | Argon clathrate | 28.90                   | -244.3                  |                     |

|                                |                       |       |        |     |
|--------------------------------|-----------------------|-------|--------|-----|
| Xe                             | Xeon                  | 36.10 | -237.1 |     |
| H <sub>2</sub> S               | Hydrogen sulfide      | 50.60 | -222.6 |     |
| CO <sub>2</sub>                | Carbon dioxide        | 54.30 | -218.9 | 54  |
| SO <sub>2</sub>                | Sulfur dioxide        | 62.30 | -210.9 |     |
| NH <sub>3</sub>                | Ammonia               | 65.50 | -207.7 |     |
| C <sub>5</sub> H <sub>12</sub> | Pentane               | 73.60 | -199.6 | 70  |
| HCN                            | Hydrogen cyanide      | 80.50 | -192.7 |     |
| C <sub>7</sub> H <sub>8</sub>  | Toluene               | 87.60 | -185.6 |     |
| NH <sub>4</sub> SH             | Ammonium hydrosulfide | 96.10 | -177.1 |     |
| H <sub>2</sub> O               | Water                 | 106.6 | -166.6 | 100 |
| S                              | Sulfur                | 201.5 | -71.65 |     |

Vapor-mobilized elements are transferred from solid materials to a coexisting vapor-phase at moderate temperature. This group includes S, Cu, Zn, As, Se, Ag, Cd, In, Te, Hg, Tl, Pb, Bi, and the halogens (F, Cl, Br, I). The vapor-mobilized volatiles are mostly added by small impactors, and so should be deposited fairly uniformly throughout the lunar regolith (Haskin *et al.*, 1991).

#### *Lunar regolith*

Regolith is a general term for the layer of fragmented and unconsolidated rock material that mantles bedrock and covers the whole lunar surface. The regolith layer develops from the continuous impact of meteoroids and the steady bombardment of charged solar and extrasolar particles (McKay *et al.*, 1991).

As soon as fresh bedrock becomes exposed, it begins to break down through impact and particle bombardment processes. The regolith layer that exists shortly after bedrock has been exposed is relatively thin (< a few cm), and various-sized impactors are able to penetrate the regolith and excavate new bedrock (McKay *et al.*, 1991). The regolith increases in thickness with time (up to a few meters), and then only less-frequent, larger impactors can penetrate the regolith and excavate new bedrock. During this stage, small, frequent impactors only disturb and ‘garden’ the existing regolith layer, so the overall regolith thickness increases more slowly (McKay *et al.*, 1991).

At the poles, the regolith has been extensively gardened and reworked and is consequently extremely fine-grained. Such grain sizes provide greater surface area for volatile adsorption. The volatile-rich upper layers of the polar regolith are then buried at greater depths by small impact processes. This preserves the volatiles by protecting them from atomic particle bombardment.

#### **Geologic context**

The polar regions are part of the most ancient terrains on the Moon, though they have been modified by subsequent cratering. The geology of the north and south poles is briefly described below.

#### *North Pole*

The geology of the region poleward of 80°N is mostly composed of crater fields approaching geometric saturation. The craters in this region are at most a few kilometers in diameter. The region also contains several large (D > 70 km) flat-floored craters, such as Peary. No craters lying entirely north of the 80° latitude line exhibit central peaks. The terrain in the study area on the nearside is mostly Imbrian-aged basin and plains material. On the farside, it is mostly Nectarian basin material and ancient pre-Nectarian cratered terrain, with dense crater clustering (USGS, 2009a).

## *South Pole*

The region poleward of 80°S is almost entirely within the South Pole-Aitken (SPA) basin (Mest *et al.*, 2011), the largest and oldest discernible impact basin on the Moon. The study area is dominated by heavily degraded impact craters ~20–100 km in diameter. The large craters are mostly flat-floored, with the exception of two craters that exhibit central peaks. Fresh, bowl-shaped craters are rare, although Shackleton is a prime example of a crater of this type. The terrain at the South Pole is mostly pre-Nectarian basin and crater material, but also includes some Nectarian and Orientale basin materials (USGS, 2009a).

### **Exploration context**

The era of lunar exploration began in the late 1950s with the Soviet Luna and American Pioneer missions, and continued into the 1970s with the Ranger, Zond, Lunar Orbiter, Surveyor, and Apollo programs. After the 1970s, there was a hiatus in lunar exploration until the 1990 launch of the Japanese Hiten spacecraft. Since that time, there has been a renewed widespread interest in returning to the Moon, and in the past two decades, American, Japanese, European, Chinese, and Indian spacecraft have begun to return large amounts of new data on the lunar polar regions.

*Clementine*: In 1994 a backscatter radar experiment was performed to remotely detect the presence of ice at depth under the lunar surface. Radio waves were beamed from Clementine into polar areas, reflected from the surface, and received on Earth by the Deep Space Network. One orbit was directly over a PSR at the South Pole, and it produced coherent backscatter consistent with the presence of water ice (Spudis *et al.*, 1998).

*Lunar Prospector*: A neutron spectrometer was flown on Lunar Prospector in 1998, and measured epithermal-, thermal-, and fast-neutron fluxes. Maps of the epithermal- and fast-neutron fluxes were produced, and depressions in epithermal-neutron fluxes were observed at both poles within PSRs. However, no measureable depression in fast neutrons was observed at the poles. This data is consistent with deposits of hydrogen in the form of water ice at depths of ~50 cm under the lunar regolith at PSRs (Feldman *et al.*, 1998).

*Chandrayaan-1*: The Indian Space Research Organization launched the Chandrayaan-1 craft in 2008, which was equipped with a VIS/NIR spectrometer, the Moon Mineralogy Mapper (M<sup>3</sup>). This instrument detected absorption features indicative of hydroxyl (both lone OH and possibly H-OH, or H<sub>2</sub>O) near 2.8 to 3.0 μm at the surface (upper 1-2 mm of regolith), with the 3.0 μm feature appearing strongest at high latitudes (Pieters *et al.*, 2009). Chandrayaan-1 also obtained polarimetric radar data with the instrument Mini-SAR, which measured coherent backscatter levels in various craters on the lunar surface. Specifically, it returned information on the ratio of radar signals returned with right- versus left-circular polarization, known as the Circular Polarization Ratio (CPR). Most high CPR readings covered an area including both a crater's interior and surrounding regions, indicating a rough or fresh surface. However, there were some anomalous craters in PSRs with elevated CPR values in crater interiors without elevated values exterior to the crater, consistent with the presence of water ice at depth in these craters (Spudis *et al.*, 2010).

*Lunar Reconnaissance Orbiter*: New LRO data are also greatly enhancing our understanding of lunar volatiles. These data sets include high-resolution imagery, topography, temperature, and hydrogen data. We have used the most current existing versions of these data sets at the time this study was conducted. In 2009, the Centaur stage of LRO's Atlas V rocket was impacted into Cabeus crater, chosen because it was a PSR at the South Pole with elevated hydrogen levels. A shepherding satellite flew through the ejecta plume and observed spectra that corresponded with the presence of the volatile compounds H<sub>2</sub>O, OH, H<sub>2</sub>S, SO<sub>2</sub>, C<sub>2</sub>H<sub>4</sub>, CO<sub>2</sub>, CH<sub>4</sub>, CH<sub>3</sub>OH.

## DATA SETS AND METHODS

In order to find sites that will address all Science Goals within Science Concept 4, we developed the following method which we divided in three main steps: pre-processing, classification and weighting in ArcMap, and post-classification analysis (Fig. 4.4). Each of those steps has been done for all five Science Goals in order to produce a map of recommendation sites for each Science Goal separately. Then, overlapping of maps for each Science Goal allowed us to produce a final map of landing site recommendations to achieve all five Science Goals within Science Concept 4. Various geospatial datasets were processed using ArcGIS 10 and ISIS software.

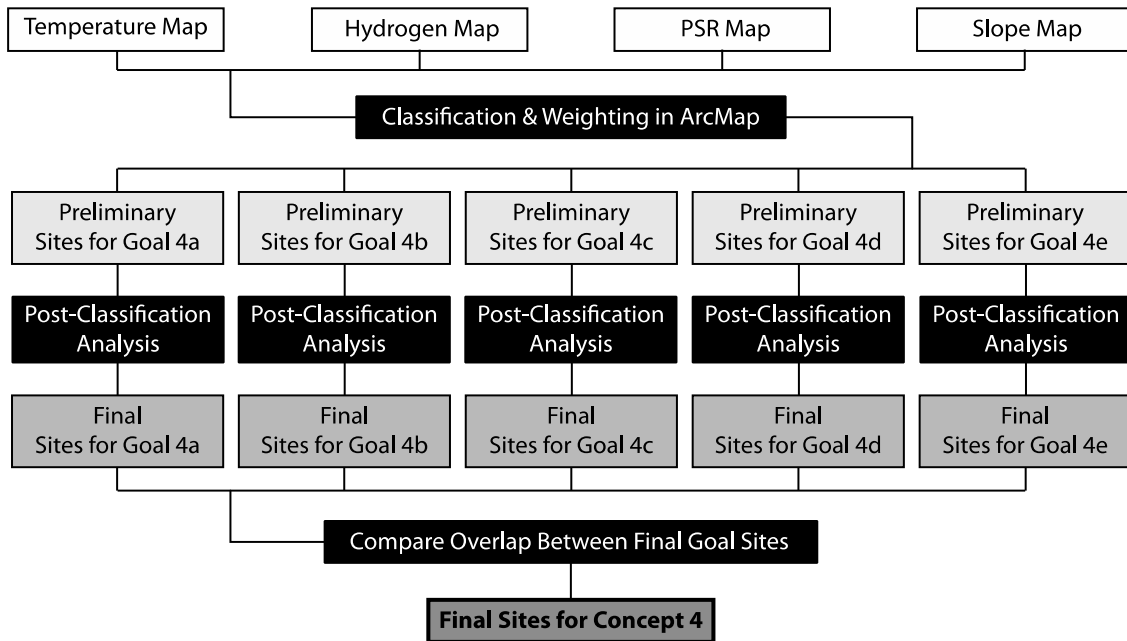


FIGURE 4.4 Overall methodology flowchart, showing the progression from data sets, at the top, down to final products, at the bottom. The main steps involved are the classification and weighting of datalayers in ArcMap for each Science Goal, the post-classification analysis, and finally the integration of the five Science Goals results. The outputs are preliminary maps showing acceptable sites to address each Science Goal, site final maps showing the recommended sites and a map showing the recommended sites to address all Science Goals at once.

### Datasets

Different datasets have been used in order to accomplish the pre-processing, classification, and post-classification analysis of the lunar polar regions. Some of them are in raster format, or images, and some of them are in vector format, or polygons.

#### *Raster layers*

Table 4.2 summarizes data images from Lunar Prospector, Lunar Reconnaissance Orbiter and Chandrayaan-1 that have been used in this study. Many image types were used and had different spatial resolution and coverage.

TABLE 4.2 Raster layers used for Science Concept 4 studies.

| Spacecraft                   | Instrument                | Layer Name                  | Type                       | Coverage Poleward of $\pm$ Latitude | Spatial resolution | Units         |
|------------------------------|---------------------------|-----------------------------|----------------------------|-------------------------------------|--------------------|---------------|
| Lunar Prospector             | Neutron Spectrometer (NS) | Hydrogen                    | Thematic                   | global                              | 30323 m            | ppm by weight |
| Lunar Reconnaissance Orbiter | Laser Altimeter (LOLA)    | Digital Elevation Model     | Scientific                 | 60°                                 | 120 m              | Meters        |
|                              |                           | Slope                       | Thematic                   | 60°                                 | 120 m              | Degrees       |
|                              |                           | Roughness                   | Thematic                   | 45°                                 | 1895 m             | Meters        |
|                              |                           | Permanently Shaded Regions  | Thematic                   | 80°                                 | 240 m              | Binary        |
|                              |                           | Shaded mosaic               | Base map                   | 75°                                 | 240 m              | -             |
|                              |                           | Diviner                     | Maximum Annual Temperature | Thematic                            | 80°                | 240 m         |
|                              | Wide Angle Camera (WAC)   | WAC mosaic                  | Base map                   | 60°                                 | 100 m              | -             |
| Chandrayaan-1                | Mini-SAR                  | Circular Polarization Ratio | Thematic                   | 80°                                 | 75 m               | Ratio         |

**Hydrogen map (LP-NS) [Plate I]** The half degree hydrogen abundance image contains data from the Lunar Prospector Neutron Spectrometer. The abundances, available for the entire Moon, were derived from epithermal neutron counts that have been corrected by thermal neutron data (Feldman *et al.* 1998; 2001). The dataset reflects the count of epithermal neutrons that have escaped from approximately 50 cm deep up to the surface. The total uncertainties related to the low-altitude epithermal neutron data poleward of  $\pm 70$  degrees latitude, including systematic and statistical contributions, are less than  $\sim 1\%$ .

**Digital Elevation Model (DEM) (LRO-LOLA) [Plate II]** This DEM is based on altimetry data acquired by the LOLA instrument through mission phase “LRO\_SM\_05”. The spatial resolution is 120 meters per pixel (horizontal), true at the poles in polar stereographic projection; elevation accuracy is  $\sim 1$  m (MIT, 2011). The elevation values for the South Pole vary approximately from -8000 m to 8000 m and from -6000 m to 3000 m for the North Pole.

**Slope map (LRO-LOLA-DEM) [Plate III]** We derived a slope image from the LOLA DEM image using the “Slope tool” in ArcGIS 10. For each cell, this tool calculates the maximum rate of change in value from that cell to its eight direct neighbors. The maximum change in elevation over the distance between the cell and its neighbors identifies the steepest downhill descent from the cell. The lower the slope value is, the flatter the terrain is; the higher the slope value is, the steeper the terrain is. If there is a cell location in the neighborhood with a “NoData” elevation value, the elevation value of the center cell will be assigned to the location. At the edge of the image, at least three cells outside the image’s extent will contain “NoData” values. These cells will be assigned the center cell’s elevation value, which will result in a flattening of the  $3 \times 3$  plane fitted to these edge cells, and will lead to a reduction in the slope. Slope is commonly measured in degrees, which uses the algorithm:

$$\text{slope\_degrees} = \frac{180}{\pi} \arctan \left( \sqrt{\left(\frac{\partial z}{\partial x}\right)^2 + \left(\frac{\partial z}{\partial y}\right)^2} \right) \quad (4.1)$$

The slope image created is of the same spatial resolution as the DEM image, which is 120 m/pixel. The slope values vary between 0 and  $\sim 80^\circ$  for both poles.

Roughness map (LRO-LOLA) [Plate IV] This data product is an image of the surface roughness of the Moon at a resolution of 16 pixels per degree ( $\sim 1895$  m/pixel) in a simple cylindrical projection re-projected into polar stereographic. This image is based on LOLA altimetry data from Laser 1 and 2 through mission phase “LRO\_SM\_05”. To derive roughness, the LOLA science team averaged the residual standard deviation of altitudes from three successive laser shots. Depending on orbital velocity, probability of detection, and spacecraft altitude, the slope baseline may vary from 30 to 120 meters. The pixel values are interpolated by the nearest-neighbor method for missing values (NASA, 2011c). Roughness values on the Moon vary between  $\sim 0.192$  to 7.466 RMS m.

Permanently Shadowed Regions (PSR) map (LRO-LOLA) [Plate V] This data product is an image of PSRs at the lunar poles at a resolution of 240 m/pixel, true at the poles in polar stereographic projection. The calculations have been made by the LOLA science team, based on the LOLA DEM “LDEM\_75N\_240M” as described in Mazarico *et al.* (2011). The values are binary and indicate whether or not a given pixel is in permanent shadow (MIT, 2011).

Shaded relief mosaic (LRO-LOLA) [Plate VI] The shaded relief mosaic has been downloaded from the Lunar Mapping and Modeling Project Portal (NASA, 2011a). This 240 m/pixel image is a shaded relief topographic model derived from LRO-LOLA altitude data.

Maximum annual temperature (LRO-Diviner) [not shown] Each pixel in this image represents the maximum annual bolometric brightness temperature over a lunar year, which corresponds to 13 LRO mapping cycles. These data represent the wavelength-integrated radiance in seven infrared Diviner channels expressed as the temperature of an equivalent blackbody (Paige *et al.*, 2010). Data provided by Dr. David Paige (personal communication).

Minimum annual temperature (LRO-Diviner) [not shown] Each pixel in this image represents the minimum annual bolometric brightness temperature over a lunar year.

Wide Angle Camera (WAC) mosaic (LRO-LROC) [Plate VII] The Wide Angle Camera (WAC) mosaic from the Lunar Reconnaissance Orbiter Camera (LROC) onboard LRO is derived from the Reduced Data Record (RDR), Level 5 Version 1.0. The spatial resolution is  $\sim 100$  m/pixel with global coverage. The principal limitation of LROC imagery is that it is illumination-dependent, a disadvantage when studying areas in permanent shadow.

Circular Polarization Ratio (CPR) (Chandrayaan-1-Mini-SAR) [Plate VIII] From February to April 2009 the Chandrayaan-1 Mini-SAR (Synthetic Aperture RADAR) instrument mapped over 95% of the lunar poles at a wavelength of 12.6 cm, in the S band (Spudis *et al.*, 2010). The Circular Polarization Ratio (CPR) values have been derived from the radar backscatter measurements by the Johns Hopkins University Applied Physics Laboratory. CPR values correspond to the ratio of power of the received signal in the same circular polarization sense (as transmitted by Chandrayaan-1) to the power of the signal received in the opposite sense. Those values are usually an indication of surface roughness on the same scale as the radar wavelength (12.6 cm). However, a high CPR value can be attributed to multiple internal reflections and/or coherent backscatter produced by low-loss material such as water ice up to a few meters deep. A high CPR value found only inside a crater could be an indication of the presence of water ice, whereas a high CPR value found both inside and outside a crater may instead be caused by a rough (*i.e.* fresh) surface. The average CPR of the lunar surface is 0.2–0.4 at a  $45^\circ$  incidence, for typical terrains. Above 0.4, CPR values are considered ‘high’.

#### *Vector layers*

Geographical shapes in Geographical Information Systems (GIS) are often expressed as vectors, such as points, lines and polygons. For this study, we used the polygons of geologic units created by the United States Geological Survey (USGS) and the Lunar Impact Crater Database from the Lunar and Planetary Institute (LPI) (Table 4.3).

TABLE 4.3 Vector layers used for Science Concept 4 studies.

| Layer Name      | Type     | Geometry | Coverage Poleward of $\pm$ Latitude | Unit          |
|-----------------|----------|----------|-------------------------------------|---------------|
| USGS Geology    | Thematic | Polygons | 45°                                 | geology units |
| Crater database | Thematic | Points   | (global)                            | -             |

Geologic units (USGS) [Plates IX and X] Geologic unit layers “L-1162 Geologic Map of the South Side of the Moon” and “L-1062 Geologic Map of the North Side of the Moon” were downloaded from the USGS Planetary GIS Web Server, PIGWAD (USGS, 2009a). These maps are part of a complete geologic reconnaissance mapping of the Moon at 1:5,000,000 scale that was meant to summarize the current state of lunar geologic knowledge as developed from the USGS Systematic Lunar Mapping Program. The maps were created mostly from Lunar Orbiter photography, supplemented in places by Zond 7 and Mariner 10 images. For our study, we used USGS geologic maps for minor descriptive purposes only.

Crater database (LPI) [Plate XI and XII] The database of impact craters was created as part of the Lunar Exploration Summer Intern Program at the Lunar and Planetary Institute in 2008 and updated in May 2011. The database contains 8,713 craters with their age and several physical characteristics (*e.g.* ejecta blanket thickness, crater volume, or melt volume).

### **Landing site selection**

Landing site selection was completed using the Spatial Analyst Tools in ArcMap. First, relevant layers were imported and pre-processed. New data sets were derived from existing layers, reclassifying each data set for subsequent weighting. Data sets were combined according to different criteria for each Science Goal in order to find suitable sites for each Science Goal. Finally, results for each Science Goal were overlapped to find suitable sites that address Concept 4 as a whole. Post-processing analysis for each result led to selection of the highest priority sites.

Plate I. Hydrogen content at the Lunar Poles

The half degree hydrogen abundance map has been derived from epithermal neutron counts (Lunar Prospector) that have been corrected by thermal neutron data (Feldman et al. 1998; 1999; 2001). They reflect the count of epithermal neutrons that have escaped from approximately 30 cm deep up to the surface. For this study, we use the hydrogen map as a proxy for the lunar volatiles.

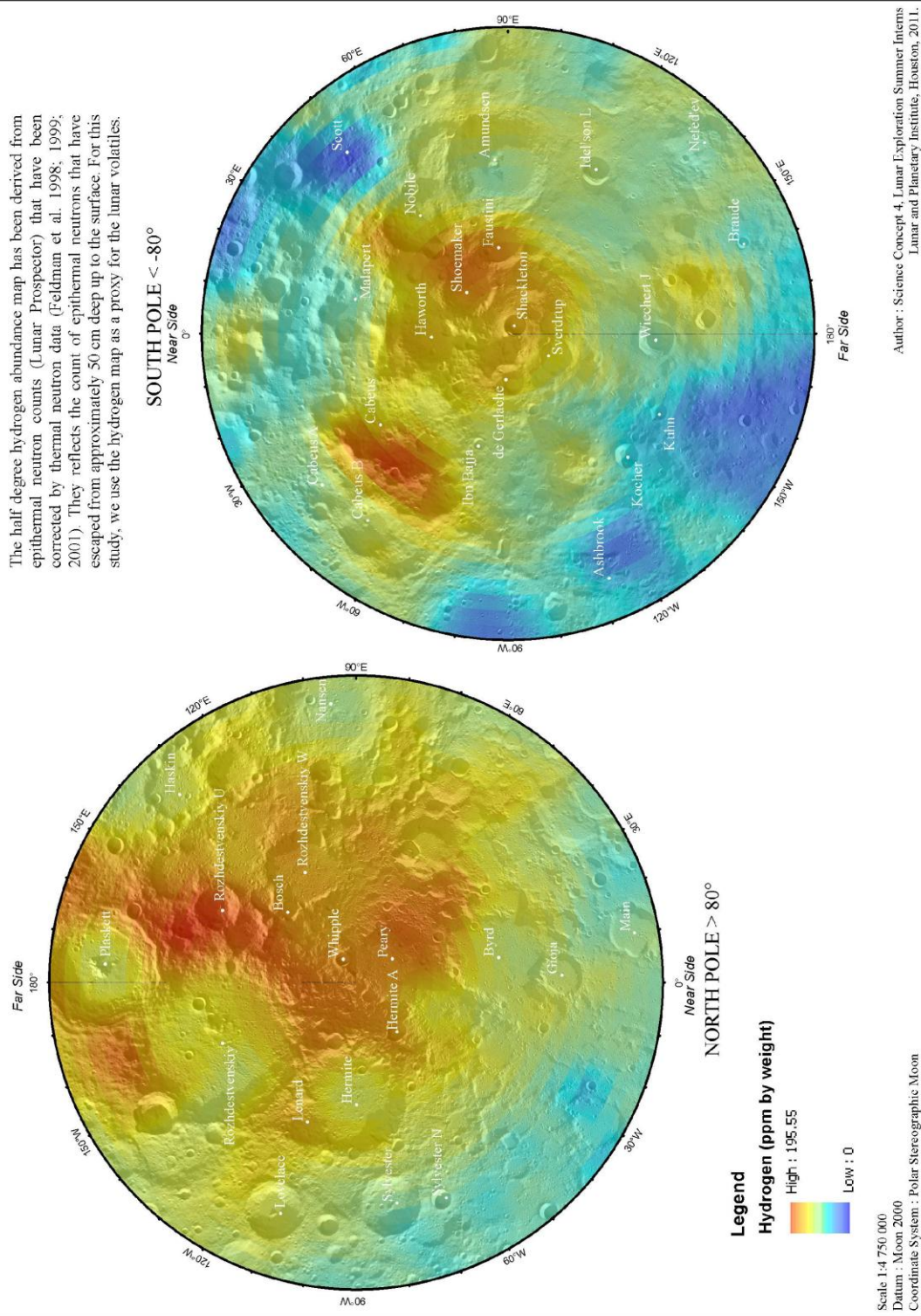
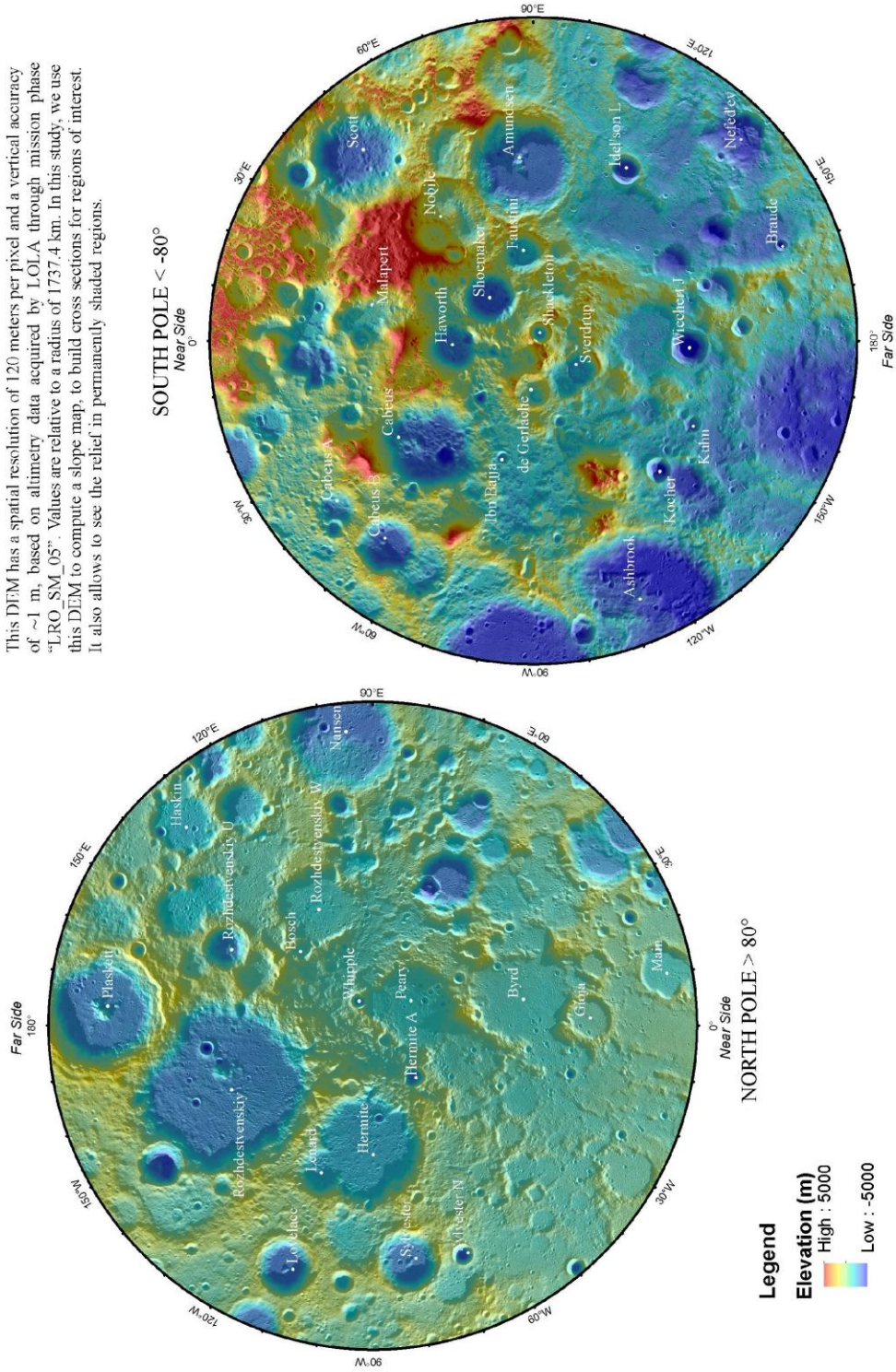


## Plate II. Digital Elevation Model of the Lunar Poles

This DEM has a spatial resolution of 120 meters per pixel and a vertical accuracy of ~1 m, based on altimetry data acquired by LOLA through mission phase "LRO\_SM\_05". Values are relative to a radius of 1737.4 km. In this study, we use this DEM to compute a slope map, to build cross sections for regions of interest. It also allows to see the relief in permanently shaded regions.



Scale 1:4 750 000  
 Datum : Moon 2000  
 Coordinate System : Polar Stereographic Moon

Author : Science Concept 4, Lunar Exploration Summer Interns  
 Lunar and Planetary Institute, Houston, 2011.

### Plate III. Slope Map of the Lunar Poles

We derived this slope map from LOLA DEM values in ArcMap. It has a spatial resolution of 120 m. This slope map has been used in the classification process for each Science Goal to avoid areas containing slopes steeper than 25 degrees.

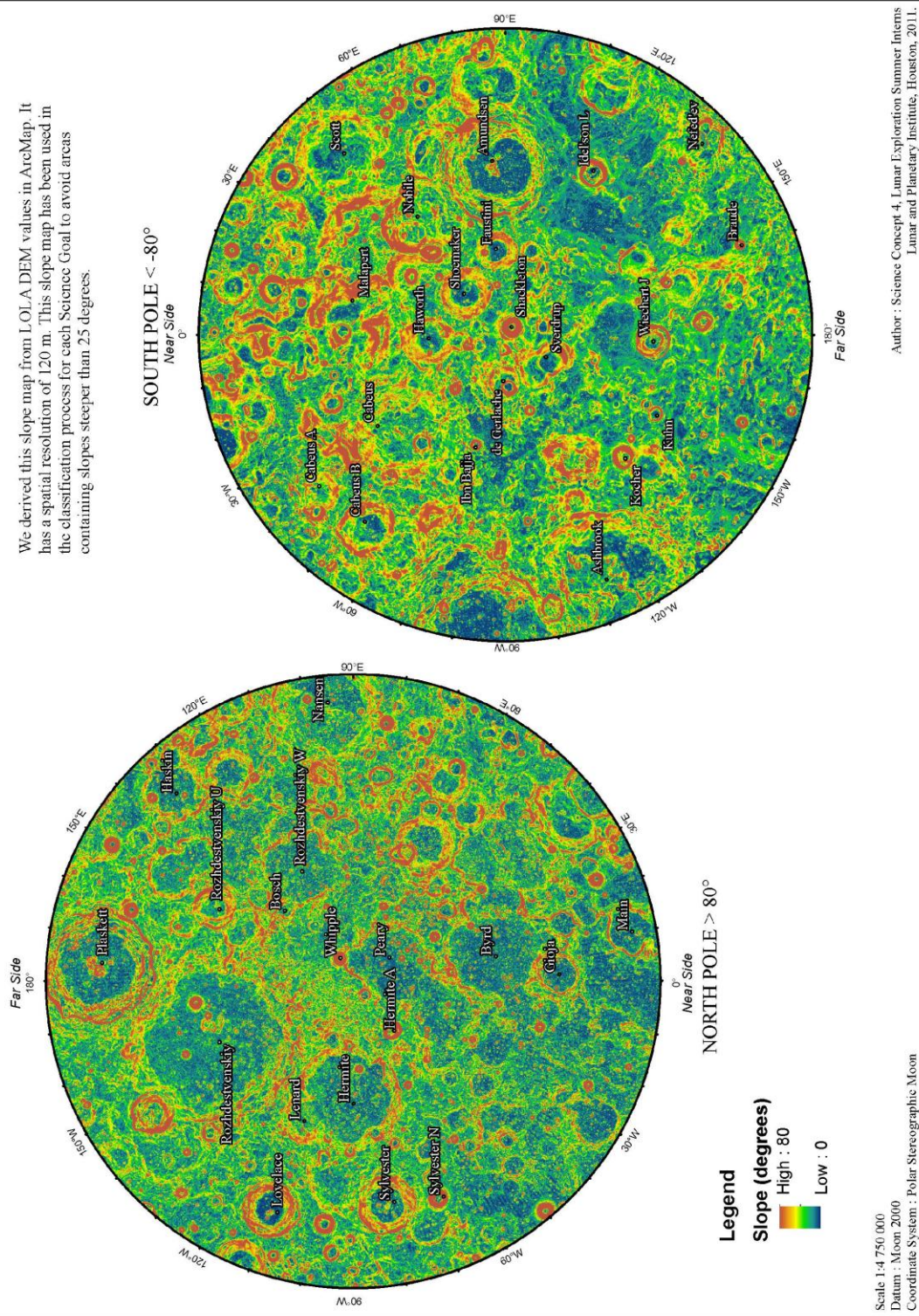
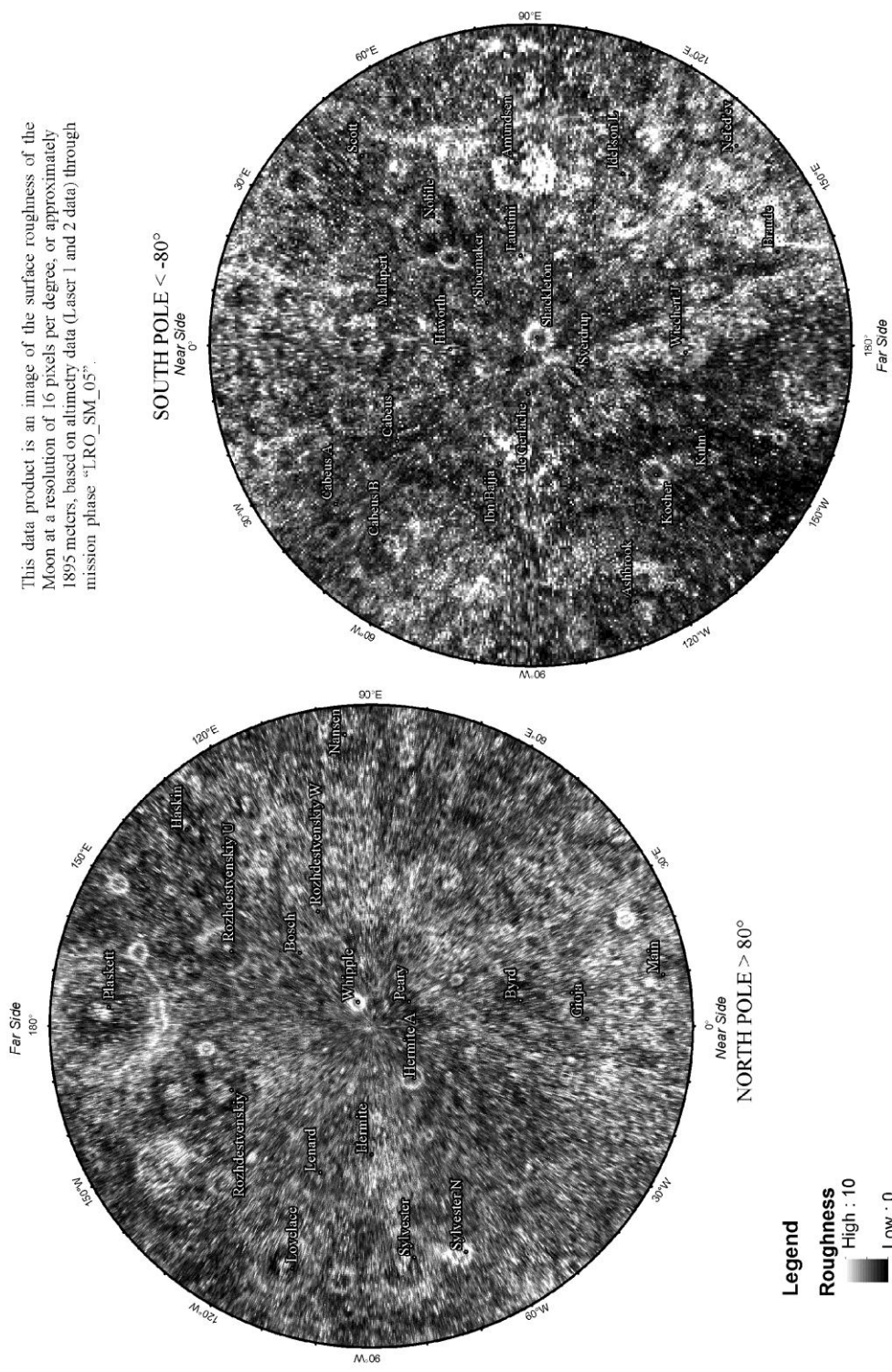


# Plate IV. Roughness Map of the Lunar Poles

This data product is an image of the surface roughness of the Moon at a resolution of 16 pixels per degree, or approximately 1895 meters, based on altimetry data (Laser 1 and 2 data) through mission phase "LRO\_SM\_05".



Author : Science Concept 4, Lunar Exploration Summer Interns  
Lunar and Planetary Institute, Houston, 2011.

### Plate V. Distribution of Permanently Shadowed Regions at the Lunar Poles

This map of the permanently shadowed regions (PSRs) at the Lunar Poles has a spatial resolution of 240 meters per pixel, true at the poles in polar stereographic projection. The calculations have been made by the LOLA science team, based on the LOLA DEM "LDEM\_75N\_240M". In our study, understanding the transport, retention and loss that operate on volatiles at permanently shaded regions is expressed by Science Goal 4c.

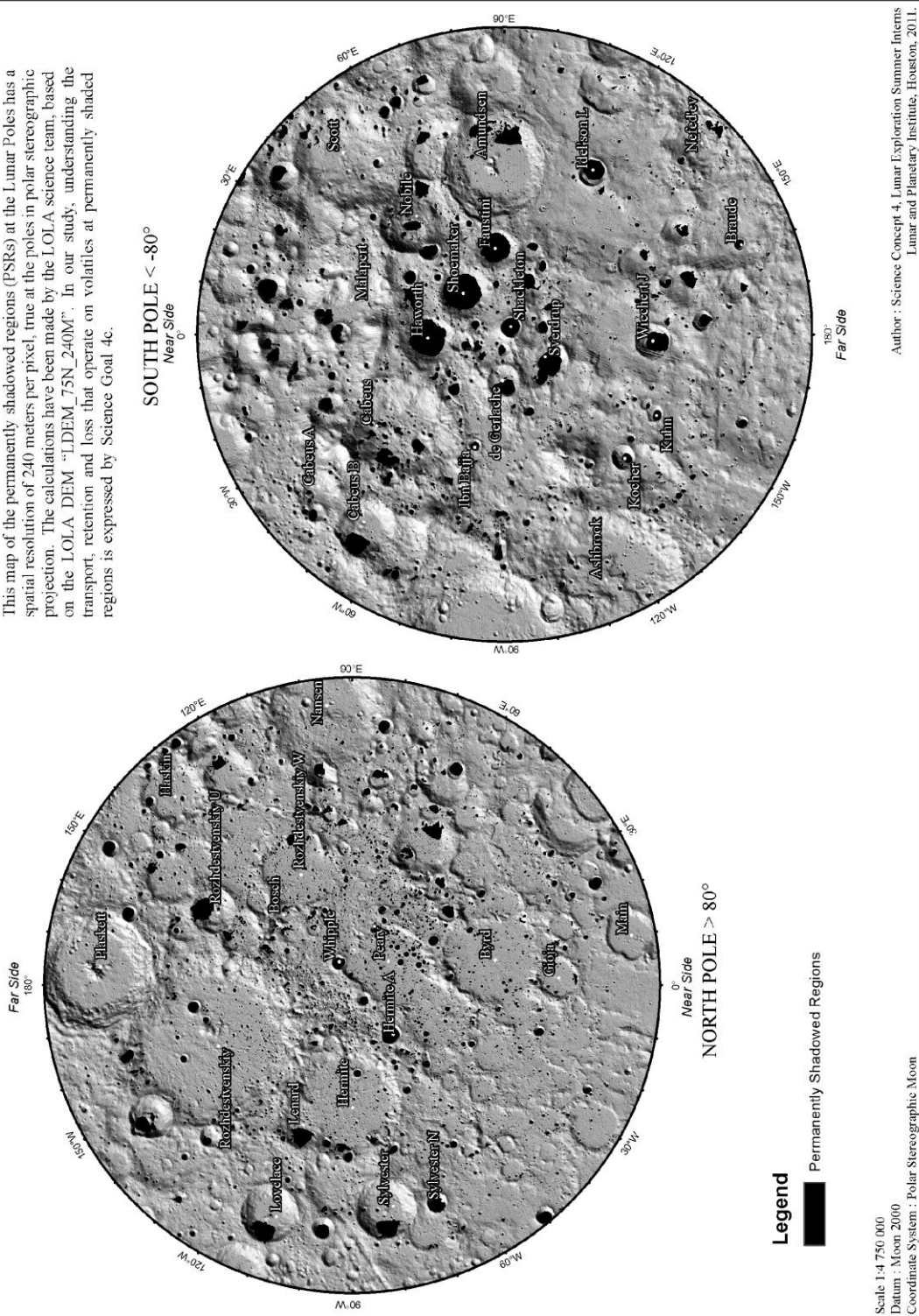
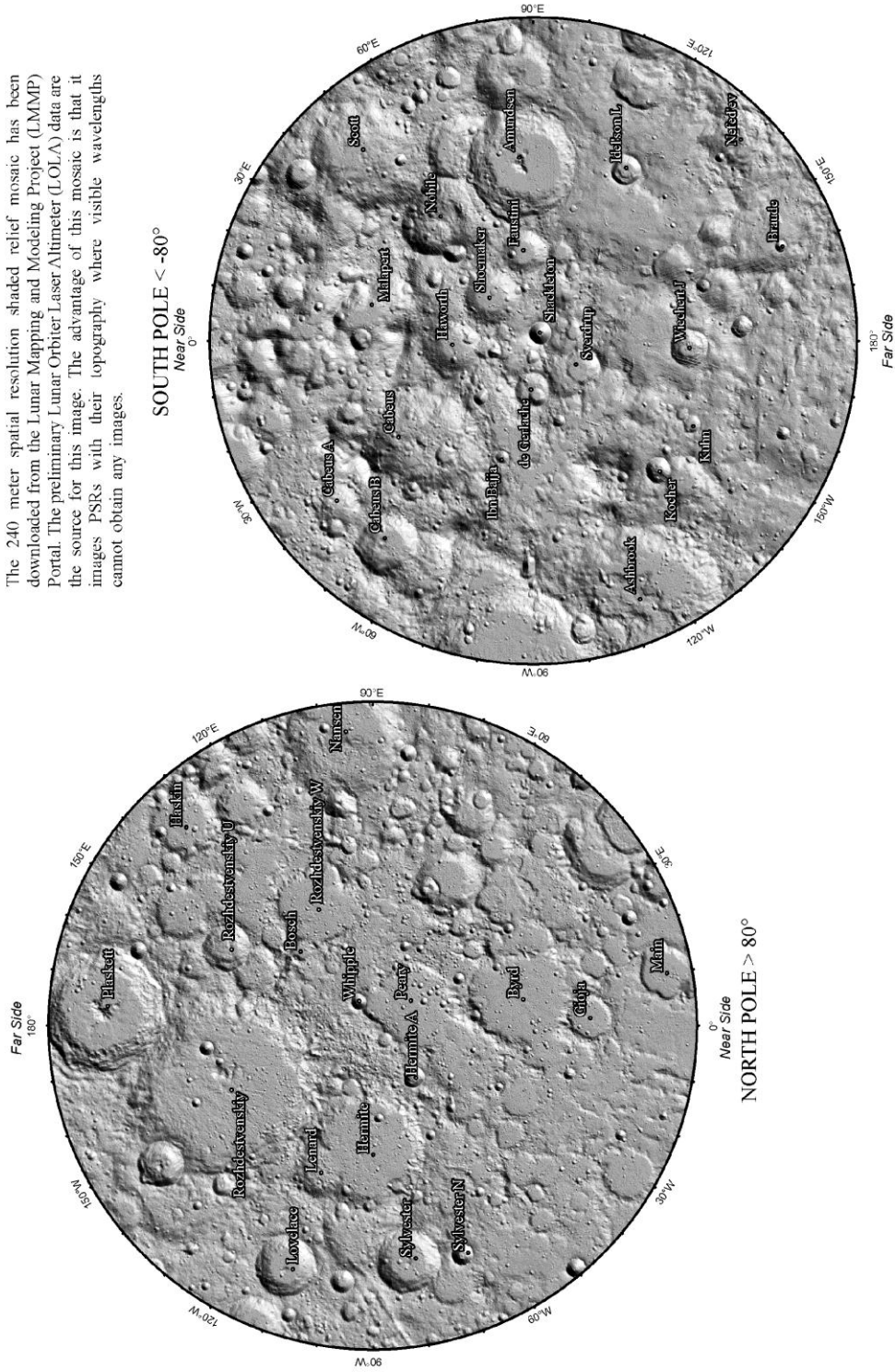


## Plate VI. Shaded Relief Mosaic of the Lunar Poles

The 240 meter spatial resolution shaded relief mosaic has been downloaded from the Lunar Mapping and Modeling Project (LMMP) Portal. The preliminary Lunar Orbiter Laser Altimeter (LOLA) data are the source for this image. The advantage of this mosaic is that it images PSRs with their topography where visible wavelengths cannot obtain any images.

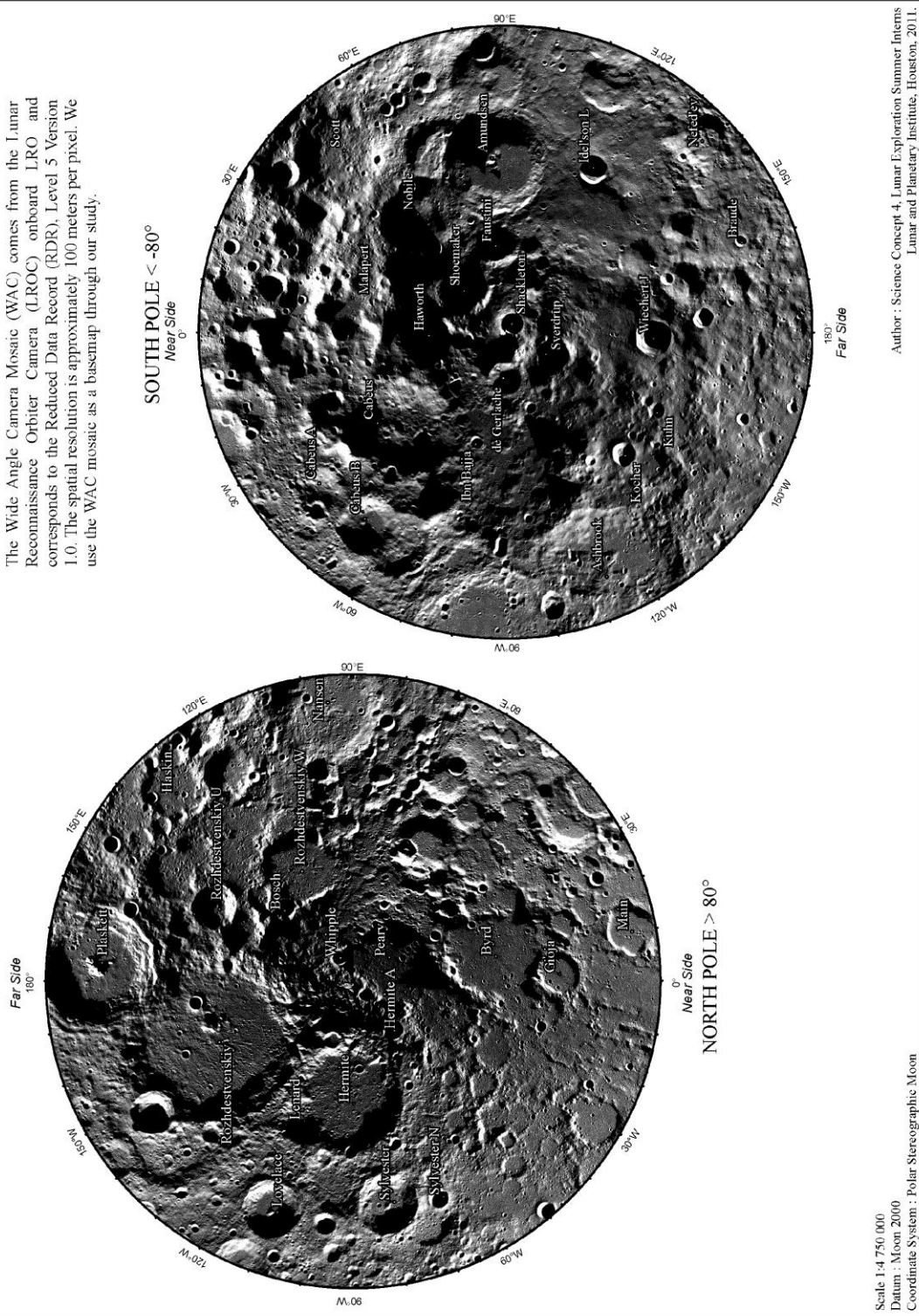


Scale 1:4 750 000  
 Datum : Moon 2000  
 Coordinate System : Polar Stereographic Moon

Author : Science Concept 4, Lunar Exploration Summer Interns  
 Lunar and Planetary Institute, Houston, 2011.

### Plate VII. Lunar Reconnaissance Orbiter Wide Angle Camera Mosaic of the Lunar Poles

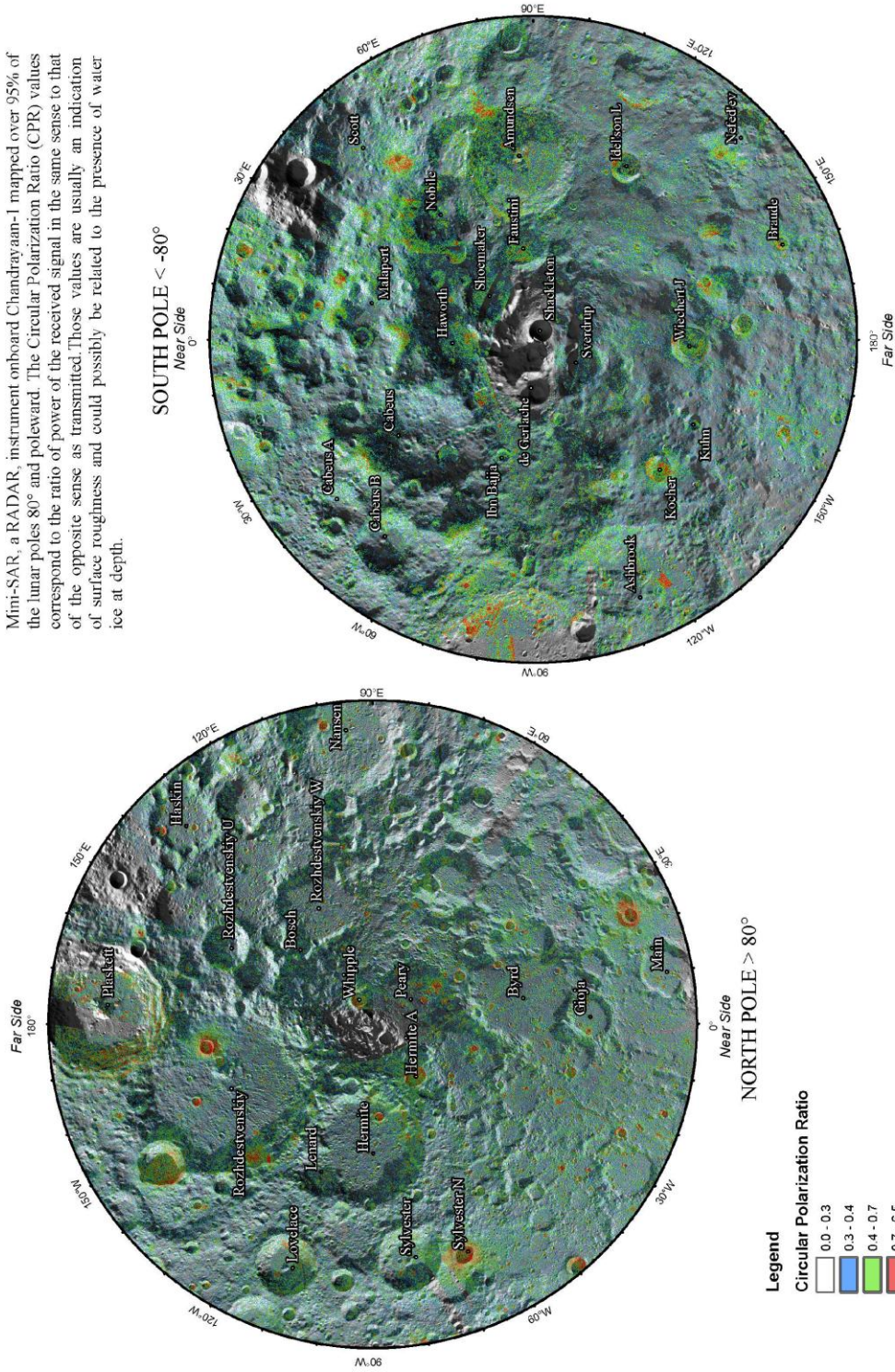
The Wide Angle Camera Mosaic (WAC) comes from the Lunar Reconnaissance Orbiter Camera (LROC) onboard LRO and corresponds to the Reduced Data Record (RDR), Level 5 Version 1.0. The spatial resolution is approximately 100 meters per pixel. We use the WAC mosaic as a basemap through our study.



Scale 1:4 750 000  
 Datum : Moon 2000  
 Coordinate System : Polar Stereographic Moon  
 Author : Science Concept 4, Lunar Exploration Summer Interns  
 Lunar and Planetary Institute, Houston, 2011.

### Plate VIII. Circular Polarization Ratio derived from Mini-SAR at the Lunar Poles

Mini-SAR, a RADAR, instrument onboard Chandrayaan-1 mapped over 95% of the lunar poles 80° and poleward. The Circular Polarization Ratio (CPR) values correspond to the ratio of power of the received signal in the same sense to that of the opposite sense as transmitted. Those values are usually an indication of surface roughness and could possibly be related to the presence of water ice at depth.

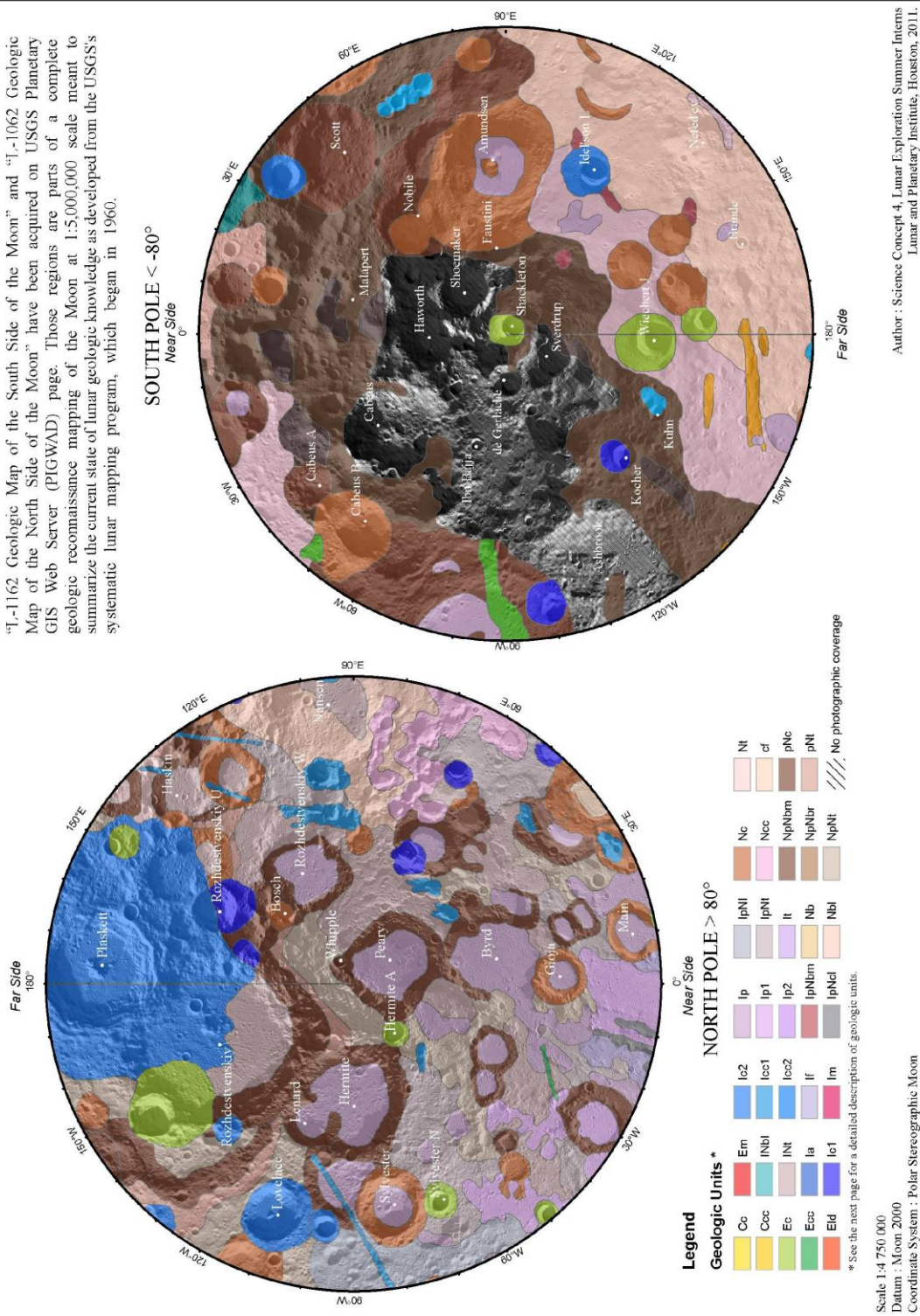


Scale 1:4 750 000  
 Datum : Moon 2000  
 Coordinate System : Polar Stereographic Moon

Author : Science Concept 4, Lunar Exploration Summer Interns  
 Lunar and Planetary Institute, Houston, 2011.

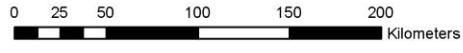
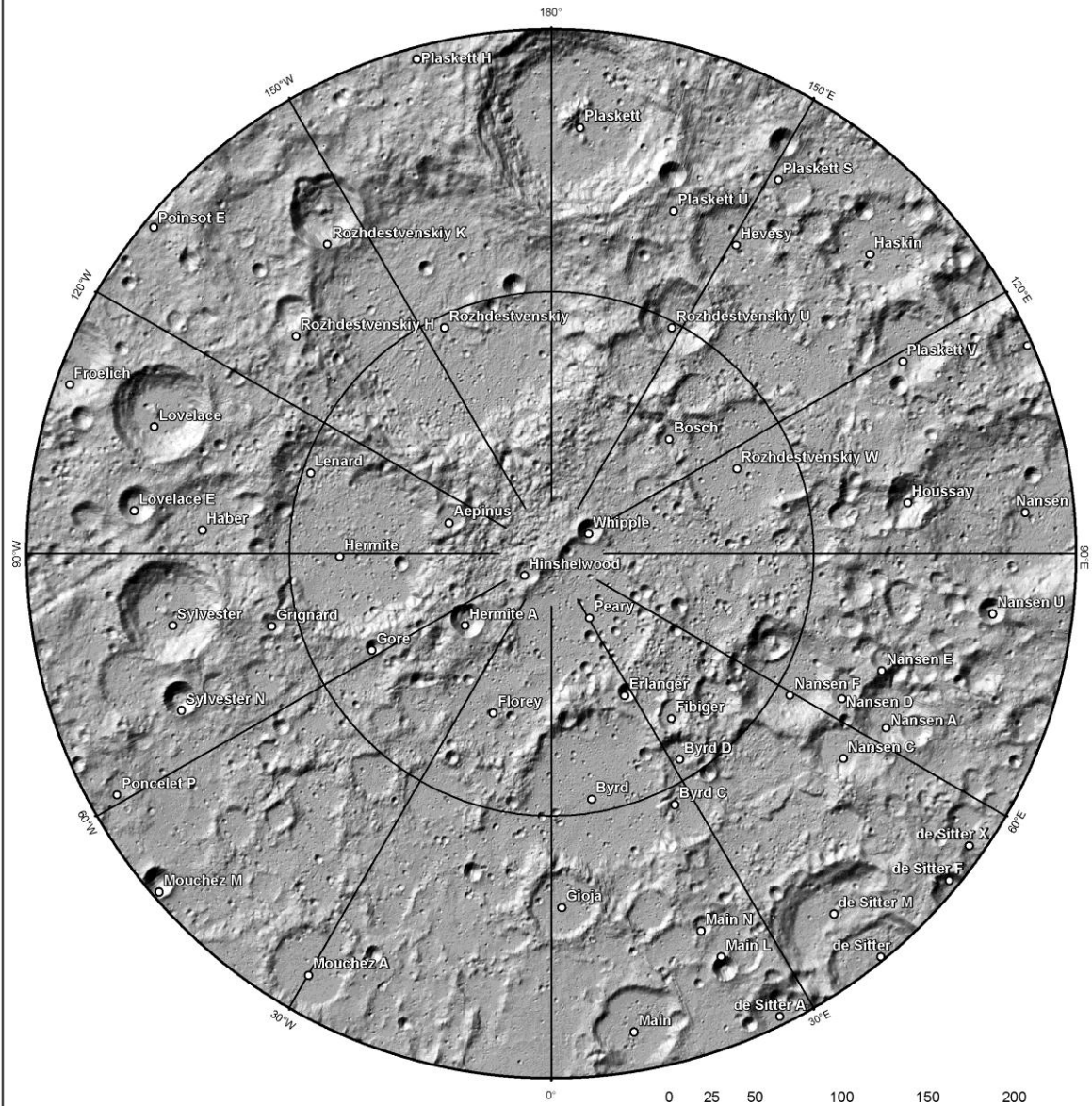
Plate IX. Map of Geologic Units at the Lunar Poles

"T-1162 Geologic Map of the South Side of the Moon" and "T-1062 Geologic Map of the North Side of the Moon" have been acquired on USGS Planetary GIS Web Server (PIGWAD) page. Those regions are parts of a complete geologic reconnaissance mapping of the Moon at 1:5,000,000 scale meant to summarize the current state of lunar geologic knowledge as developed from the USGS's systematic lunar mapping program, which began in 1960.



| Unit Symbol | Unit Name                               | Major Group                    | Epoch   | Unit Description   |
|-------------|---|--------------------------------|---|--|
| Cc          | Material of Rayed Craters               | Crater Materials               | Copernican System                             | Material of Rayed Craters, Copernican System                                     |
| Ccc         | Material of Crater Chain                | Crater Materials               | Copernican System                             | Material of Crater Chain, Copernican System                                      |
| Ec          | Material of Fresh Craters               | Crater Materials               | Eratosthenian System                          | Material of Fresh Craters, Eratosthenian System                                  |
| Ecc         | Material of Crater Chain                | Crater Materials               | Eratosthenian System                          | Material of Crater Chain, Eratosthenian System                                   |
| Eld         | Dark Material                           | Mare and Dark Mantle Materials | Eratosthenian or Imbrian Systems              | Dark Material, Eratosthenian or Imbrian Systems                                  |
| En          | Younger Mare Material                   | Mare and Dark Mantle Materials | Eratosthenian System                          | Younger Mare Material, Eratosthenian System                                      |
| INbl        | Undivided Lineated Basin Material       | Basin Materials                | Imbrian and Nectarian Systems                 | Undivided Lineated Basin Material, Imbrian and Nectarian Systems                 |
| INt         | Terra Material                          | Other Terra Materials          | Imbrian and Nectarian Systems                 | Terra Material, Imbrian and Nectarian Systems                                    |
| Ia          | Alps Formation                          | Basin Materials                | Imbrian System                                | Alps Formation, Imbrian System   |
| Ic1         | Material of Moderately Subdued Craters  | Crater Materials               | Imbrian System                                | Material of Moderately Subdued Craters, Imbrian System                           |
| Ic2         | Material of Moderately Fresh Craters    | Crater Materials               | Imbrian System                                | Material of Moderately Fresh Craters, Imbrian System                             |
| Icc1        | Material of Crater Clusters and Chains  | Crater Materials               | Imbrian System                                | Material of Crater Clusters and Chains, Imbrian System                           |
| Icc2        | Material of Crater Clusters and Chains  | Crater Materials               | Imbrian System                                | Material of Crater Clusters and Chains, Imbrian System                           |
| If          | Fra Mauro Formation                     | Basin Materials                | Imbrian System                                | Fra Mauro Formation, Imbrian System  |
| Im          | Older Mare Material                     | Mare and Dark Mantle Materials | Imbrian System                                | Older Mare Material, Imbrian System  |
| Ip          | Undivided Plains Material               | Other Terra Materials          | Imbrian System                                | Undivided Plains Material, Imbrian System  |
| Ip1         | Older Plains Material                   | Other Terra Materials          | Imbrian System                                | Older Plains Material, Imbrian System  |
| Ip2         | Younger Plains Material                 | Other Terra Materials          | Imbrian System                                | Younger Plains Material, Imbrian System  |
| IpNbm       | Material of Imbrium Basin Massifs       | Basin Materials                | Imbrian, Nectarian, and pre-Nectarian Systems | Material of Imbrium Basin Massifs, Imbrian, Nectarian, and pre-Nectarian Systems |
| IpNcl       | Material of Lineated Craters            | Crater Materials               | Imbrian, Nectarian, and pre-Nectarian Systems | Material of Lineated Craters, Imbrian, Nectarian, and pre-Nectarian Systems      |
| IpNI        | Imbrian Lineated Basin Material         | Basin Materials                | Imbrian, Nectarian, and pre-Nectarian Systems | Imbrian Lineated Basin Material, Imbrian, Nectarian, and pre-Nectarian Systems   |
| IpNT        | Terra Material                          | Other Terra Materials          | Imbrian, Nectarian, and pre-Nectarian Systems | Terra Material, Imbrian, Nectarian, and pre-Nectarian Systems                    |
| It          | Terra Material                          | Other Terra Materials          | Imbrian System                                | Terra Material, Imbrian System   |
| Nb          | Undivided Basin Material                | Basin Materials                | Nectarian System                              | Undivided Basin Material, Nectarian System                                       |
| Nbl         | Lineated Basin Material                 | Basin Materials                | Nectarian System                              | Lineated Basin Material, Nectarian System  |
| Nc          | Material of Subdued Craters             | Crater Materials               | Nectarian System                              | Material of Subdued Craters, Nectarian System                                    |
| Ncc         | Material of Crater Clusters and Chains  | Crater Materials               | Nectarian System                              | Material of Crater Clusters and Chains, Nectarian System                         |
| NpNbm       | Material of Humboldtianum Basin Massifs | Basin Materials                | Nectarian and pre-Nectarian Systems           | Material of Humboldtianum Basin Massifs, Nectarian and pre-Nectarian Systems     |
| NpNbr       | Material of Rugged Basin, Terra         | Basin Materials                | Nectarian and pre-Nectarian Systems           | Material of Rugged Basin, Terra, Nectarian and pre-Nectarian Systems             |
| NpNt        | Terra Material                          | Other Terra Materials          | Nectarian and pre-Nectarian Systems           | Terra Material, Nectarian and pre-Nectarian Systems                              |
| Nt          | Terra Material                          | Other Terra Materials          | Nectarian System                              | Terra Material, Nectarian System   |
| pNc         | Material of Highly Subdued Craters      | Crater Materials               | pre-Nectarian System                          | Material of Highly Subdued Craters, pre-Nectarian System                         |
| pNt         | Terra Material                          | Other Terra Materials          | pre-Nectarian System                          | Terra Material, pre-Nectarian System   |

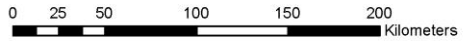
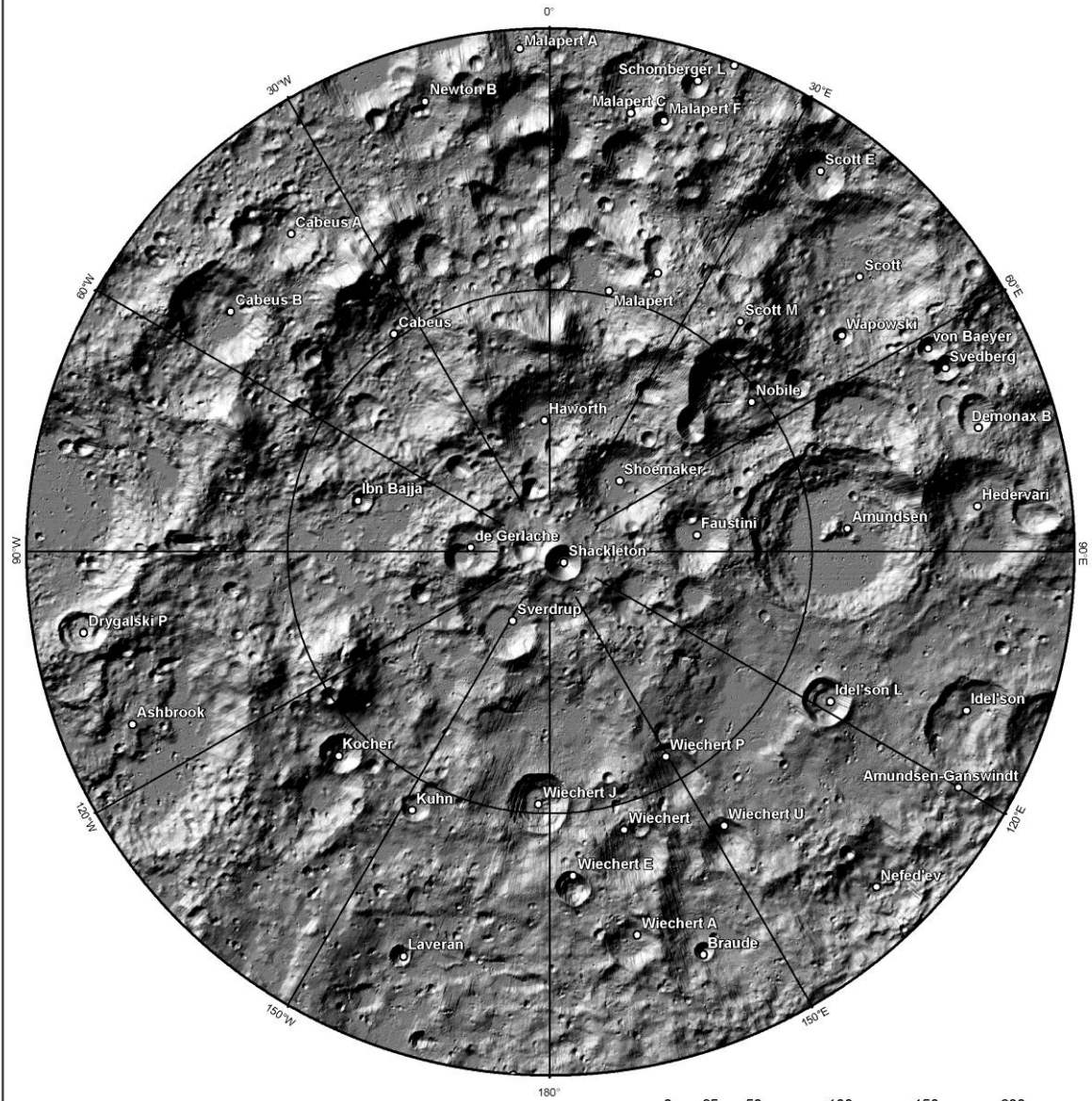
# Plate X. Map of the Lunar North Polar Region



The database of impact craters, referred here as the Crater Database, was created as part of the Lunar Exploration Summer Intern Program at the Lunar and Planetary Institute in 2008 and updated in May 2011. The database contains 8713 craters and is based on a database created by Jonathan McDowell.

Scale : 3 000 000  
 Datum : Moon 2000  
 Coordinate System : Polar Stereographic Moon  
 Basemap : LOLA Shaded Relief  
 Author : Science Concept 4, Lunar Exploration Summer Interns, Lunar and Planetary Institute, Houston, 2011.

# Plate XI. Map of the Lunar South Polar Region



The database of impact craters, referred here as the Crater Database, was created as part of the Lunar Exploration Summer Intern Program at the Lunar and Planetary Institute in 2008 and updated in May 2011. The database contains 8713 craters and is based on a database created by Jonathan McDowell.

Scale : 3 000 000  
 Datum : Moon 2000  
 Coordinate System : Polar Stereographic Moon  
 Basemap : LOLA Shaded Relief  
 Author : Science Concept 4, Lunar Exploration Summer Interns, Lunar and Planetary Institute, Houston, 2011.

## SCIENCE GOAL 4A: DETERMINE THE COMPOSITIONAL STATE (ELEMENTAL, ISOTOPIC, MINERALGOIC) AND COMPOSITIONAL DISTRIBUTION (LATERAL AND DEPTH) OF THE VOLATILE COMPONENT IN LUNAR POLAR REGIONS

### Introduction

Remote sensing has aided understanding of the lateral and vertical distribution of potential lunar volatiles. The Neutron Spectrometer onboard Lunar Prospector mapped the hydrogen content over the entire Moon for the top 50 cm of regolith and showed a clear enhancement at the lunar poles (Feldman *et al.*, 1998). However, the Neutron Spectrometer data alone is not sufficient to distinguish between hydrogen and different hydrogenated volatile species (Feldman *et al.*, 2000). Feldman *et al.* (2001) later found that the largest concentrations of hydrogen at the poles coincide with Permanently Shadowed Regions (PSRs). They concluded that a significant portion of the hydrogen detected at the poles was most likely to be in the form of water molecules. Pieters *et al.* (2009) later analyzed Moon Mineralogy Mapper (M3) spectra and found distinct absorption bands at 2.8 and 3.0  $\mu\text{m}$  that could be attributed to OH and/or H<sub>2</sub>O present in the top 1–2 mm of the lunar surface. The strongest absorption features were found near the poles in cooler regions and seemed to coincide with several fresh craters in feldspathic terrain. They observed a general lack of correlation with previous neutron measurements, suggesting that the formation and retention of OH and H<sub>2</sub>O are continuous surficial processes. Cheek *et al.* (2011) believe that, in the region they studied, the space weathering process increased the concentration of adsorbed OH and H<sub>2</sub>O. The Mini-SAR instrument onboard Chandrayaan-1 also found what is believed to be water ice at the poles (Spudis *et al.*, 2010). This radar instrument, emitting a circular polarized signal, allowed the calculation of the circular polarization ratio (CPR), which is the ratio of the signal received in the same sense as transmitted to that received in the opposite sense. A high CPR value both interior and exterior to a crater is believed to be the result of a rough surface, indicative of a fresh crater. Spudis *et al.* (2010) suggest that a high CPR value found only inside a crater is consistent with the presence of water ice at depths up to 2–3 m. According to their results, ice would be heterogeneously distributed within many, but not all, small craters near the North Pole.

Remote sensing has also provided useful information about hydrogen content on the lunar surface. The Lunar Exploration Neutron Detector (LEND) onboard LRO was used to determine where at the South Pole an impactor should be sent to allow measurement of the volatiles released by the impact. The Cabeus crater displayed the highest hydrogen concentration in the South Polar Region, corresponding to an estimated content of 0.5 to 4.0% water ice by weight depending on the thickness of the overlying dry regolith layer (Mitrofanov *et al.* 2010). The LRO Centaur upper stage rocket impacted within a PSR detected within Cabeus as part of the Lunar Crater Observation and Sensing Satellite (LCROSS) mission. The Shepherding Spacecraft of that mission monitored the impact site and the resulting ejecta (Schultz *et al.* 2010), revealing the presence of emission lines that could have been caused by Ag, CN, CO, CO<sub>2</sub>, H<sub>2</sub>O, Na, NH, NH<sub>2</sub> and OH. The presence of OH could be due to either the thermal dissociation of H<sub>2</sub>O or desorption off of grain surfaces. NH and NH<sub>2</sub> emission lines in LCROSS spectra are believed to come from the regolith. Na was also observed in the spectra and is interpreted as coming from near but not on the surface. Colaprete *et al.* (2010) reported a detection of  $5.6 \pm 2.9\%$  of water ice in the regolith at the LCROSS impact site, based on measurements of the ejecta. The Lyman Alpha Mapping Project (LAMP) ultraviolet spectrometer onboard LRO observed a distinctive plume generated by the LCROSS impact which contained H<sub>2</sub>, CO, Hg, Ca and Mg (Schultz *et al.*, 2010; Gladstone *et al.*, 2010).

Over the past few decades, sample measurements have revealed complementary information on the volatile content of the Moon. All sample measurements have been done on Apollo samples, which were all located in nearside equatorial regions, thus limiting the extent to which interpretation can be extended to polar regions. At those equatorial regions, volatiles such as H, N, C, and O have been found in a variety of locations in various compounds (Arnold *et al.*, 1979). Quantities of these species are not low: C, for example, is believed to have concentrations of ~17% per cubic meter, which is similar to terrestrial abundances (Haskin *et al.*, 1992). Recently, there has been a confirmed occurrence of graphite in an impact-melt breccia from Apollo 17, providing additional evidence for lunar C (Steele *et al.*, 2010). In addition, Apollo 17 and 15 samples contained orange and green glass beads, respectively, that were found to be enriched in volatile elements (*e.g.* Zn, Pb, S, F, Cl) and also covered by a thin condensed volatile coating (Meyer *et al.*, 1975).

More recently, lunar apatite has been intensively studied because it is the most common volatile-bearing mineral phase in lunar rocks. It can thus provide information about magmatic volatiles from a large variety of lunar lithologies (Boyce *et al.*, 2010; McCubbin *et al.*, 2011). Up to now, the studied apatite grains revealed a high abundance of F, a varied abundance of Cl, and suggest the presence of OH (McCubbin *et al.*, 2011). It also appears that apatites, at least from Apollo 14, are very similar to terrestrial apatites in their abundance of H, Cl and S (Boyce *et al.*, 2010).

### Significance

Understanding the volatile state and distribution of polar volatiles will also be very important in establishing a permanent base on the Moon. There may be enough H in relatively small patches of regolith to provide rocket fuel for many years, and such deposits could easily be extracted by heating (Haskin, 1992). However, it is yet unknown whether tentative volatiles at the poles exist in the regolith in the form of patches or layers, and where they may be most concentrated (Fig. 4.5). A better understanding of the size and distribution of volatile deposits would allow greater efficiency in implementing in-situ resource utilization (ISRU) techniques, thereby allowing increased returns from future lunar sorties.

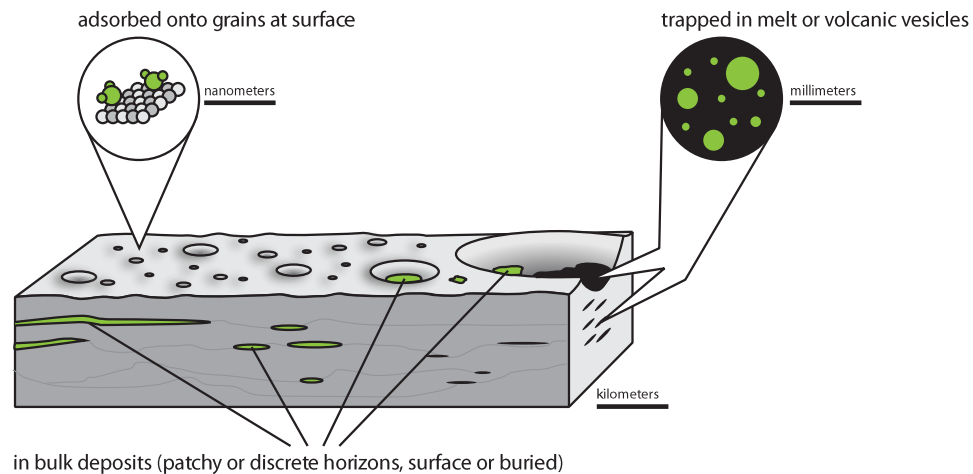


FIGURE 4.5 Schematic of possible volatile locations near the lunar surface at microscopic, hand-lens, and macroscopic scales.

### Methods

In order to find suitable landing sites that could help determine the compositional state (elemental, isotopic, mineralogic) and compositional distribution (lateral and depth) of the volatile component in lunar polar regions, we used four data layers: (1) the maximum annual temperature, (2) the distance from PSRs, (3) the slope, and (4) the hydrogen content. We conducted a classification and a post-classification analysis in ArcMap.

### Classification

We first reclassify the raster values according to scores from 1 to 4, with 1 being the most scientifically interesting and 4 being the least. We assigned each layer an equal weight and combined them with the Raster Calculator in ArcMap. Table 4.4 summarizes the science site selection criteria, scores and weights based on those layers.

The maximum annual temperature is used to assess the stability of lunar volatiles. According to Zhang and Paige (2010), most volatiles are stable below 54 K, corresponding to the sublimation point of  $\text{CO}_2$ . We then chose to assign a score of 1 for all temperatures of 0–54 K, a score of 2 to temperatures ranging between 54–70 K (chose because of the sublimation point of  $\text{C}_5\text{H}_{12}$  at 73.6 K), a score of 3 to the 70–100 K range (corresponding to the sublimation point of  $\text{H}_2\text{O}$  at 106.6 K), and a score of 4 to temperatures above 100 K.

PSRs at the lunar poles may serve as one of the most important reservoirs for volatiles. The presence of these cold surfaces adjacent to the hot surfaces of the Moon may allow cold trapping of volatile material that has been introduced to the surface. Therefore, we chose scores from highest to lowest based on distance from PSRs: 1 for locations within a PSR, 2 for locations within 1 km, 3 for locations 1–5 km away, and 4 for locations 5–10 km away. Locations farther than 10 km from a PSR have been excluded from our classification. This distance is comparable with the maximum allowed ‘walk-back’ distance for astronauts on the lunar surface.

Slopes on the lunar surface have also been used in classification. Our classification scheme was informed by current hardware design constraints; the highest score has been assigned to slopes below 25° and the lowest score to slopes steeper than 30°.

TABLE 4.4 Classification criteria for Science Goal 4a.

| Criteria                              | Score | Weight | Purpose  |
|---------------------------------------|-------|--------|--|
| <b>Maximum Annual Temperature (K)</b> |       |        |  |
| 0–54                                  | 1     | 25%    | Low volatility (CO <sub>2</sub> sublimation)                   |
| 54–70                                 | 2     |        | Medium volatility (C <sub>5</sub> H <sub>12</sub> sublimation) |
| 70–100                                | 3     |        | Medium-high volatility (H <sub>2</sub> O sublimation)          |
| >100                                  | 4     |        | Highest volatility of most volatiles                           |
| <b>Distance from PSR (m)</b>          |       |        |  |
| 0                                     | 1     | 25%    | Within PSR   |
| 0–1000                                | 2     |        | Short daily walking distance from PSR                          |
| 1000–5000                             | 3     |        | Medium daily walking distance from PSR                         |
| 5000–10000                            | 4     |        | Maximum daily walking distance from PSR                        |
| <b>Slope (°)</b>                      |       |        |  |
| 0–25                                  | 1     | 25%    | High accessibility   |
| 25–27.5                               | 2     |        | Intermediate accessibility                                     |
| 27.5–30                               | 3     |        | Intermediate to low accessibility                              |
| > 30                                  | 4     |        | Low accessibility to inaccessibility                           |
| <b>Hydrogen content (ppm)</b>         |       |        |  |
| >150                                  | 1     | 25%    | Enhanced polar hydrogen content                                |
| 100–150                               | 2     |        | Elevated polar hydrogen content                                |
| 50–100                                | 3     |        | Medium polar hydrogen content                                  |
| 0–50                                  | 4     |        | Normal equatorial hydrogen content                             |

Finally, several elemental abundances have been remotely sensed and calibrated by the Lunar Prospector Neutron Spectrometer, such as Fe, Ti, Ga, Sm and H (Lucey *et al.*, 2006). We use H as a proxy for all lunar volatiles and defined classification ranges and score values according to Feldman *et al.* (2000), who define the average equatorial hydrogen content as being approximately 50 ppm.

## **Post-Classification Analysis**

The result of the classification process is a map having pixels values ranging between 1 and 4, 1 being a perfect match of our classification criteria. To refine our results, we decided to keep values between 1 and 1.25, meaning that one of the input layers could have had a score of 2 instead of a perfect match. Areas smaller than 57,600 m<sup>2</sup> (a single pixel at our second-coarsest resolution of 240 m/pixel) were deleted. We then conducted a post-classification analysis, taking into consideration the geologic or spatial context of those areas, to single out sites that maximize potential science return.

## **Site Recommendations**

Site recommendations resulting from the above analysis are shown in Fig. 4.6.

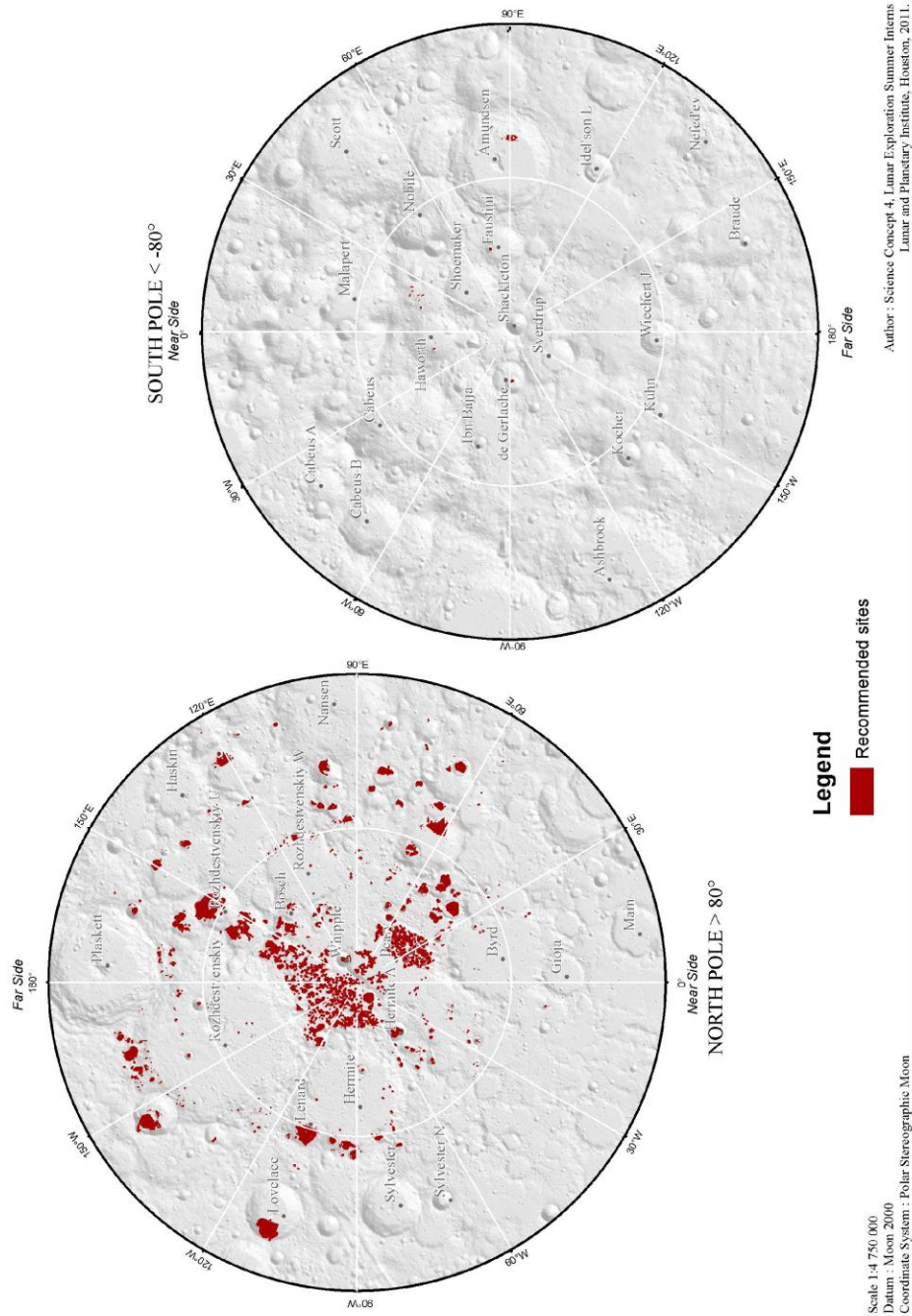
### *North Pole*

Science Goal 4a can be addressed at many more places at the North Pole than at the South Pole (Fig. 4.7). In general, the North Pole is characterized by high density of small PSRs. A high concentration of small sites can be found in the area between Hermite and Peary craters. Many smaller areas are also present on the northern wall of Hermite, Rozhdestvensky, and Rozhdestvensky W craters. Small areas cover the northern half of Peary crater floor as well as its wall. Large areas within craters could also address Science Goal 4a, such as the northern walls and floors of Rozhdestvensky U, Rozhdestvensky K, Lenard, Nansen F, and Lovelace craters. These sites are very similar to the Amundsen site at the South Pole.

### *South Pole*

Only a few South Pole sites were selected through the classification and post-classification processes (Fig. 4.8). These are mostly concentrated above 84° latitude. The largest site is found on the northeastern part of the floor of Amundsen crater. Other smaller sites are found within smaller craters in Faustini, Haworth, and de Gerlache craters. Small sites are concentrated in an elevated area between Haworth and Nobile craters. Because of its size and location, Amundsen probably represents the best crater to address Science Goal 4a at the South Pole. Sites there are within a PSR (and therefore are very cold) but are surrounded by warmer regions that are mostly illuminated. Also, Amundsen crater exhibits a central peak and walls that have slopes shallower than 25°, allowing easier exploration.

# Site Recommendations to Address Science Goal 4a



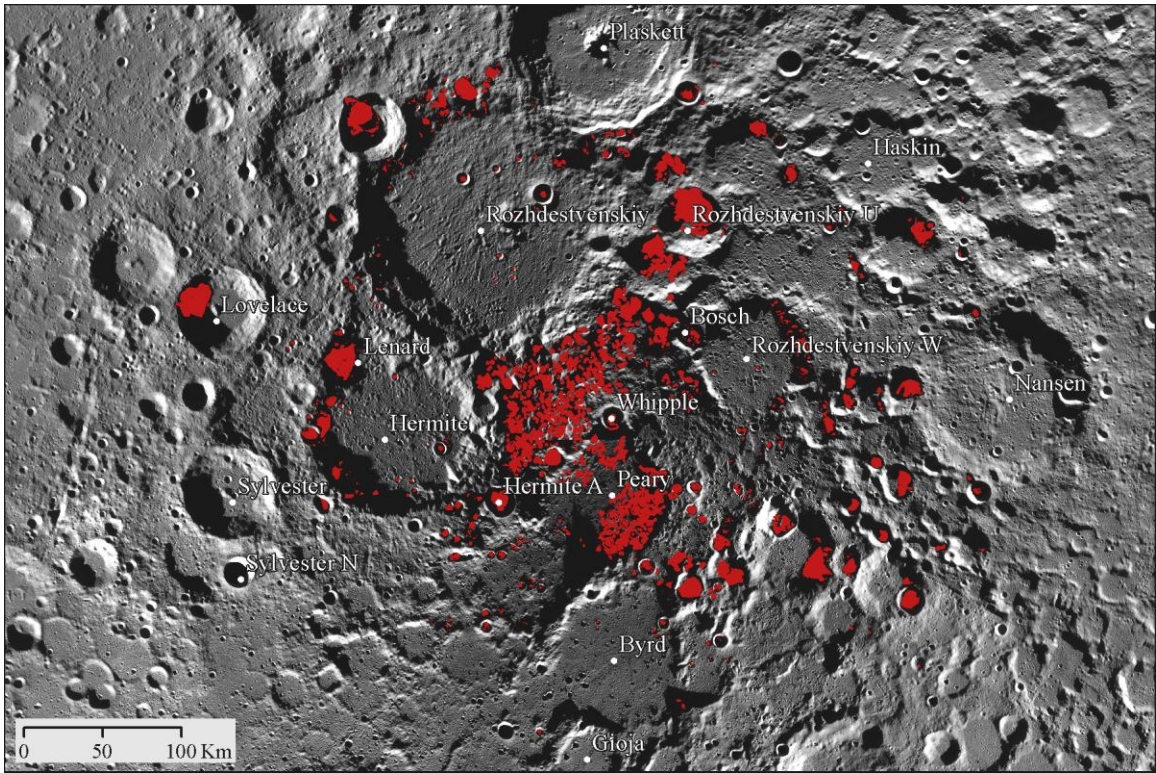


FIGURE 4.7 Enhanced view of recommended sites in the north polar region satisfying Science Goal 4a.

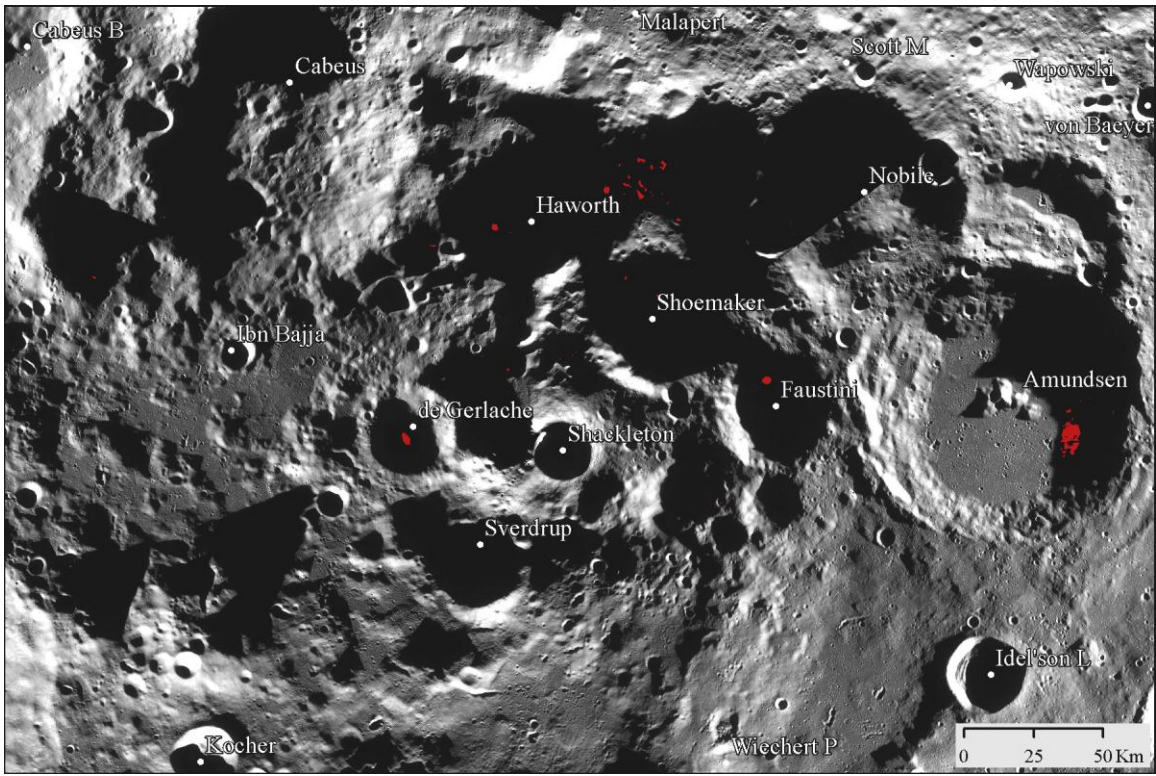


FIGURE 4.8 Enhanced view of recommended sites in the south polar region satisfying Science Goal 4a.

## SCIENCE GOAL 4B: DETERMINE THE SOURCE(S) FOR LUNAR POLAR VOLATILES

### Introduction

Volatiles can arrive on the lunar surface from five potential sources: solar wind, impacting comets and asteroids, lunar outgassing, ions from the Earth's magneto-tail, and extrasolar particles. Understanding what these sources are can provide important constraints on the volatile budget of the Moon. This in turn informs studies of volatile modification and storage processes by providing initial conditions and system inputs. The rate at which volatiles have accumulated on the lunar surface over time also has important implications for solar history (Science Goal 4e).

### Current understanding

The primary source of lunar volatiles is individual atoms coming from the solar wind (Crider and Vondrak, 2000; 2002) (Fig. 4.9). These are delivered constantly and homogeneously across the lunar surface, even in Permanently Shadowed Regions (PSRs), where they are carried in by Earth's magnetic field. The main species present from this source are H, C, O, and N (Haskin, 1992).

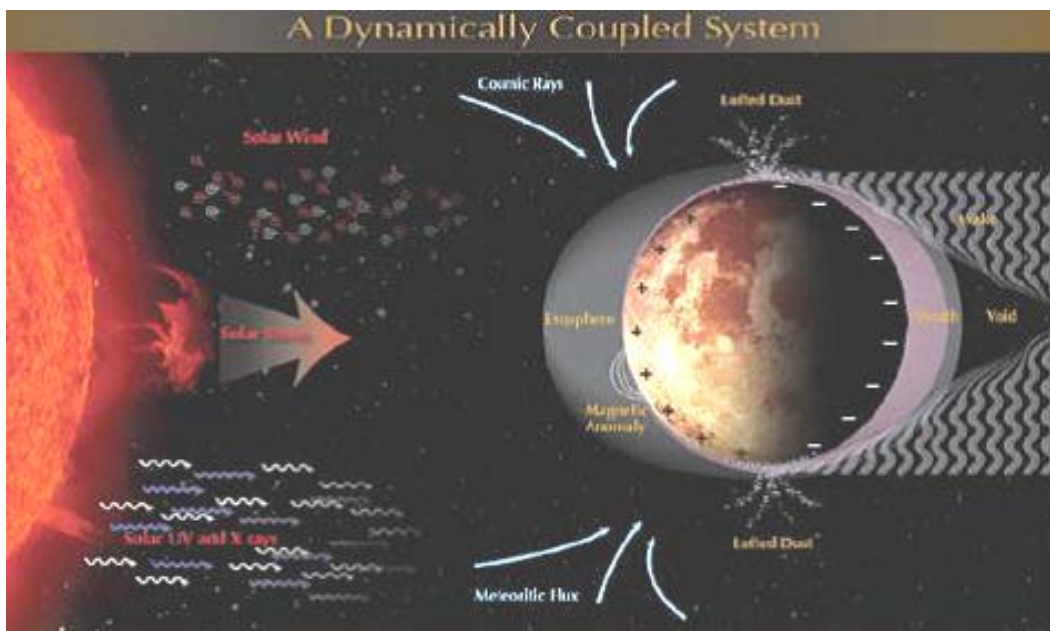


FIGURE 4.9 Schematic of solar wind processes on or near the Moon. Figure taken from Farrell *et al.* (2011)

The other main source for volatiles on the Moon is incoming material from comets or 'wet' asteroids (those with large amounts of hydrated minerals) (Watson *et al.*, 1961; Arnold, 1979; Butler, 1997). This is an episodic source, but for small impactors it can be considered to be temporally uniform. Comets have been cited as a possible source for Earth's oceans, and are thought to deliver a substantial quantity of water to the Moon as well (Lucey, 2009). Indeed, over the past 2 Gyr, some  $10^{13}$  kg of water have been delivered to the lunar surface by comets, and this flux indicates a surface density of  $\sim 0.5$  kg  $m^{-2}$  (Clark, 2009).

Apollo images revealed areas of the Moon with low numbers of craters and high albedo, which are interpreted to be young ( $\sim 10$  Myr old) and outgassing features (Schultz *et al.*, 2006). None of these features fall within our polar study area (latitudes poleward of  $80^\circ$ ), although transport processes may have relocated volatiles from outgassing sites to polar regions.

Earth is also a source of lunar volatiles – ions stripped from the upper atmosphere can become trapped at the lunar poles as the Moon passes through Earth's magnetotail (Lucey, 2009). The Moon is in the Earth's magnetosphere for six days of every orbit, or about 21% of the time. This process provides  $\sim 100$  times more proton flux than direct solar wind implantation (Starukhina, 2002). While older research

suggested that this effect would be countered by the shielding effect of Earth's magnetotail against galactic cosmic rays, more recent work shows that the magnetotail likely provides no shelter from galactic cosmic rays >10 MeV (Case *et al.*, 2010).

Extrasolar dust may also provide volatiles to the lunar surface. The Solar System passes through giant molecular clouds on timescales of tens to hundreds of Myr; when this occurs, these interstellar clouds may deposit dust or icy grains directly onto the lunar surface (Lucey, 2009).

### **Significance**

One of the most important reasons for understanding polar volatile sources is the need for a better understanding of the lunar volatile budget in these regions. Science Goal 4a focuses on the present state and distribution of volatiles, and Science Goal 4c on the processes that alter the distribution of volatiles, but an answer to the questions within Science Goal 4b would provide the initial conditions for these other goals. The volatile budget is also important in terms of understanding how transient some of these deposits may be in relation to the thermal cycling of the lunar surface.

An understanding of volatile sources on the lunar poles bears relevance for other areas of Solar System science. The main contributors to the lunar volatile budget are likely to be solar wind and micro-meteoroids, which are both prevalent throughout the Solar System, and which likely play a large role in the volatiles on other airless bodies, such as Mercury. If interstellar particles are a component, these would also be relevant for other surfaces aside from the Moon. The volatiles at the lunar poles may also give us information about particles in the Earth's magnetosphere. If these particles are implanted on the lunar surface and stored for long periods of time in cold traps, then it is possible that they record information about Earth's geomagnetic history.

Finally, polar volatiles sourced from within the Moon itself must have arrived there during lunar formation or subsequent heavy bombardment, and so could provide useful information about the process of lunar formation. Their abundances are also a useful constraint on models of lunar formation and could aid understanding in lunar origin.

### **Methods**

In order to find suitable landing sites that could help determine the source(s) for lunar polar volatiles as stated in Science Goal 4b, we used only the classified slope layer. We conducted a classification and a post-classification analysis in ArcMap 10.

### **Classification**

We first reclassified the raster values as scores from one to four, with one being the most scientifically interesting sites and four being the least. Since there was only one layer used for the classification, we assigned 100% of the weight to that layer in ArcMap. Our slope classification scheme was informed by current hardware design constraints: the highest score has been assigned to slopes below 25° and the lowest score to slopes steeper than 30°.

There are no apparent outgassing sites poleward of 80° latitude (*e.g.* Schultz *et al.*, 2006; Lawson *et al.*, 2005), though such places would have been prime locations to test the volatile content of the lunar interior. We assume that small craters and the top few centimeters of the regolith could provide useful information about volatile sources but these features are ubiquitous and are more important for mission operations than landing site consideration.

### **Site recommendations**

Results from classification (Fig. 4.10) show that Science Goal 4b is not very constraining in the selection of specific landing sites. Since the only data used in the classification analysis is the slope map, most lunar locales would satisfy this goal. Moreover, the sites excluded from the results of Science Goal 4b are the same sites excluded from other Science Goals on the basis of slope. In addressing Science Goal 4b, sampling strategy is more important than site location. Therefore, we recommend sampling bright, fresh features as well as contrasting areas around these locations. Such young features should be present everywhere on the Moon, and their detection may have to wait until landed missions identify them or until they are detected from focused comparison of Lunar Orbiter and LROC NAC images.

### Site Recommendations to Address Science Goal 4b

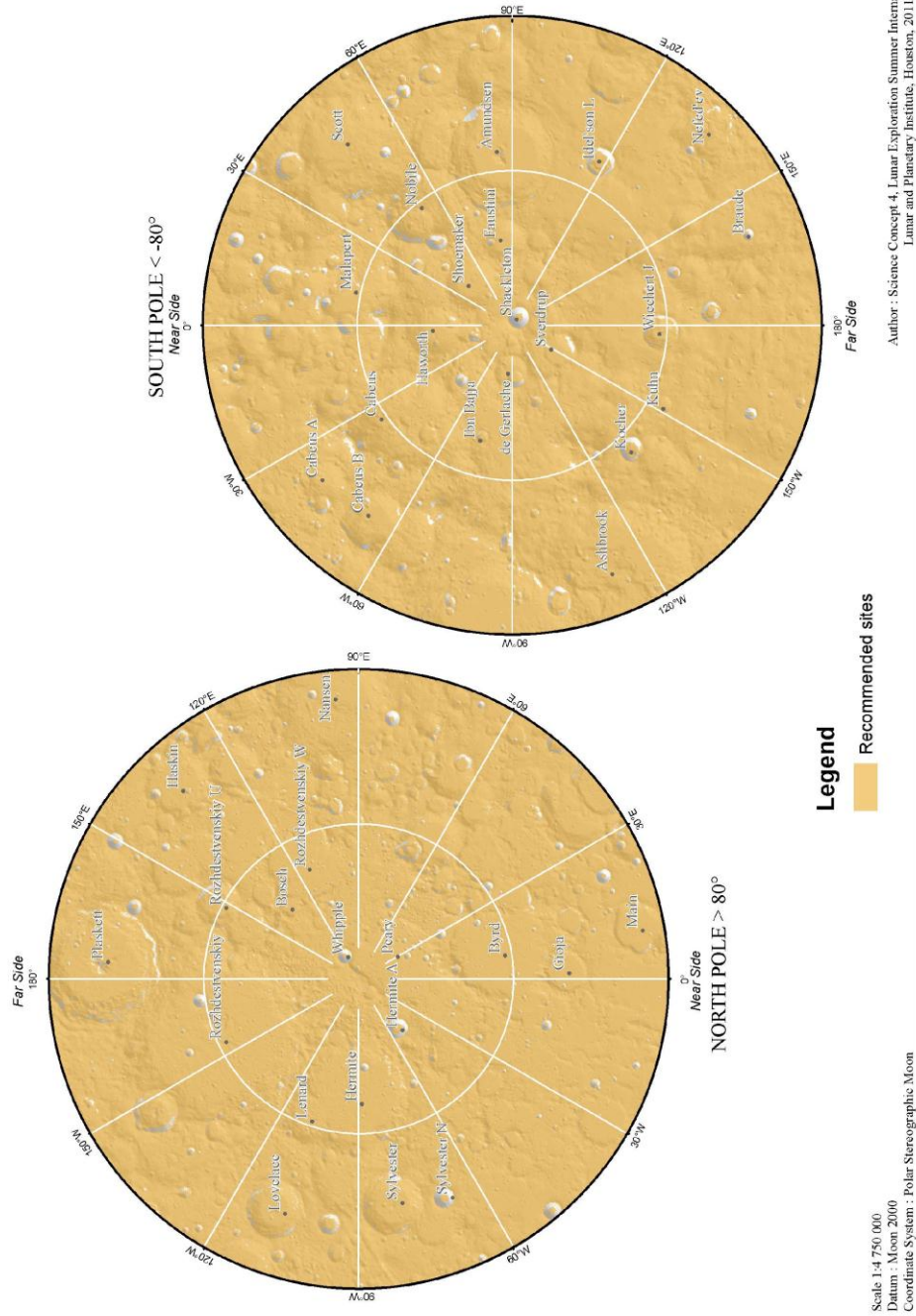


FIGURE 4.10 Site recommendations to address Science Goal 4b.

## SCIENCE GOAL 4C: UNDERSTAND THE TRANSPORT, RETENTION, ALTERATION, AND LOSS PROCESSES THAT OPERATE ON VOLATILE MATERIALS AT PERMANENTLY SHADED LUNAR REGIONS

### Introduction

Questions concerning processes that alter the state or distribution of volatiles on the lunar surface are broadly applicable to similar processes on other airless bodies (*e.g.*, the way in which these processes interact with Permanently Shadowed Regions (PSRs) is of great interest for Mercury, in particular). Study of these processes is difficult in terrestrial laboratories, and so a return to the Moon would prove invaluable for bettering our understanding of them. Finally, it is important to understand these processes fully before future missions damage the pristine lunar exosphere (NRC 2007). The processes by which volatiles are transported, retained, altered, and lost are described in the following subsections.

### Transport

The amount of volatiles in a given deposit is a function of efficiency of the various transport and loss mechanisms (Fig. 4.11). There are many ways that volatiles can move across the lunar surface, including electrostatic levitation, random ballistic walk, thermal diffusion, impact vaporization, and impact gardening.

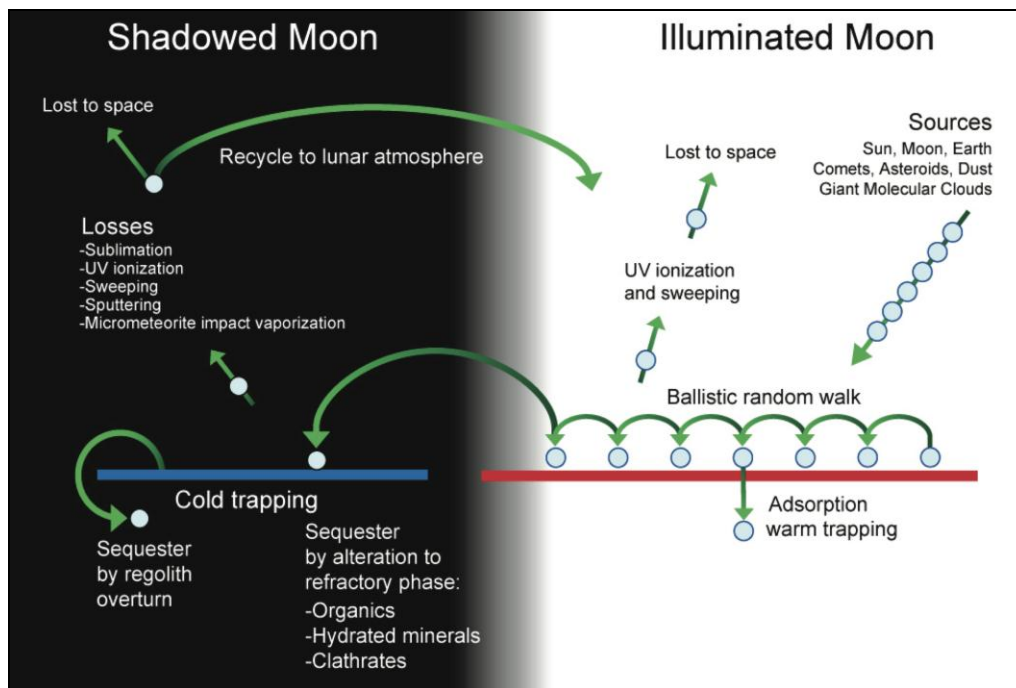


FIGURE 4.11 Schematic of various mechanisms that affect lunar volatiles (from Lucey, 2009).

#### *Electrostatic levitation*

Small ( $\sim 1 \mu\text{m}$ ) grains on the lunar surface can be caused to levitate by becoming positively charged by plasma and photoemission of electrons from solar UV and X-rays. They then fall back to the surface after a certain period of time after becoming neutralized. While levitated, grains can be transported laterally by electric fields or if the dust has an intrinsic horizontal velocity component. Transport occurs in a photoelectron sheath above the surface. Grain size controls the height of levitation:  $0.1 \mu\text{m}$  grains can be raised to 100 km above the surface, while  $5 \mu\text{m}$  grains can only reach  $\sim 10 \text{ cm}$  above the surface. This is based on the 'dynamic fountain model' for lunar dust (Stubbs *et al.*, 2006). Levitated positively charged grains will tend to move across the terminator to negatively charged regions through this process (Berg, 1978).

### *Random ballistic walk*

Hydrogen can move through the lunar exosphere by a process known as random ballistic walk (Crider and Vondrak, 2000; 2002; 2003). Incident protons from the solar wind electrically interact with the lunar surface which can neutralize them, backscattering ~1% of the incident protons and leaving ~99% implanted in the regolith. Implanted H atoms may remain in the regolith until chemically reacting with local atoms, or until they are removed via sputtering or diffusion. Particles that leave the lunar surface travel on individual ballistic paths, and those that are not lost to ionization from ultraviolet radiation or solar wind will return to the surface some distance away (see Fig. 4.11). After landing, particles thermally equilibrate with local surface materials until this process repeats itself. It should be noted that regardless of the release mechanism for the first hop, every subsequent hop is considered to be a thermal desorption with a Maxwellian distribution (Crider and Vondrak, 2002).

According to calculations by Crider and Vondrak (2000) using H abundance data from the Lunar Prospector Neutron Spectrometer (LP-NS), it would take 7 Ma for the solar wind to supply the cold traps with the observed  $4.99 \times 10^{37}$  H atoms. However, if the H is only found as part of H<sub>2</sub>O molecules, the time required for solar wind implantation is 100 Ma. Via ballistic hopping and associated loss processes the absolute minimum time to transport volatiles to the lunar poles is ~83 ka, even assuming the most favorable solar wind H concentrations and that every H atom reaches a polar cold trap. This timeframe increases to ~83 Ma with less favorable assumptions (Crider and Vondrak, 2000). These numbers are based on a constant solar wind flux, so they are not representative of any solar wind particles except for H, and do not apply to any source of lunar volatiles except for solar wind (Crider and Vondrak, 2002).

### *Thermal diffusion*

Individual atoms of volatiles, such as H, may diffuse along thermal gradients from the surface to greater depths. When surface temperatures are below ~95 K, this process becomes largely ineffective, and volatiles are more likely to remain at or near the surface (Siegler *et al.*, 2010). This is important, because some other processes (*e.g.* levitation, ballistic random walk, sputtering, and gardening) act only on particles at the surface, and so thermal diffusion may help shield volatiles from these processes.

### *Impact vaporization*

Volatiles can also be mobilized if they are vaporized during an impact event. This process can remove volatiles from cold trap areas (Crider and Vondrak, 2003), and is in fact largely insensitive to PSRs and surface temperatures. According to Monte Carlo simulations by Butler (1997), however, 85% of particles vaporized from an impact into a PSR would very quickly be re-sequestered by cold trapping.

### *Gardening*

Impact gardening is the process of moving material within the top portion of the lunar regolith by small meteorite bombardment. This results in churning of the regolith, exposing previously buried material to ultraviolet radiation and solar wind sputtering. Crider and Vondrak (2003) reported that the lunar regolith becomes gardened down to a depth of about 1.6 m in ~1 Ga. The rate at which new material is exposed can provide constraints on the effectiveness of retention of volatiles in cold traps.

### **Retention**

The primary way in which volatiles are retained on the Moon is by mineral-grain adsorption, though the adsorptive capacity of lunar regolith is 10–100 times less than that of terrestrial soil (Vondrak, 1974). This process is continually active in the top few  $\mu\text{m}$  of the regolith, where solar wind particles are bound to the surfaces of individual grains at the top of the regolith.

The saturation rates of volatiles in lunar regolith are important because they control which material is stored and which is lost in a given location. The amount of time it takes to reach saturation varies with depth: the top 1–3 mm of freshly exposed regolith become saturated in 10–100 ka, while the top 1–2 m will not be saturated for 400–900 Ma. Both of these timescales assume that overturn occurs by gardening and not by the influence of large impacts (Crider and Vondrak, 2002; Johnson and Baragiola, 1991).

Impact gardening by small meteorites serves to bury volatiles, which greatly increases the amount of time that they can be retained. The survival time of a buried volatile deposit depends on its composition,

thickness and burial depth. This effect is even more pronounced in low-temperature areas; in PSRs, buried ice deposits could be stable for billions of years (Vasavada *et al.*, 1999).

In addition to impact gardening and burial, shadowed regions halt the levitation of small particles that may be moving across the lunar surface by electrostatic levitation. Colwell *et al.* (2004) suggests that this leads to a buildup of finer-sized grains in PSRs on Eros, leading to the ‘ponds’ observed there. Such an effect may also be possible on the Moon. Finer-grained regolith has more surface area available for volatile adsorption, and so can retain more volatiles. Interestingly, this is a way that PSRs may aid retention of volatiles that is temperature-independent.

### **Alteration**

There are several key processes by which volatiles on the lunar surface are altered from their original states. For example, volatiles can be broken down by alpha particles, incorporated into clathrates or hydrated minerals, undergo organic synthesis. Alteration processes are important both because it would be helpful to know in what form you might expect to find volatiles (*e.g.* for ISRU), and because the varying states of volatiles have different physical properties (*e.g.* sublimation point).

#### *Alpha particles*

When solar wind alpha particles hit the lunar surface, they can impart their energy to H<sub>2</sub>O molecules, breaking them apart into H and OH. This can happen any time an H<sub>2</sub>O molecule is exposed to the solar wind, which happens at or above the surface (during a ballistic hop, for example) (Crider and Vondrak, 2000).

#### *Clathrate hydrates*

Clathrates are a type of compound where the molecular structure of one substance entrains the molecules of another. In a clathrate hydrate, the ‘host’ molecule is water, and the ‘guest’ molecule is a volatile substance. There has been some evidence of this kind of compound on the Moon. Apollo 11, 12, 14, 15, and 16 samples have a ubiquitous CH<sub>4</sub> (methane) component. The assumption is that these are products of interactions between solar wind and lunar regolith (Duxbury *et al.*, 2001). When the water molecules are ice, this prevents diffusion of the entrained volatiles into the near-vacuum lunar exosphere. The idea is that surficial CH<sub>4</sub> gas could get buried under water ice, diffuse into the ice and (given the right temperatures and pressures) form clathrates. These compounds would likely be stable at temperatures under around 150 K (Duxbury *et al.*, 2001).

#### *Hydrated minerals*

There has been some suggestion that hydrated minerals, particularly ilmenite, could account for a majority of the hydrogen at the lunar poles, particularly in small (<10 km) craters. At temperatures between 95 and 110 K, surface ices would move down into the regolith through thermal diffusion. This migration may then lead to the formation of hydrated minerals from reactions with dry silicates in the regolith at depth (Cocks *et al.*, 2002).

#### *Organic synthesis*

*In-situ* production of organics from indigenous inorganic material is possible because of the special combination of three conditions in cold traps: a feedstock of organic elements, an energy source for driving the chemical reactions, and high enough temperatures for reactions to occur (Lucey, 2000).

### **Loss**

Loss of volatiles from the lunar surface can happen in several ways. The dominant loss processes during volatile transport is photodissociation, or ionization and dissociation of volatiles by photons during a ballistic hop (Crider and Vondrak, 2000).

Thermally-driven sublimation is also an important mechanism for volatile loss; volatiles heated above their sublimation points escape from the lunar surface and enter the exosphere. Cold trapping can prevent this from occurring, but PSRs are not found equatorwards of 80°. Water ice buried under a 10 cm layer of regolith has loss rates from 10<sup>-6</sup>–100 kg m<sup>-2</sup> Ga<sup>-1</sup>, depending on temperature (Schorghofer and Taylor, 2007).

Exposed surface volatile deposits can also be eroded by ‘sputtering’, the displacement implanted H atoms when cosmic rays or charged particles from the solar wind penetrate into the regolith (Crider and Vondrak, 2003; Starukhina, 2002). For exposed H<sub>2</sub>O ice, the loss rate by sputtering is 10<sup>3</sup> kg m<sup>-2</sup> Ga<sup>-1</sup> when the temperature is between 70–120 K (Schorhofer and Taylor, 2007).

### Significance

Understanding the way in which volatiles move around and off of the lunar surface is a vital part of understanding where they can be found. Volatile transport is a process that involves many different sub-mechanisms, including temperature-dependent grain-volatile interactions which have not or can not be studied in terrestrial laboratories. Thus, the Moon is an ideal natural laboratory for examining these processes. Also, transport, retention, alteration, and loss of volatiles likely occurs via similar mechanisms on all airless bodies. Finally, studying movement of volatiles into and out of the lunar exosphere must occur before future human and robotic missions further alter the pristine lunar polar environment.

### Methods

In order to find suitable landing sites to help understand the transport, retention, alteration, and loss processes that operate on volatile materials at permanently shaded lunar regions, we used four data layers: (1) the maximum annual temperature, (2) the distance from PSRs, (3) the slope and (4) the hydrogen content. We conducted a classification and a post-classification analysis in ArcMap.

### Classification

We first classify the raster values according to scores from 1 to 4, 1 being the most valuable and 4 being the least. We assigned each layer an equal weight and combined them with the Raster Calculator in ArcMap. Table 4.5 summarizes the science site selection criteria, scores and weights based on those layers.

The main difference between the classification for Science Goal 4c and that for other Science Goals is that here we used two different maximum annual temperature ranges: under 54 K, to look at retention, and from 90–130 K to look at transport (specifically thermal diffusion). The 54 K limit was common to several other goals, and represents a temperature just below the sublimation point of CO<sub>2</sub>. Downward diffusion of water ice does not occur below ~90 K, and is most efficient at 110–130 K (Schorhofer and Taylor, 2007).

PSRs, slope and hydrogen content have also been used in the classification process. Their classification criteria and weights are the same as for science goal 4a.

TABLE 4.5 Classification criteria for Science Goal 4c.

| Criteria                              | Score | Weight | Purpose                                 |
|---------------------------------------|-------|--------|---|
| <b>Maximum Annual Temperature (K)</b> |       |        |   |
| 0-130                                 | 1     | 25%    | Allows downward migration of volatiles  |
| >130                                  | 4     |        | Does not allow downward migration       |
| <b>Distance from PSR (m)</b>          |       |        |   |
| 0                                     | 1     | 25%    | Within PSR                              |
| 0-1000                                | 2     |        | Short daily walking distance from PSR   |
| 1000-5000                             | 3     |        | Medium daily walking distance from PSR  |
| 5000-10000                            | 4     |        | Maximum daily walking distance from PSR |
| <b>Slope (°)</b>                      |       |        |   |
| 0–25                                  | 1     | 25%    | High accessibility                      |
| 25–27.5                               | 2     |        | Intermediate accessibility              |
| 27.5–30                               | 3     |        | Intermediate to low accessibility       |
| > 30                                  | 4     |        | Low accessibility to inaccessibility    |

| <b>Hydrogen content (ppm)</b> |   |     |                           |
|-------------------------------|---|-----|---------------------------|
| >150                          | 1 | 25% | Enhanced hydrogen content |
| 100–150                       | 2 |     | Elevated hydrogen content |
| 50–100                        | 3 |     | Medium hydrogen content   |
| 0–50                          | 4 |     | Normal hydrogen content   |

### **Post-Classification Analysis**

The result of the classification process is a map of locations at the lunar polar regions with elevated hydrogen concentrations, temperatures <130 K, low slopes, and minimal distances to PSRs. The polygons shown on this map match the above criteria, but their geologic or spatial context is not taken into account. The purpose of post-classification, then, is to generate such a map in order to single out sites that maximize potential science return.

We generated two different sets of post-classified polygons, one calling out temperatures below 54 K and one with temperatures in the 90–130 K range. The lower temperatures indicate areas with the best potential for volatile storage, while the higher-temperature regions are important for studying the process of thermal diffusion of volatiles into the regolith. For each of these two maps, polygons were kept that matched its respective temperature range. This was done visually by overlaying a classified maximum annual temperature map over the set of all polygons for 4c and looking for polygons that contained areas of the given temperature.

The set of polygons containing areas with maximum temperatures of 90–130 K closely matched the original set of classified polygons. This is because the classification process called for temperatures under 130 K, and the upper end of this range was more common than the lower end. Polygons with maximum temperatures under 54 K were rarer, but it is important to note that a transect from any of these polygons to a well-illuminated area will cross isotherms with temperatures of 90–130 K. Because of this, when we incorporated our post-classification results for Science Goal 4c into the final results for Concept 4 as a whole, we use the set of polygons from this lower temperature range. Figure 4.12 shows the results of this process, with the upper and lower temperature ranges appearing in different shades of green.

### **Site recommendations**

There are a large number of sites to address Science Goal 4c at either pole. At the North Pole, areas from both of the temperature regimes in our result ( $T < 54$  K and  $90$  K  $< T < 130$  K) are small and patchy. Away from the pole, regions of 90–130 K become more continuous in distribution, because of larger-scale cratered terrain. Regions also exist with sites in both temperature ranges. In these locations, it would be possible to sample across isotherms, gaining information about regolith at different temperatures, and thus, volatiles that are undergoing different processes.

#### *North polar region*

In the colder temperature regime (maximum annual temperatures  $< 54$  K), our result is generally characterized by small locations, particularly in the Intercrater Polar Highlands (IPH) between Hermite, Peary, and Rozhdestvenskiy craters. Sites also exist on the bases and walls of large craters, such as in Hermite, Peary, and Lenard craters.

For the warmer (90–130 K) temperature range, a similar pattern exists, but with more sites present (Fig. 4.13). Larger areas exist in the floors and walls of moderately-sized craters such as Lovelace, Rozhdestvenskiy U, and Nansen F and A. Rozhdestvenskiy U is notable also for its high hydrogen abundances and the large area matching Science Goal 4c selection criteria.

#### *South polar region*

For the colder temperatures considered, there are few sites, mostly in the floors of Haworth, Shoemaker, Faustini, de Gerlache, and Amundsen craters (Fig. 4.14). These areas are fairly extensive (tens of kilometers across). There are also a few locations between Shackleton and Haworth, and to the northwest of Shoemaker crater.

Sites in the warmer temperature range include Shackleton, Sverdrup, Nobile, Cabeus and Cabeus B, Wiechert, and Idel'son L. Amundsen also shows areas in this temperature regime.

### Site Recommendations to Address Science Goal 4c

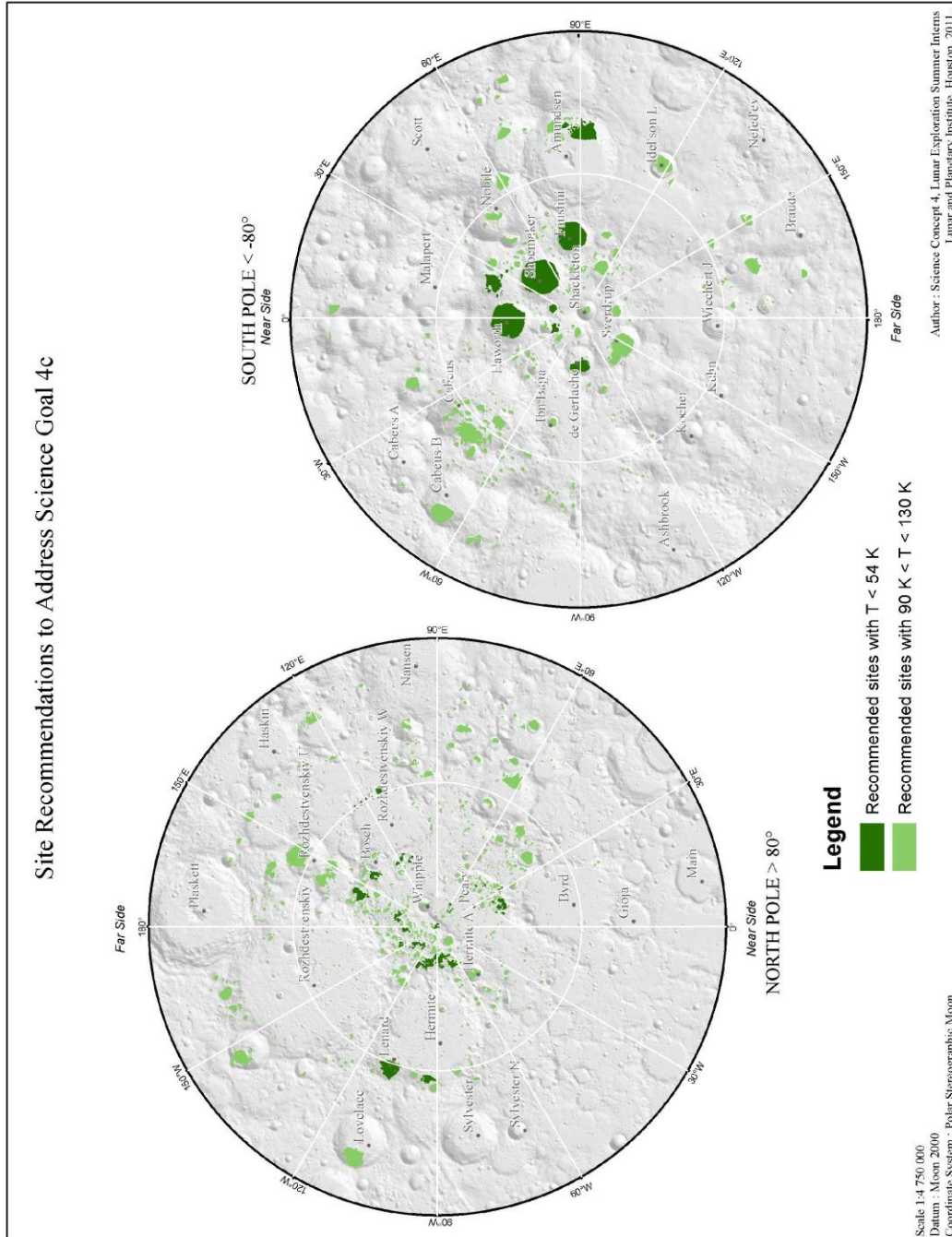


FIGURE 4.12 Site recommendations to address Science Goal 4c.

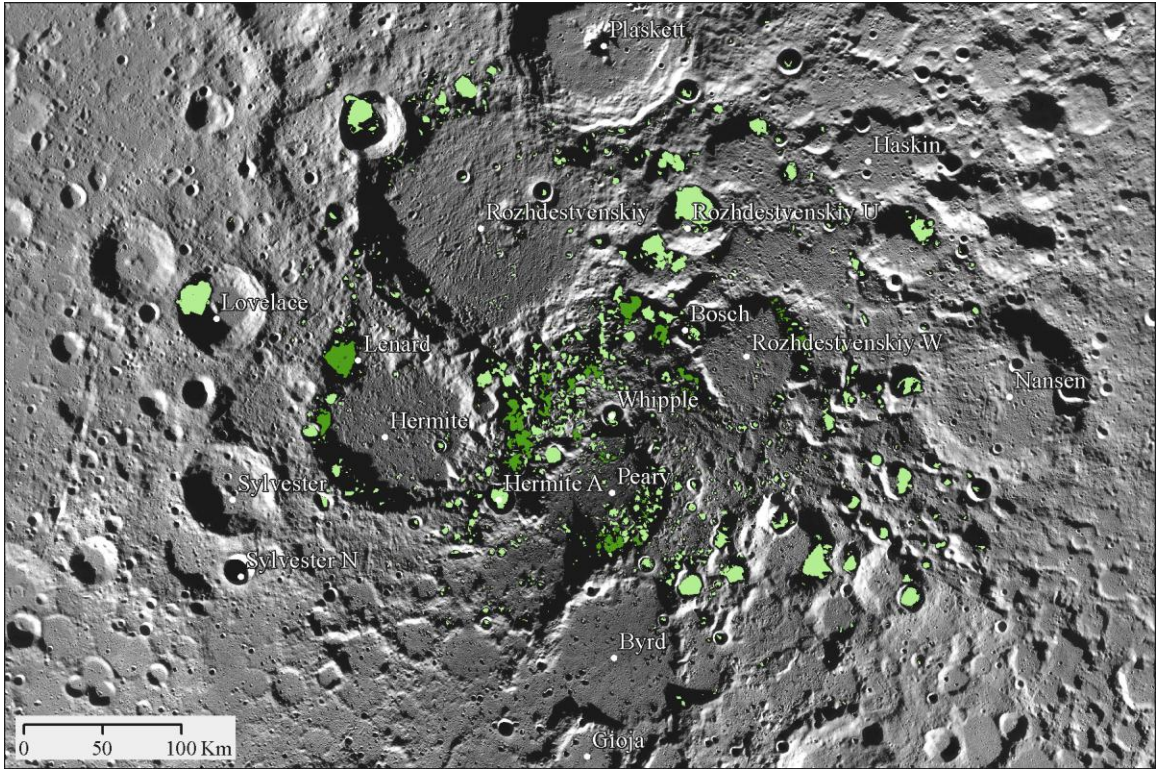


FIGURE 4.13 Enhanced view of recommended sites in the north polar region satisfying Science Goal 4c.

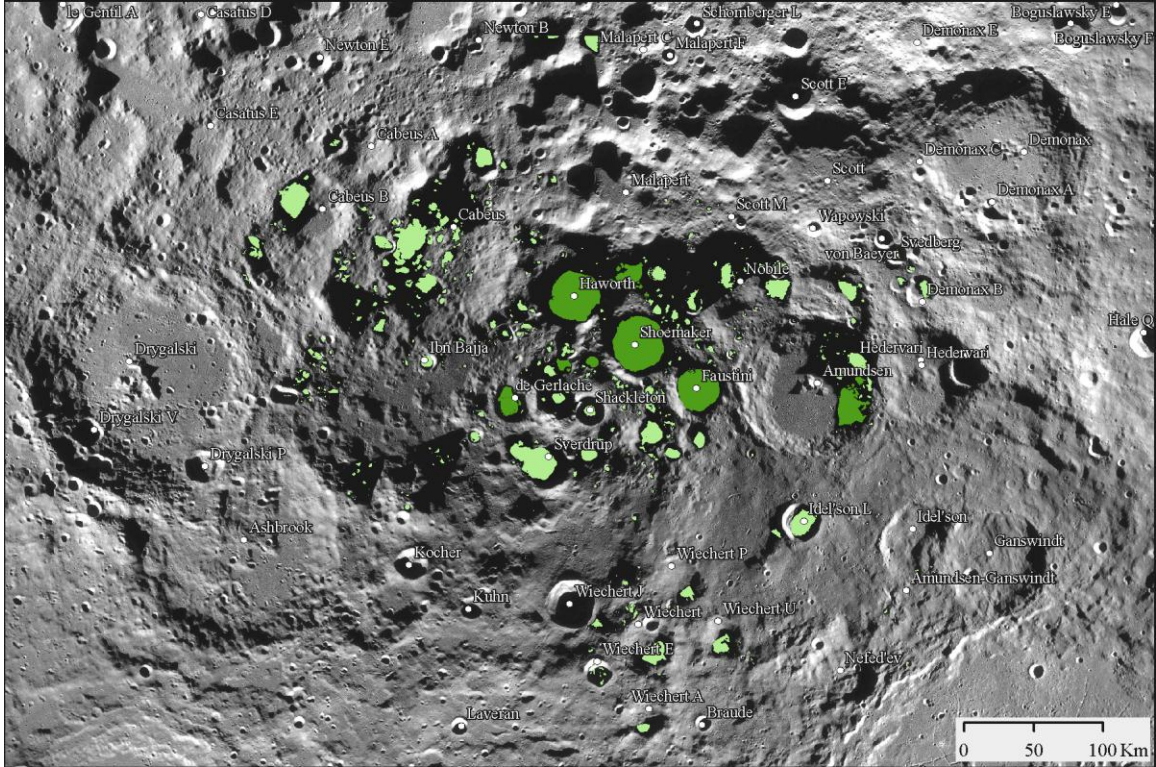


FIGURE 4.14 Enhanced view of recommended sites in the south polar region satisfying Science Goal 4c.

## SCIENCE GOAL 4D: UNDERSTAND THE PHYSICAL PROPERTIES OF THE EXTREMELY COLD (AND POSSIBLY VOLATILE RICH) POLAR REGOLITH

### Introduction

All existing surface samples of the Moon come either from equatorial Apollo missions or from lunar meteorites of unknown provenance. Because of this, the physical properties of the regolith at the equator are comparatively well understood; the analysis of returned samples and drill cores provides information about mineralogical and chemical properties of lunar regolith from the equator (McKay *et al.*, 1991). Properties of lunar regolith are summarized in Table 4.6. The *in situ* bulk density is approximately 1.30 g/cm<sup>3</sup> at the surface and the *in situ* porosity ranged around 44–52%, although these values have been found to vary between localities (Carrier *et al.*, 1991). The concentration of hydrogen in regolith up to a depth of 2 m is ~50 µg/g (Haskin, 1992). Generally the volatile content at the poles varies within the range of ~0.1 to 1.8kg per 0.1 kg/m<sup>3</sup> of H, and ~1 to 20 g per 0.1kg/m<sup>3</sup> of H (noble gases) (Haskin, 1992).

TABLE 4.6 Example properties of lunar regolith. Beach sand is provided as a familiar substance for comparison. Data from \*Carrier *et al.*, 2005; †Carrier *et al.*, 1991; ‡Haskin *et al.*, 1992

| Parameter          | Lunar regolith: surface | Lunar regolith: 50 cm depth | Typical beach sand | Units |
|--------------------|-------------------------|-----------------------------|--------------------|-------|
| Particle size      | 0.002–2.000 *           | 0.002–2.000 *               | 0.063–2.000        | mm    |
| Bulk density       | 1.50 †                  | 1.74 †                      | 2.65               | g/cm3 |
| Porosity           | 52 †                    | 44 †                        | 40                 | %     |
| Concentration of H | 50 ‡                    | 50 ‡                        | Varies             | µg/g  |
| Particle shapes    | Spherical to angular‡   | Spherical to angular‡       | Rounded, spherical | -     |

At the polar regions, extremely low temperatures (50–70 K) (Vasavada *et al.*, 1999) can have a drastic effect on regolith properties such as bulk density and conductivity (Carrier *et al.*, 1991). Not only are surface temperatures lower at the poles, but subsurface temperature profiles are likely also different due to the temperature of the surrounding material. Figure 4.15 shows some important temperatures for volatiles on the lunar surface.

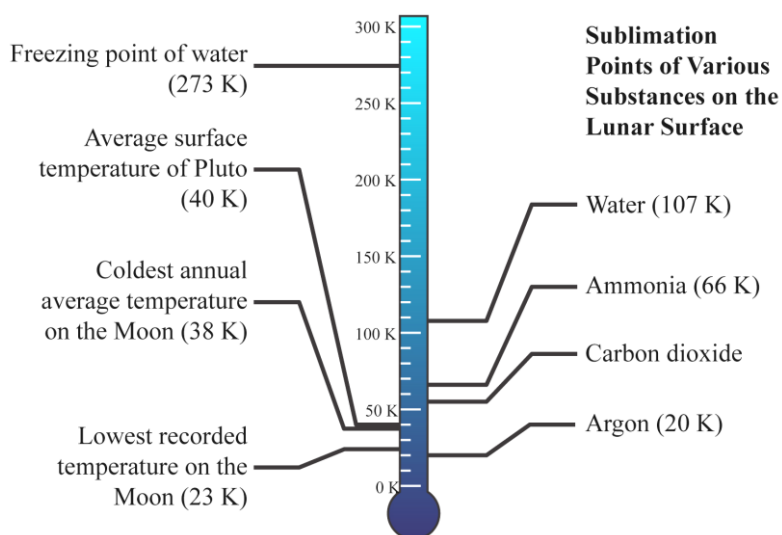


FIGURE 4.15 Diagram showing some important temperatures for Science Goal 4d, on the right, with other temperatures provided for context on the left.

In addition to direct thermal effects on the regolith, the cold temperatures at the lunar poles can indirectly affect regolith by allowing the presence of water and other volatiles. The presence of water, specifically, can encourage formation of agglutinates, small lunar soil particles (mineral grains and glasses) bonded together by impact glasses (McKay *et al.*, 1991, p. 296). An abundance of these extremely porous particles will increase the overall porosity of a sample of regolith containing them. Agglutinates already comprise at least half of the volume of a mature regolith (McKay *et al.*, 1991), and so their effect on bulk regolith properties is nontrivial. It is also possible that the extremely cold temperatures at the lunar poles may inhibit glass formation, leading to fewer agglutinates and therefore lower bulk porosity.

Space weathering can also play a role in determining the physical properties of polar regolith. Generally, the regolith may be much finer grained at the lunar poles as a result of the late heavy bombardment and a lack of subsequent large-scale volcanism (Hartmann, 2003). Finer-grained material at the lunar poles would not only affect regolith permeability, but would also provide more grain surface area for bonding of volatiles.

### Significance

The primary importance of understanding the physical properties of the lunar polar regolith is that the state of these surface materials may determine the ease or difficulty of volatile extraction from the regolith (NRC, 2007). Such deposits, as explained throughout this report, would greatly facilitate future human presence on the lunar surface, and could also provide support for human or robotic exploration by providing a local fuel source. Lunar surface activity related to extraction of these volatiles also requires a detailed understanding of the physical conditions of the polar regolith to ensure safe operations. In addition, volatile-rich polar PSRs would provide a useful analog to other airless bodies such as asteroids or Mercury.

Direct measurement of polar regolith in permanently shadowed regions (PSRs) may be the only way of characterizing these materials. Sample return at such low temperatures would be difficult, and the same samples raised to higher temperatures likely would not have the same physical properties. Therefore, a return to the moon for in-situ measurements is the only viable way to address Science Goal 4d.

### Methods

In order to find suitable landing sites that could help understand the physical properties of the extremely cold (and possibly volatile rich) polar regolith we used three data layers: (1) the maximum annual temperature, (2) the slope and (3) the hydrogen content. We conducted a classification and a post-classification analysis in ArcMap.

### Classification

We first classify the raster values according to scores from 1 to 4, 1 being the most valuable and 4 being the least. We assigned a higher weight to the maximum annual temperature due to the focus on the extremely cold regions. We assigned the slope and the hydrogen content equally lower weights. The three layers were then combined with the Raster Calculator in ArcMap. Table 4.7 summarizes the science site selection criteria, scores and weights based on those layers. Classification of the three layers and score values are the same as for Science Goal 4a.

TABLE 4.7 Classification criteria for Science Goal 4d.

| Criteria                              | Score | Weight | Purpose   |
|---------------------------------------|-------|--------|---|
| <b>Maximum Annual Temperature (K)</b> |       |        |   |
| 0–54                                  | 1     | 40%    | Low volatility (CO <sub>2</sub> volatility)                   |
| 54–70                                 | 2     |        | Medium volatility (C <sub>5</sub> H <sub>12</sub> volatility) |
| 70–100                                | 3     |        | Medium-high volatility (H <sub>2</sub> O volatility)          |
| >100                                  | 4     |        | High volatility of most volatiles                             |

| <b>Slope (°)</b>              |   |     |                                      |
|-------------------------------|---|-----|--------------------------------------|
| 0–25                          | 1 |     | High accessibility                   |
| 25–27.5                       | 2 | 30% | Intermediate accessibility           |
| 27.5–30                       | 3 |     | Intermediate to low accessibility    |
| >30                           | 4 |     | Low accessibility to inaccessibility |
| <b>Hydrogen content (ppm)</b> |   |     |                                      |
| >150                          | 1 |     | Enhanced hydrogen content            |
| 100–150                       | 2 | 30% | Elevated hydrogen content            |
| 50–100                        | 3 |     | Medium hydrogen content              |
| 0–50                          | 4 |     | Normal hydrogen content              |

### Post-Classification Analysis

The result of the classification process is a map of locations at the lunar poles with elevated hydrogen concentrations, very low temperatures, and low slopes (unlike Science Goals 4a, 4c, and 4e, PSRs were not part of this classification). The areas shown on this map match the above criteria, but their geologic or spatial context is not taken into account. The purpose of post-classification, then, is to generate such a map in order to single out sites that maximize potential science return.

We manually removed every polygon that was not either in a region of low maximum annual temperature (<105 K) or of high CPR; we assessed these regional criteria visually using the appropriate data layers. The final results for this process are shown in Fig. 4.16.

### Site recommendations

As the focus of Science Goal 4d is the study of physical properties of extremely cold regolith, the highest-priority landing sites had a maximum annual temperature  $\leq 54$  K (usually within PSRs).

#### *North polar region*

Our results show that a relatively small number of sites in the north polar region satisfy the constraints of Science Goal 4d, most of which fall north of the  $85^\circ$  latitude line (Fig. 4.17). The best and most extensive regions are found in Lenard and Rozhdestvenskiy W craters ( $D = 47$  km and  $D = 90$  km, respectively). Other sizeable areas can be found near the south wall of Hermite crater, and on the floor of Peary crater. There are also a number of small areas located in the Intercrater Polar Highlands (IPH), bounded by Bosch, Rozhdestvenskiy, Hermite, and Peary craters.

#### *South Polar Region*

For the south polar region, the distribution of possible landing sites is very similar to Science Goal 4a (Fig. 4.18). A small concentration of regions are observable mostly on the floors of medium-to-large craters close the poles. These include Amundsen, Faustini, Haworth, and de Gerlache craters, as well as the plains west of Shoemaker.

### Discussion

The results from the North and South Poles of the Moon were quite similar; neither pole contained many sites that satisfied Science Goal 4d. Note however that the site recommendations shown in Fig. 4.16 were selected for extreme cold to maximize science returns. Sampling regolith in different geologic units and from different morphologies is important for contrast with the results for regolith from the coldest areas.

### Site Recommendations to Address Science Goal 4d

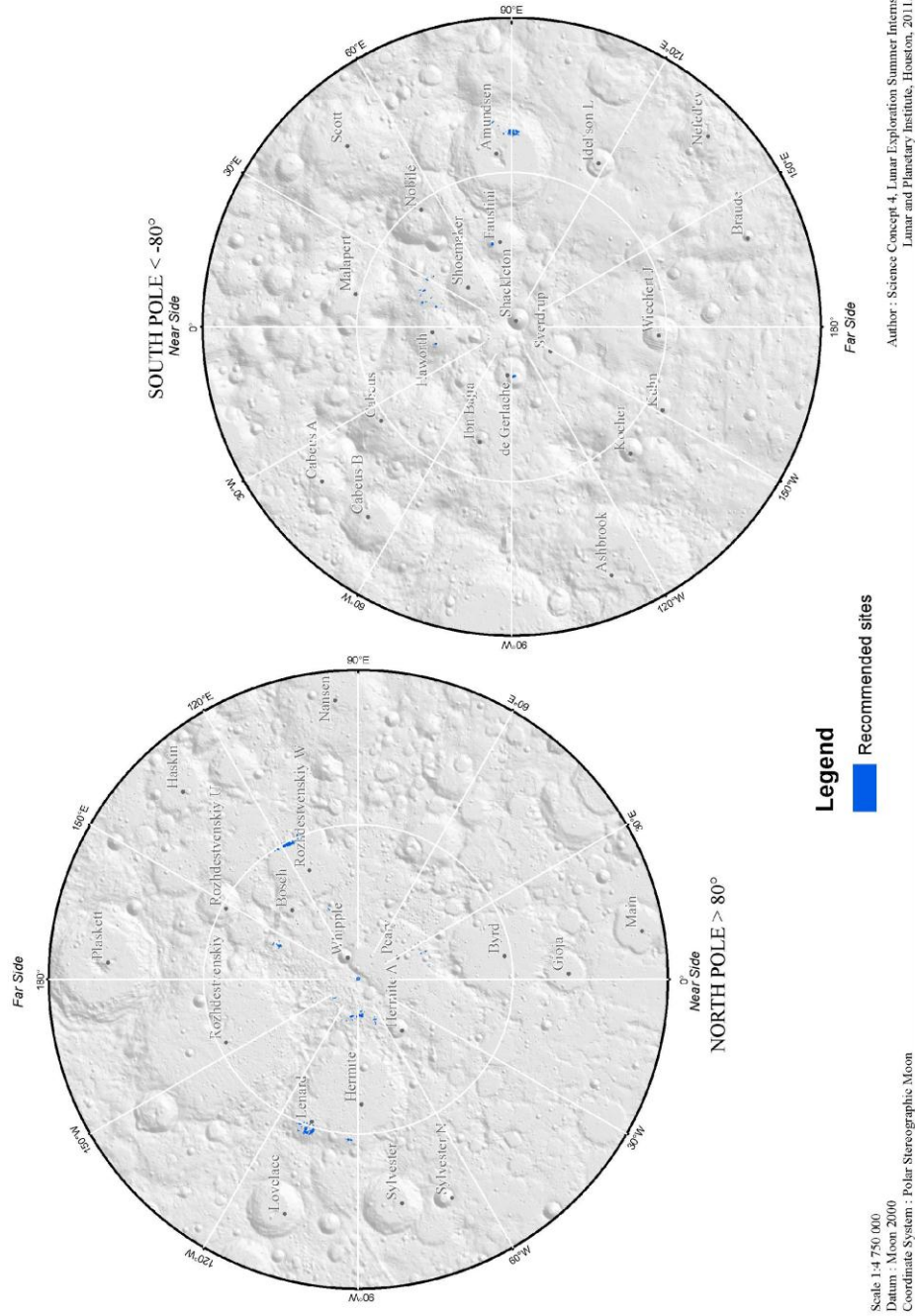


FIGURE 4.16 Site recommendations to address Science Goal 4d.

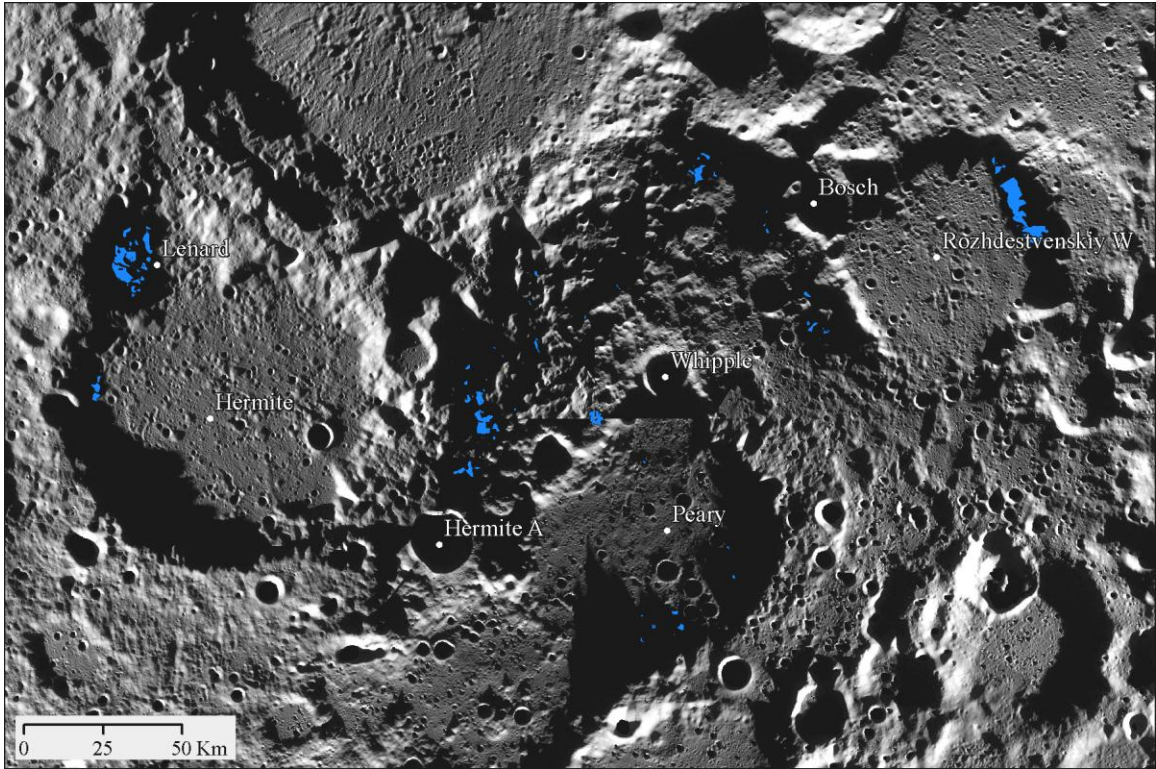


FIGURE 4.17 Enhanced view of recommended sites in the north polar region satisfying Science Goal 4d.

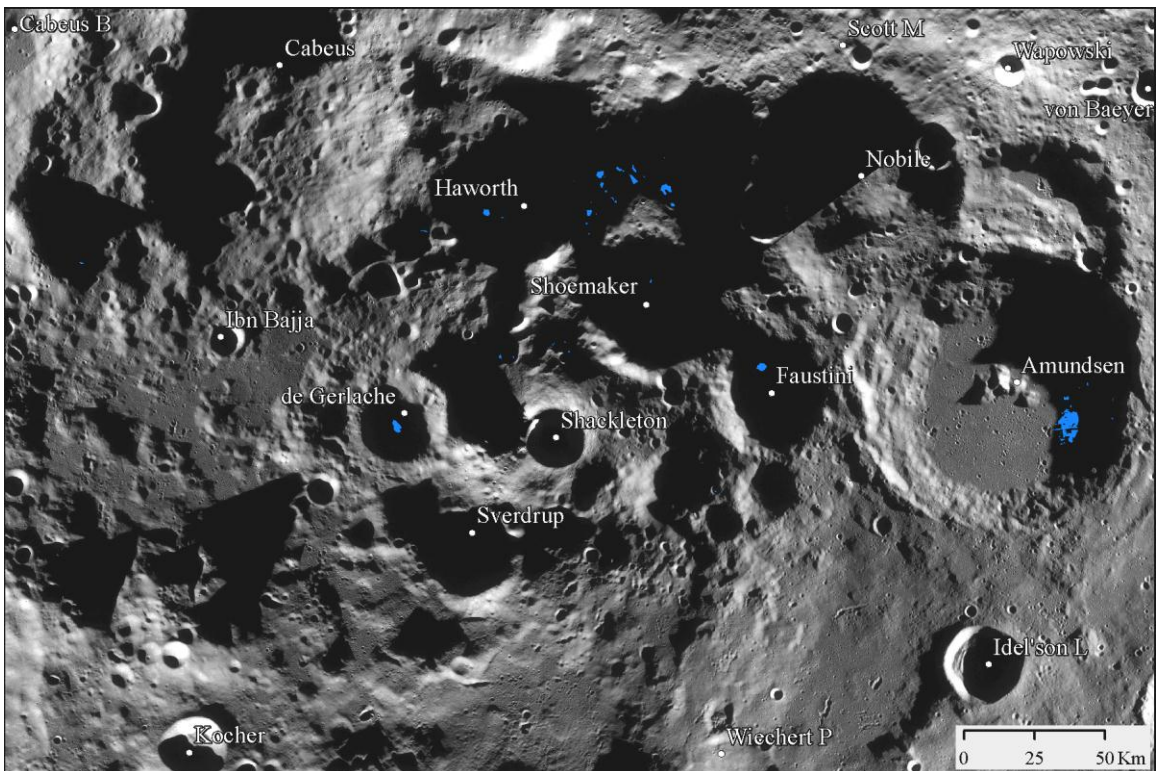


FIGURE 4.18 Enhanced view of recommended sites in the south polar region satisfying Science Goal 4d.

## **SCIENCE GOAL 4E: DETERMINE WHAT THE COLD POLAR REGOLITH REVEALS ABOUT THE ANCIENT SOLAR ENVIRONMENT**

### **Introduction**

The extremely cold temperatures at the lunar polar regions, particularly in PSRs, may have allowed the preservation of a longer record of solar activity than is present in samples from equatorial regions that have been heated and cooled on a diurnal cycle. When lunar regolith is heated, it releases volatile elements as gases, notably particles that had been implanted in that regolith by the solar wind. In deeper regolith, these particles may be quite old, meaning that they were implanted at a different time in our Sun's evolution. Thermal outgassing from equatorial soils shows a nitrogen signature (N), for example, that does not appear to match solar composition models, but because of the high temperatures in these areas, it is unclear whether that signature is due to a real anomaly in solar composition or to post-implantation diffusion or fractionation processes. A study of regolith in polar PSRs may help resolve this issue, as it has not been extensively heated, and so is unlikely to have suffered similar post-implantation modification (NRC, 2007).

Solar wind particles implanted in polar regolith and preserved in PSRs would help fill an important temporal gap in our knowledge of the Sun. Through time, lunar obliquity has varied up to 77° (Siegler *et al.*, 2011), though the Moon's obliquity has been relatively constant over the past 2 Ga (Siegler *et al.*, 2011a; 2011b, Ward *et al.*, 1975, Arnold *et al.*, 1979). It follows that modern-day PSRs have likely been shadowed for roughly the past 2 Ga, with the oldest PSRs being those closest to the poles. Thus, the epoch of solar history measureable at the lunar polar regions extends from the present back to around 2 Ga. According to Lal *et al.* (1991) meteorite and lunar records can reveal solar history for the first 0.5 Ga of solar system history and the last <10 Ma, but times between these are not readily interpretable. Recent (<10 Ma) energetic solar particles do not show any marked variation from present-day particles. Core tube samples of regolith have an antiquity (time since they acquired their characteristic SW signature) of ~3 Ga (Kerridge *et al.*, 1979) and this raises the possibility that future deep regolith cores could reveal soils with similar antiquities. If such data can successfully be interpreted, they may place constraints on and context for the claims of (1) (Newkirk *et al.*, 1979) that the SW flux was ~2 times its current rate 3.5 Ga ago; and of (2) (Eugster *et al.*, 1983) that impact-exhumed Apollo 17 soils (74001 & 73261) likely contain trapped noble gases from 3.6 and 2.5 Ga, respectively.

### **Significance**

Understanding solar history greatly aids our understanding of past climates on Earth. Knowing the solar output over terrestrial history would, for example, help place constraints on past climate variability on Earth. Another promising avenue for study is the possibility of noble gas 'snow' in PSRs or other cold polar regions. The coldest temperatures measured on the Moon are below 23 K (Paige *et al.*, 2011), which puts them in the same temperature range as the stability of xenon (Xe), krypton (Kr), and argon (Ar) (Zhang *et al.*, 2010). This means that there is a possibility that noble gases could be frozen out of the lunar exosphere in these places and possibly sequestered in the regolith, at least for short periods of time. Because the lowest average temperatures on the Moon are around 38 K (Paige *et al.*, 2011), long-term solid-state storage of noble gases seems unlikely, but periodic 'trap-and-release' cycles may be more common. This provides an interesting analog for periodic comets, which may undergo similar temperature fluctuations as they change distance from the Sun.

### **Methods**

In order to find suitable landing sites that could help determining what the cold polar regolith reveals about the ancient solar environment we used three data layers: (1) the minimum annual temperature, (2) the distance from PSRs and (3) the slope. We conducted a classification and a post-classification analysis in ArcMap.

### **Classification**

We first classify the raster values according to scores from 1 to 4, 1 being the most valuable and 4 being the less. We assigned the three layers weights of 33%, 34%, and 33%, respectively. We then combined the layers with the Raster Calculator in ArcMap. In the classification of Science Goal 4e, we decided to use the minimum annual temperature instead of the maximum annual temperature that has been used in the

classification for all other science goals up to now. The reason for that is to look at sites that have the potential for ‘trap-and-release’ of noble gases, particularly xenon (Xe), krypton (Kr), and argon (Ar).

### **Post-Classification Analysis**

The result of the classification process is a map having pixels values ranging between 1 and 4, 1 being a perfect match of our classification criteria. To refine our results, we decided to keep values between 1 and 1.33, meaning that one of the input layer could have had a score of 2 instead of a perfect match. Keeping only the perfectly matched areas resulted in so few sites that we decided to relax our constraints. We then conducted a post-classification analysis to take into consideration the geologic or spatial context of those areas. The purpose of the post-classification analysis is to generate such a map in order to single out sites that maximize potential science return.

We manually removed every area that was not either in a region of low minimum temperature (<54 K), high CPR, or elevated hydrogen levels (> 100 ppm); we assessed these regional criteria visually using their respective data layers. The final results are shown in Fig. 4.19.

### **Site recommendations**

Science Goal 4e can be addressed in most extremely cold regions (<54 K). The map of recommended sites required that areas be PSRs and have the coldest minimum annual temperatures, though we included cold non-PSR regions in order to observe diurnal effects on SW content, especially regarding noble gas gain and loss.

#### *North polar region*

Figure 4.20 shows a close-up view of the recommended landing sites to address Science Goal 4e at the north polar region. The recommended sites are found on the wall and floor of large craters, having a diameter larger than 50 km, such as Rozhdestvenskiy W, Lovelace, Hermite, Nansen F, and Plaskett V. They are also found on smaller craters such as Rozhdestvenskiy K, Lenard, Houssay, Hinshelwood, and Whipple, as well as in smaller craters on the floor of large craters like Rozhdestvenskiy, Hermite, Peary, Rozhdestvenskiy W, Florey, and Byrd. The Intercrater Polar Highlands also contain many small interesting sites.

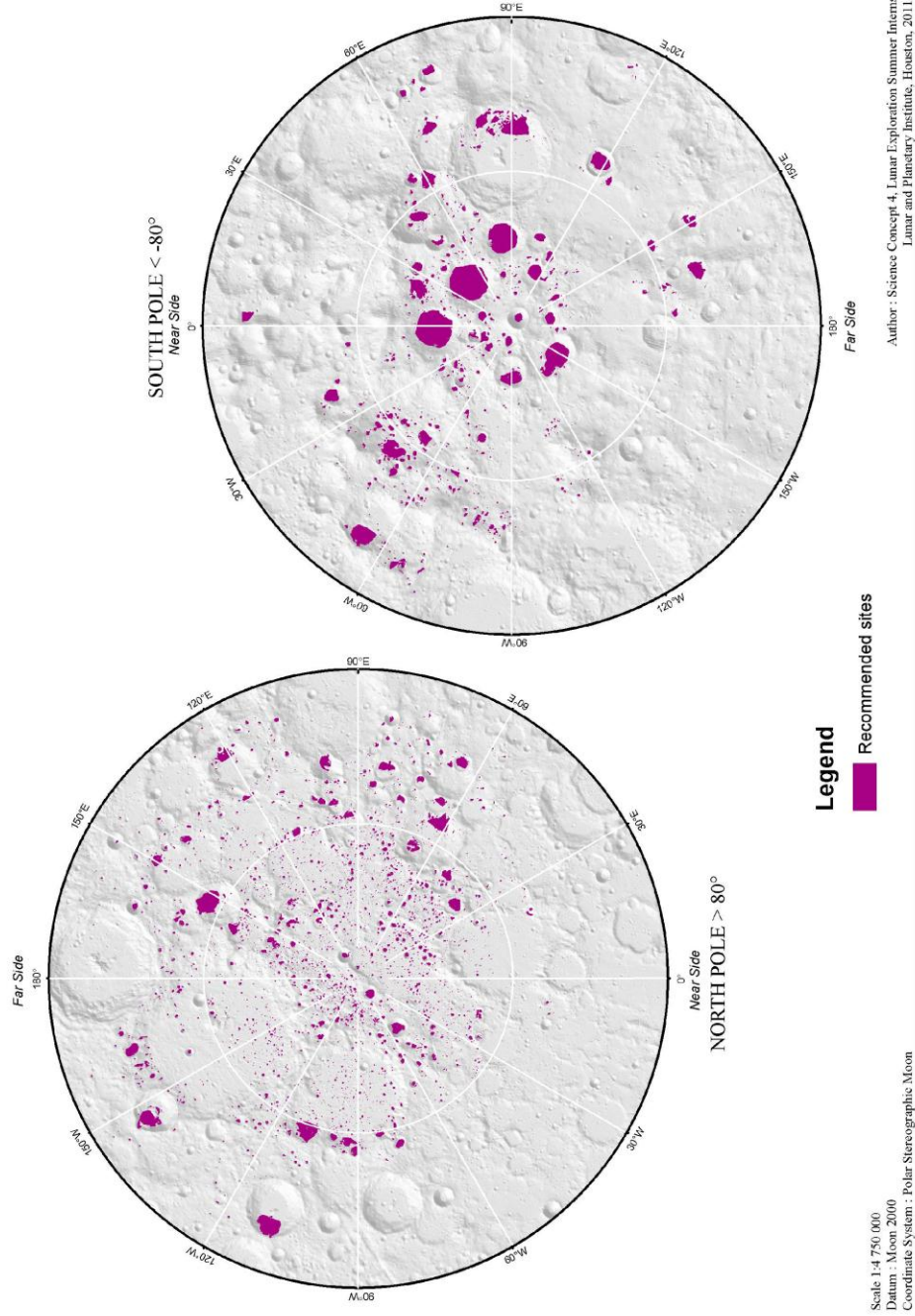
#### *South polar region*

Many sites also can address Science Goal 4e in the south polar region. Figure 4.21 shows a close-up view of the recommended landing sites there, found in large craters such as Cabeus, Cabeus B, Amundsen, Idel'son, Shoemaker, Haworth, and Nobile as well as in smaller craters such as Faustini, Wiechert, Wiechert U, Wiechert P, Sverdrup, de Gerlache, and on the floor of Skackleton.

### **Discussion**

Qualitatively, the south polar region has a more consolidated site distribution than the north, particularly around the circum-polar craters of Haworth, Shoemaker, and Faustini. Specifically, the south polar region has ~46% the number of sites than the north, although the south has almost 4,000 km<sup>2</sup> more Science Goal coverage than the north pole. Regions where Science Goal 4e coverage is in large areas are more desirable in that they allow for sampling from a greater variety of geologic morphologies. In this regard, the south polar region is preferred.

# Site Recommendations to Address Science Goal 4e



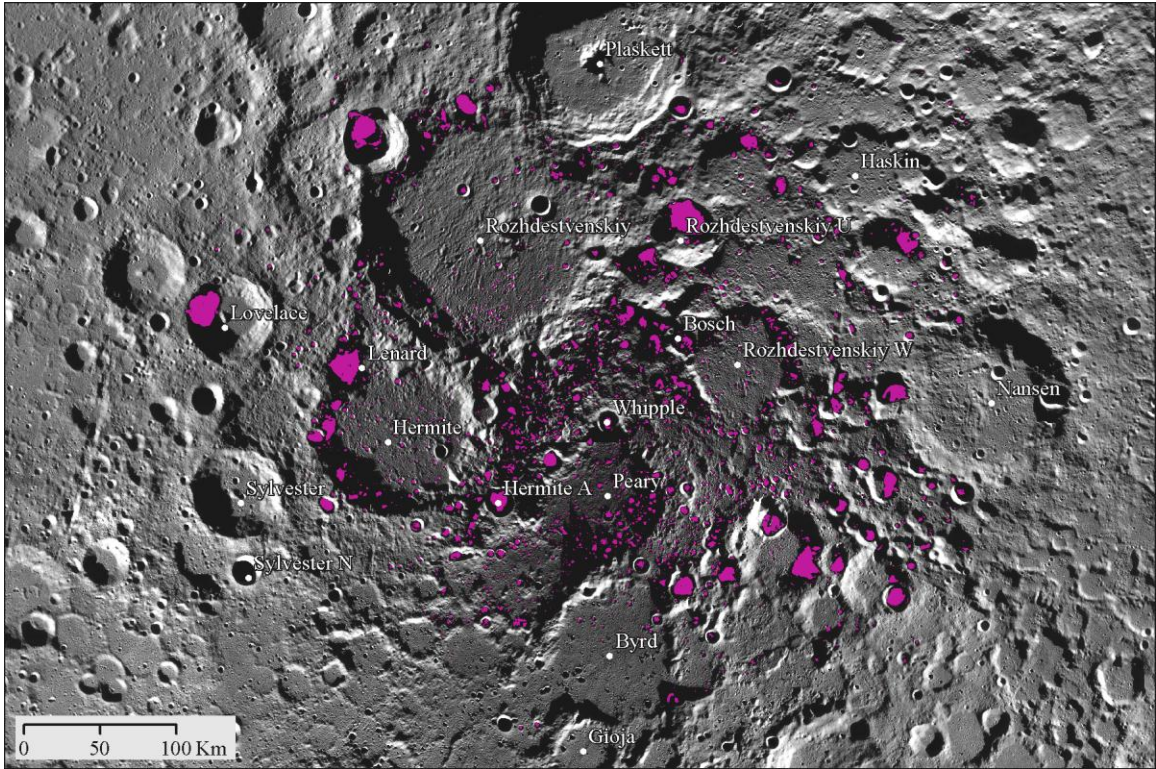


FIGURE 4.20 Enhanced view of recommended sites in the north polar region satisfying Science Goal 4e.

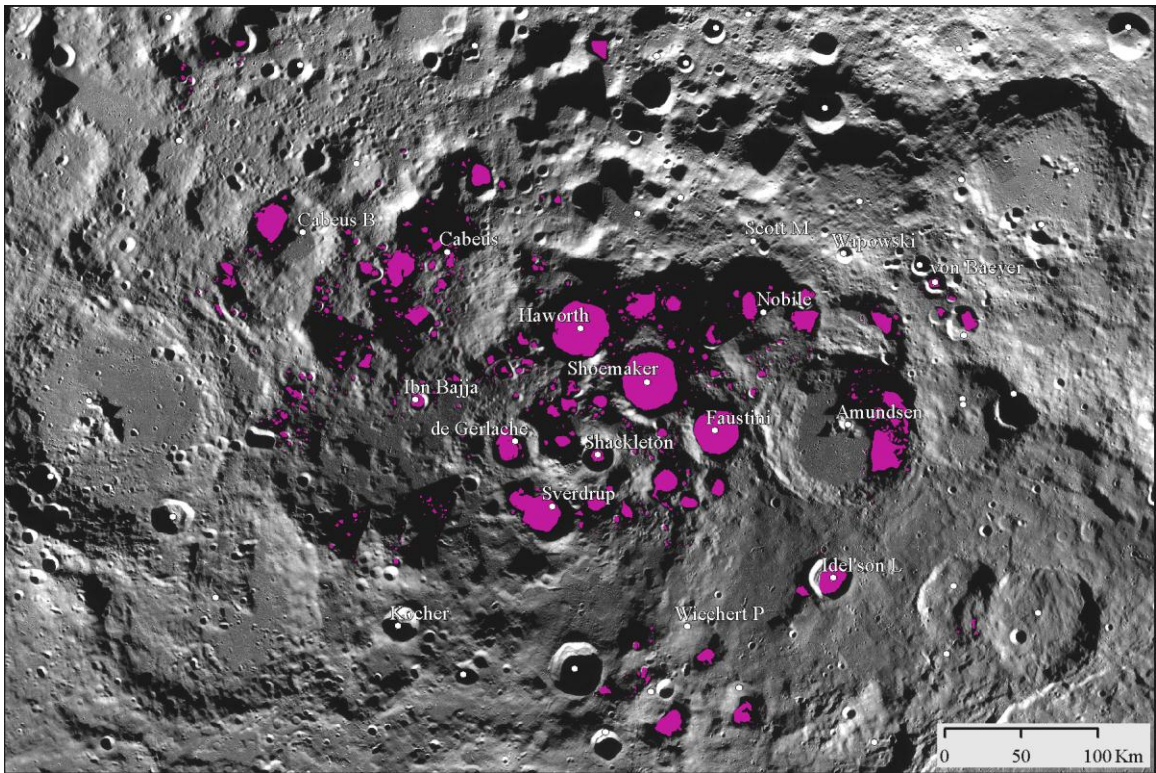


FIGURE 4.21 Enhanced view of recommended sites in the south polar region satisfying Science Goal 4e.

## INTEGRATED RESULTS FROM ALL SCIENCE GOALS

### Introduction

Up to this point, we have addressed the Science Goals within Concept 4 on an individual basis and identified locations where the potential science return can be maximized. A broad variety of sites could be studied with a multiple-mission campaign, with landing sites chosen to maximize return for each goal. In this type of multi-mission architecture, the Science Goal maps would be used independently, with the same recommendations as given in each Science Goal section.

In order to conduct the most science at the fewest number of stations, a single-mission architecture would be more efficient, even one with limited mobility. By this framework, it would be desirable to find sample locations where all five Science Concept 4 Science Goals overlap. This approach will not give the breadth of data possible in a multiple-mission design, but would still allow a mission to address the vast majority of key questions for each Science Goal and for Concept 4 as a whole.

### Methods

To find the sites where all Science Goals could be achieved simultaneously, we overlapped the sites that had been determined for each separate Science Goal. Science Goal 4b was the least constraining, while Science Goals 4a and 4d were the most constraining, meaning that they placed the most limitations on the overlapping Science Goal sites. Since the data used for this overlapping came from our previous post-classification analysis, no further processing or validation was required.

### Site recommendations and discussion

By sampling areas where all Concept 4 Science Goals may be addressed simultaneously, the probability of mission success is increased. In this section we list potential sites where the scientific return can be maximized at both the North and South Poles. Figure 4.22 shows these sites in a map similar to those shown for individual Science Goals.

#### *North polar region*

The areas that satisfy all Science Goals for Concept 4 at the north polar region can be seen in Fig. 4.23, which includes insets to allow better viewing of the sites. There are very few sites where all goals overlap in the north polar region. Generally, these are patchy areas related to degraded crater morphologies, particularly in the Intercrater Polar Highlands (IPH) near the geographic North Pole. The largest continuous region of Science Goal overlap is in Lenard crater ( $D = 48$  km). Other notable areas include sites on the floor of Peary crater, and on the southern walls of Rozhdestvenskiy W, Hermite, and Peary craters. There are more areas on the North Pole than at the South Pole that can address all five Science Goals simultaneously.

#### *South polar region*

Figure 4.24 shows all sites at the south polar region satisfying all Science Goals simultaneously. In the south polar region, many sites can be found in the bottoms of smaller craters within larger craters. This is the case for Faustini, de Gerlache, Haworth, Shoemaker, and some of the near-polar highlands/intercrater areas. The largest Science Goal overlap site at the South Pole is Amundsen crater ( $D = 105$  km), which is also a convenient site because there are a range of morphologies present on the crater floor, allowing contrasting areas with different physical or thermal properties.

### Discussion

Both poles have very few sites where all Science Goals of Concept 4 can be addressed simultaneously. In south polar regions, the only site of notable size is on the north floor and wall of Amundsen crater. In the north polar regions, there are slightly more acceptable locations that satisfy all Science Goals, but these sites are still fairly rare. The most prominent grouping of sites at the North Pole can be seen in Lenard crater. Note that, as has been the case for individual Science Goal sections, the maps shown in Fig. 4.22 are probably more selective than is absolutely necessary. Many sites at both poles are PSRs, for example, or have elevated or high H content.

Site Recommendations to Address All Science Goals within Concept 4

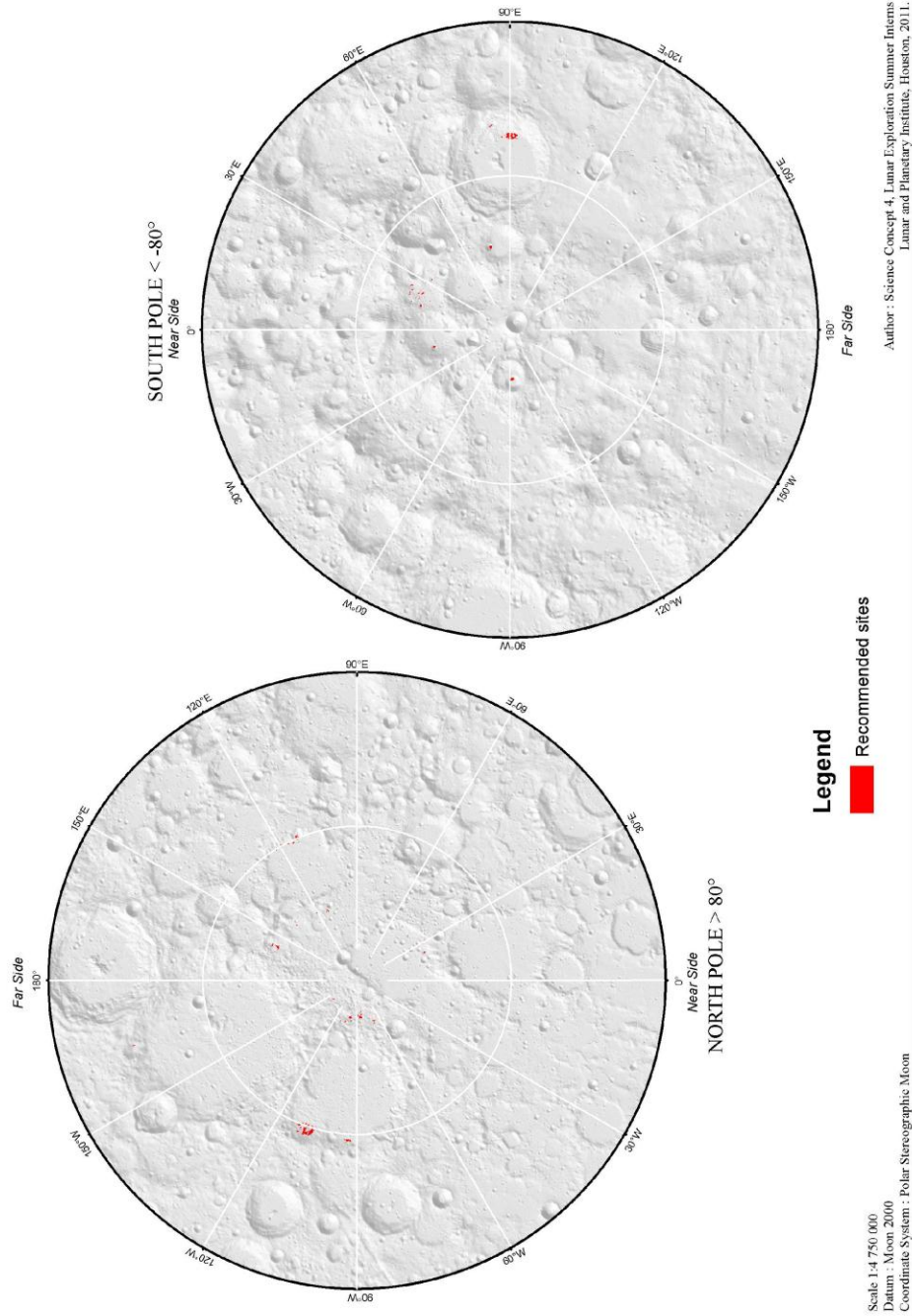


FIGURE 4.22 Site recommendations to address all Science Concept 4 Science Goals simultaneously.

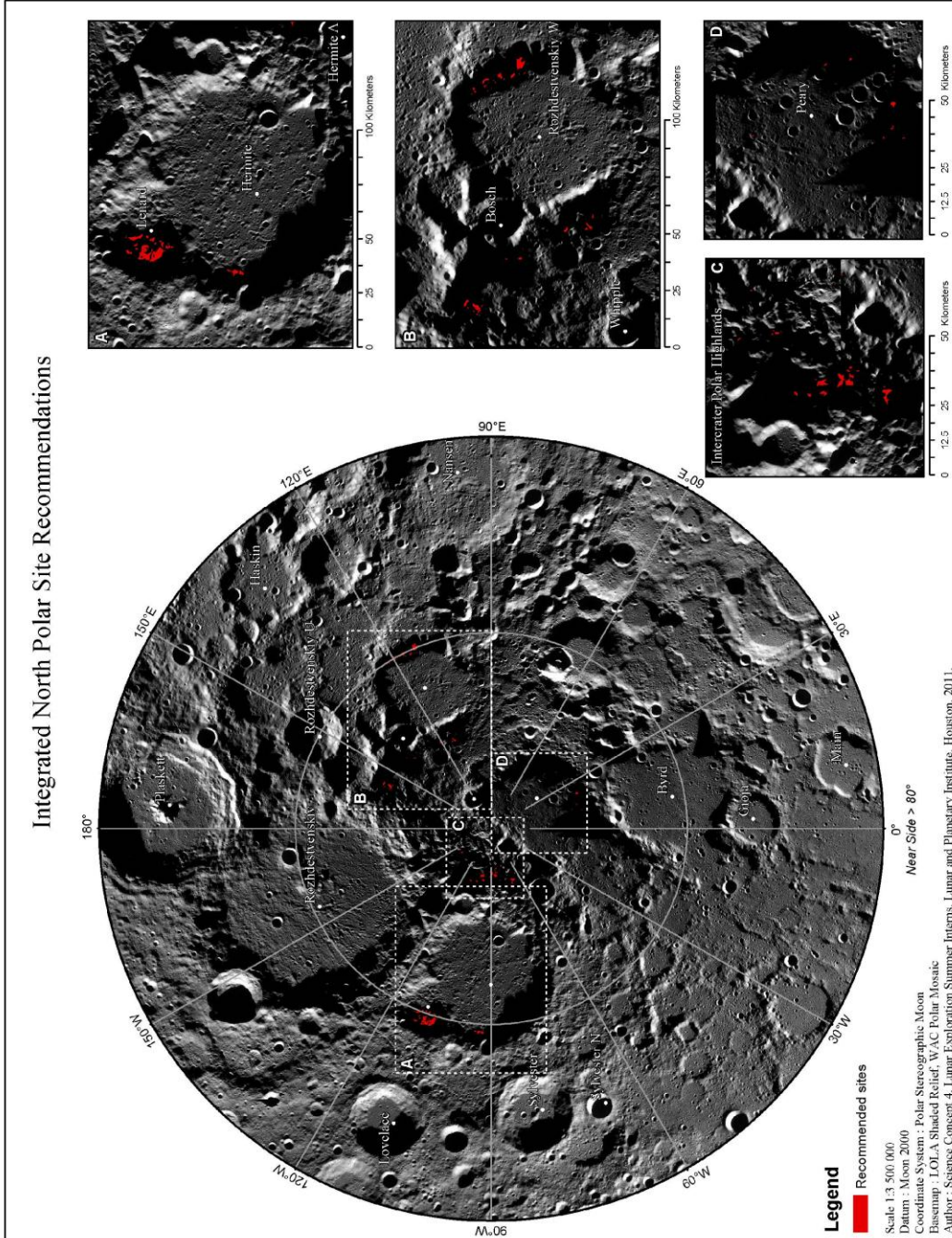


FIGURE 4.23 Enhanced view of recommended sites in the north polar region satisfying all Science Concept 4 Science Goals simultaneously.

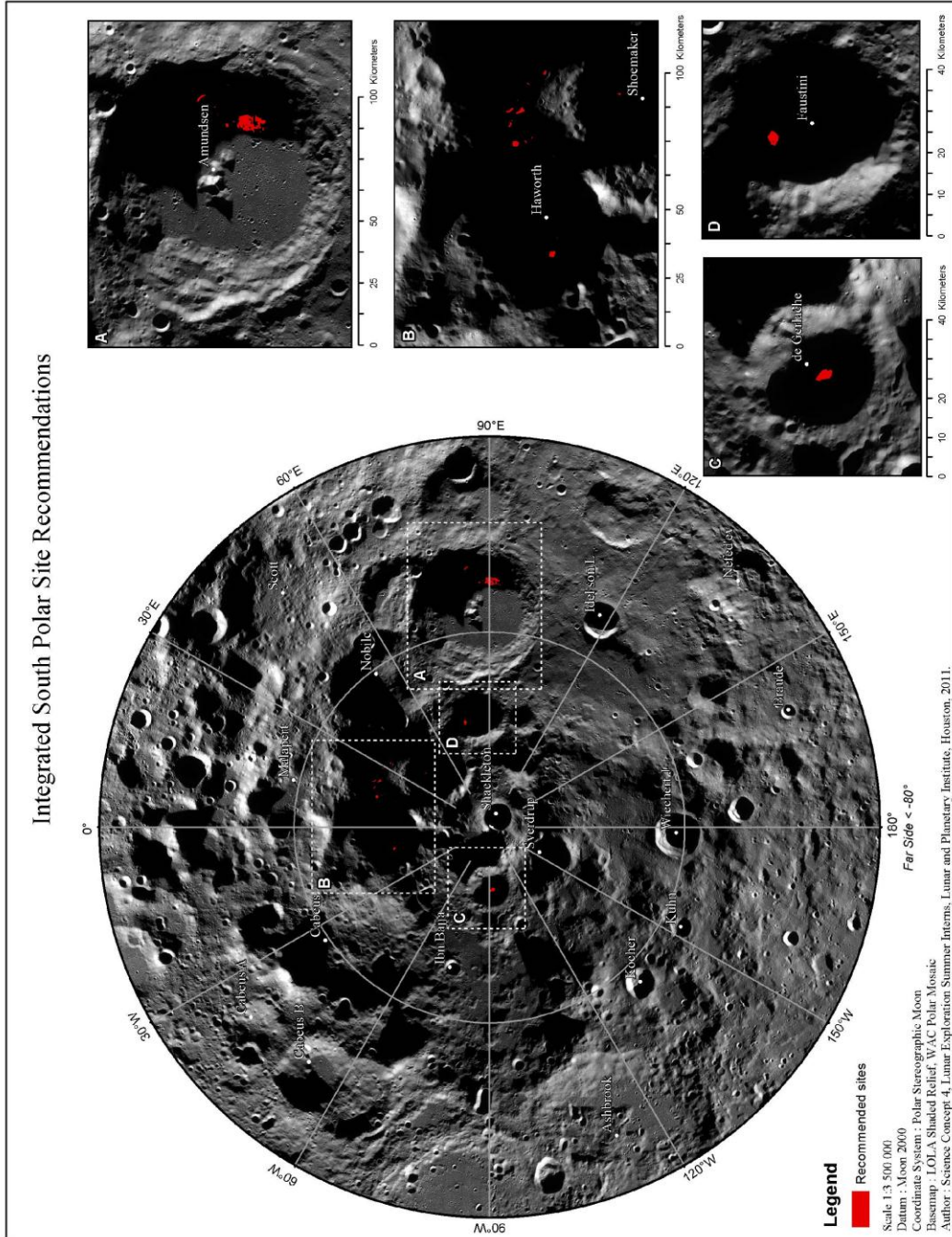


FIGURE 4.24 Enhanced view of recommended sites in the south polar region satisfying all Science Goals simultaneously.

## CASE STUDIES

After compiling lists of recommended landing sites based on individual and integrated Science Goals, we conducted case studies for two regions. These case studies are in-depth examinations of where the Science Goals can be addressed within specific geologic and geographic contexts. We also considered basic mission operations in terms of overall exploration architecture and science station distribution. The two case studies are the Hermite-Peary highlands (North Pole) and Amundsen Crater (South Pole).

### **Rationale for station selection based on Science Goal**

The common constraint for all Science Goals is navigability; this was dictated by slopes less than 25° as derived from a Lunar Orbiter Laser Altimeter Digital Elevation Model (LOLA-DEM) (Plate III). We used other constraints for the various Science Goals below.

#### *4a: Composition and distribution*

The locations chosen to address Science Goal 4a are those with elevated hydrogen values as derived from the Lunar Prospector Neutron Spectrometer (LP-NS) data and those within Permanently Shadowed Regions (PSRs). Also, they have the lowest annual maximum temperature as derived from LRO Diviner data.

#### *4b: Sources of volatiles*

Science Goal 4b can be addressed in any navigable location. Fresh craters provide the least ambiguous information on volatile sources. Small, fresh craters may be identified by eye in virtually any location based on the following criteria: (1) brightness of material, (2) crispness of rim and angularity of blocky, near-rim ejecta, and (3) lack of smaller over-printing craters. While close examination and comparison of Lunar Orbiter IV and V and Lunar Reconnaissance Orbiter Camera - Narrow Angle Camera (LROC-NAC) images could reveal new craters less than 50 years old, such a time-intensive undertaking was beyond the scope of this report. Therefore, we did not consider fresh craters as a landing site constraint; instead, astronaut crews could sample fresh craters wherever they find them.

#### *4c: Volatile transport, retention, alteration, and loss in PSRs*

The sites where Science Goal 4c phenomena are best addressed (1) have the highest hydrogen content as determined from LP-NS; (2) have the lowest annual maximum temperatures as derived from Diviner data; (3) are in PSRs and on PSR borders near sunlit areas; and (4) are in and around very fresh craters as visually identified by the crew.

#### *4d: Physical properties of extremely cold polar regolith*

Science Goal 4d can be best addressed in places with the lowest maximum annual temperature that are not in PSRs. Locations with the highest hydrogen content were also considered.

#### *4e: Ancient solar environment*

For Science Goal 4e we primarily considered diurnal temperature trapping of noble gases and other volatiles. Because of this, our favored regions (1) have minimum annual temperatures lower than 54 K; (2) contain PSRs; (3) are near PSR/sunlit borders; and (4) have contained PSRs for the longest possible times.

#### *CPR: A special dataset*

Circular polarization ratio (CPR) data from the Mini-SAR instrument is a proxy for decimeter-scale roughness and water ice (Spudis *et al.*, 2010). CPR values are locally heterogeneous, so we propose crews land with a local remote sensing Mini-SAR-type instrument package or repurpose the lunar module's landing radar to record CPR data. These data can be processed and interpreted on Earth leading to a high-spatial-resolution CPR map that could precisely inform astronaut traverses.

### **Amundsen crater (South Pole)**

Amundsen crater, centered at 84.6° S, 85.6° E, is a complex, central-peak crater ~100 km in diameter. It is only one of three discernable complex craters poleward of 80° S and is the youngest south polar complex crater. Amundsen formed in the late Nectarian, but its floor has a crater density consistent with an

Imbrian age (USGS, 2009a). The entire crater sits within the South Pole-Aitken (SPA) impact basin, which is the oldest (pre-Nectarian) and largest (~2600 km diameter) discernable lunar impact crater (Stuart-Alexander, 1978). Because of the great depth of SPA (~18 km of vertical relief), the mineralogy is likely intermediate with deep crustal or shallow mantle material mixing with feldspathic highlands material (Mest, 2011).

Approximately 9% of the interior of Amundsen crater is in permanent shadow and ~6% of the interior satisfies all five of the NRC (2007) Concept 4 Science Goals. A 43 km<sup>2</sup> region directly north of our proposed landing site is one such region in which all five Science Goals could be addressed. Many of these regions are on the floor of Amundsen, making for convenient access. We chose Amundsen crater for this case study because it has many easily-accessible sites that address all or most Science Goals. A broad range of geologic features is also present within Amundsen; these include crater floor materials (melt and/or volcanics), crater walls, wall slumps from higher on the crater wall or rim, and central peak material. It also contains many smaller craters with varying degrees of degradation. Sampling these various morphologies may place constraints on distribution of volatiles, partially addressing Science Goal 4a.

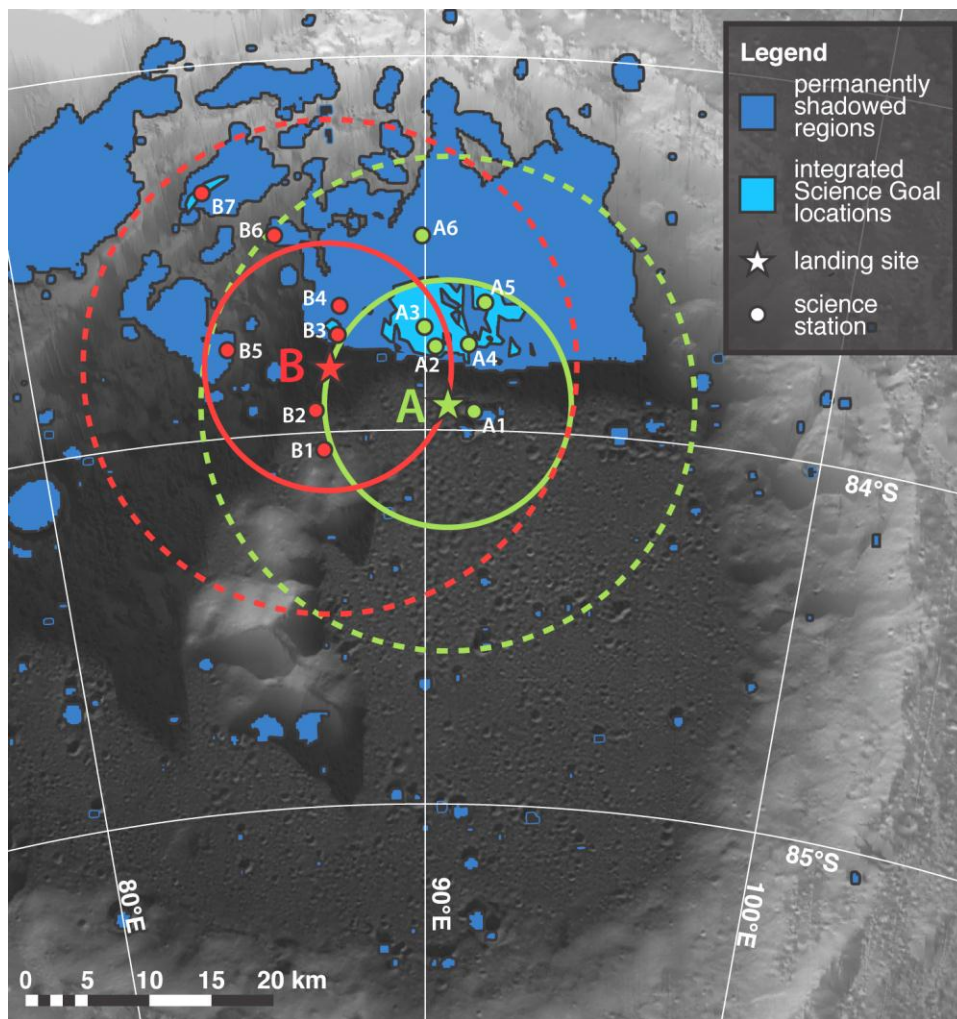


FIGURE 4.25 Amundsen Crater interior, showing PSRs (dark blue), sites where all five Science Concept 4 Science Goal can be met (light blue), proposed landing sites (stars), and proposed science stations (circles). Radii of 10 and 20 km from the landing sites are shown as solid and dashed lines, respectively. Base map is LRO/WAC/LOLA shaded relief.

### Landing sites

We identified two landing sites (A and B) on the floor of Amundsen crater that are lit up to ~25% of a lunation (Zuber *et al.*, 2011). Those sites provide access to stations within PSRs while providing a base of operations in an illuminated region. Having the ability to establish stations in both sunlit regions and adjacent PSRs also has several scientific advantages. The stations outside of PSRs can serve as experimental controls for the processes that affect volatile distribution within PSRs. Contrasts between the two regions can also be used to evaluate transport mechanisms. Remotely observed circular polarization ratios (CPR) (Zhang and Paige, 2010) also vary around both landing sites, providing an opportunity to groundtruth the global data set and test the effects of ground ice and surface roughness on those CPR values. Temperatures derived from the Diviner radiometer (Paige *et al.*, 2010) also helped define station locations. The two sites are shown in Fig. 4.25.

TABLE 4.8 Amundsen landing sites and science stations.

| Site | Station | Lat    | Long  | Science Goals addressed | Description/reasoning  |
|------|---------|--------|-------|-------------------------|--|
| A    | 1       | -83.95 | 91.12 | 4c, 4e                  | diurnal temperature variation, proximal to simple crater morphologies                      |
|      | 2       | -83.78 | 90.17 | 4a, 4b, 4c, 4d, 4e      | flat terrain   |
|      | 3       | -83.72 | 89.89 | 4a, 4b, 4c, 4d, 4e      | near degraded crater rim   |
|      | 4       | -83.77 | 90.91 | 4a, 4b, 4c, 4d, 4e      | access to crater ejecta; on a degraded crater rim that is over-printed by a younger crater |
|      | 5       | -83.65 | 91.34 | 4a, 4b, 4c, 4d, 4e      | access to possible slump material  |
|      | 6       | -83.48 | 89.79 | 4c, 4e                  | temperature variation, access to terrace material  |
| B    | 1       | -84.04 | 87.25 | -                       | diurnal temperatures (not in a PSR), access to base of central peak                        |
|      | 2       | -83.94 | 87.05 | -                       | fresh crater material, in small PSR with temperature variation                             |
|      | 3       | -83.74 | 87.69 | 4a, 4b, 4c, 4d, 4e      | consistent low temperatures (27.8 K = T min; 41.5 K = T ave; 52.0 K = T max)               |
|      | 4       | -83.66 | 87.79 | 4c, 4e                  | access to possible slump material  |
|      | 5       | -83.76 | 84.99 | 4c, 4e                  | temperature variation, access to debris slump material                                     |
|      | 6       | -83.47 | 86.31 | 4a, 4b, 4c, 4d, 4e      | access to crater material on wall terrace  |
|      | 7       | -83.34 | 84.77 | 4a, 4b, 4c, 4d, 4e      | access to terrace material   |

Site A (83.93°S, 90.45°E) consists of six science stations (Table 4.8), all with elevated hydrogen levels (~110–123 ppm [Feldman *et al.*, 1998]), navigable slopes (< 15° [Zuber *et al.*, 2011]), and with temperatures (Paige *et al.*, 2010) ranging from ~23–100 K and averaging ~40–50 K. Stations A1 and A6 address three of the five NRC Science Goals (b, c, and e), while Stations A2 to A5 address them all. The maximum temperature ( $T_{\max}$ ) distribution places constraints on stations' expected volatile abundance based on volatiles' sublimation points. Volatile sublimation temperatures (Feldman *et al.*, 1998) near the  $T_{\max}$  of the stations include CO<sub>2</sub> and hydrogen sulfide (Stations A2 to A5); water and ammonium hydrosulfide (A1); and toluene (A6).

These stations explore the distribution of volatiles in several geologic sites that will have variable regolith properties and potentially cavities for icy deposits, while also providing access to geology that address other NRC (2007) goals. Station A1 is in a small PSR amidst an interesting complex of overlapping, asymmetric simple craters. Station A2 is on flat terrain while Stations A3 and A4 are on degraded crater rims, though the latter is also near fresh craters and their ejecta. Station A5's location on a debris slump will allow sampling of a range of lithologies, particularly from higher on Amundsen's wall

and rim, while Station A6 is on the terraced wall. All but Station A6 are within the 10 km astronaut walk-back safety zone.

*Site B* (83.82°S, 87.53°E) consists of seven science stations (Table 4.8); all have elevated hydrogen levels (between ~98–125 ppm [Feldman *et al.*, 1998]), slopes <6° (Zuber *et al.*, 2011), and temperatures (Paige *et al.*, 2010) ranging from ~23–239 K with an average of ~37–73 K. Stations B1 and B2 address none of the science goals directly, but serve as controls. Stations B3, B6, and B7 address all five of the Science Concept 4 Science Goals, while Stations B4 and B5 address Science Goals 4b, 4c, and 4e. Site B also allows sampling in various geologic regimes. Station B1 is in a diurnal region at the base of Amundsen’s central peak. Station B2 is in a small PSR on the bottom of a small, fresh crater while Station B3 is on the flat Amundsen floor very near the terraced walls. Stations B4 and B5 are on different debris slumps, allowing for sampling of stratigraphically higher and laterally diverse material. Station B6 samples a simple crater on Amundsen’s terrace. Station B7 also samples the terrace, though in a location that also satisfies all five NRC goals.

### *Conclusions*

Amundsen crater is a prime area for studying lunar volatiles. Its geologic diversity, elevated hydrogen abundances, cold PSRs adjacent to warmer diurnal regions, and overall accessibility make it an appealing and interesting target for future lunar missions from both science and mission planning perspectives. This is in contrast to the more limited science opportunities at Shackleton crater, which has steeper walls, simpler geology, and whose interior is entirely in permanent shadow.

### **Intercrater Polar Highlands (North Pole)**

Centered at 285°E, 89°N, the IPH is ~4000 km<sup>2</sup> in area and consists of rugged, hummocky terrain bounded by Peary, Rozhdestvenskiy, and Hermite craters. The IPH is relatively homogeneous due to its age and near-complete crater saturation (USGS, 2009). The majority of the region has been characterized as pre-Nectarian (~4.60–3.94 Ga) and Nectarian (~3.94–3.86 Ga) in age, which is bounded by highly subdued pre-Nectarian crater material (USGS, 2009). Within the IPH there are also a few young craters of Erastosthenian age (3.2–1.1 Ga), namely Hermite A. The IPH contains abundant PSRs that are smaller, but more numerous, than those at the South Pole (see Lemelin *et al.*, 2012). PSRs within the IPH are typically <10 km in diameter, occupying small topographic lows that are often degraded simple craters. These regions have not been illuminated by the Sun in at least 2 Ga (Siegler *et al.*, 2011) and, thus, act as ‘cold traps’ for volatiles migrating from other regions on the lunar surface (Watson *et al.*, 1961). Orbital measurements indicate that the IPH region has enhanced hydrogen abundances (>150 ppm; [Feldman *et al.*, 1998]), low average temperatures (<54 K; [Paige *et al.*, 2010]), and high circular polarization ratio (CPR) values (Spudis *et al.*, 2010). The Mini-SAR CPR data suggest that ice may be heterogeneously distributed within many small craters near the North Pole and be at least tens of wavelengths (~2–3 m) thick.

Because the IPH region lacks substantial topographic highs, temperatures remain consistently cold (~23–54 K average annual temperatures), and there is little direct sunlight. Models suggest the entire region experiences ~0–25% illumination over a period of four full (18.6 earth-year) cycles (Mazarico *et al.*, 2011). While this is suboptimal for generation of solar power during a mission, the situation can be improved by installing solar panels in nearby well-lit areas or mounted on ~10-meter-high masts. Alternatively, radiogenic power sources could be used. Because of the patchwork nature of the PSRs in the IPH, landing can occur in sunlit regions (attractive for solar power) and short drives can then access the PSRs for measurements and sample collection.

### *Landing sites*

We have identified two sites that can provide access to areas with overlapping science objectives and that have slopes suitable for rover operations. Each area consists of 3 to 5 geologic stations located within a 10 km radius (for extravehicular activity safety reasons) of a flat ( $\leq 1^\circ$  slopes) landing site. All stations can be reached following rover-accessible paths (slopes <20°), and are located in areas where all Science Concept 4 Science Goals can be addressed. Multiple core samples (to depths of 3 m) collected in a grid-like fashion would address Science Goal 4a locally, as well as Science Goals 4d and 4e due to the stations’ low annual average temperatures of ~31–39 K. Sampling regolith to depths of 3 m is required to verify potential subsurface water ice as suggested by high CPR values at some stations. Samples collected at stations situated in variable terrains (*e.g.* crater rim/floor) partially address Science goals 4a and 4c. To

address Science Goals 4b and 4c, ion and particle collectors could be set up to assess volatile flux at the boundary of the PSR in which each station resides. In order to fully address Science Goal 4c, regolith core samples could be collected not only at each station, but also outside and on the borders of their respective PSRs. The two sites are shown in Fig. 4.26.

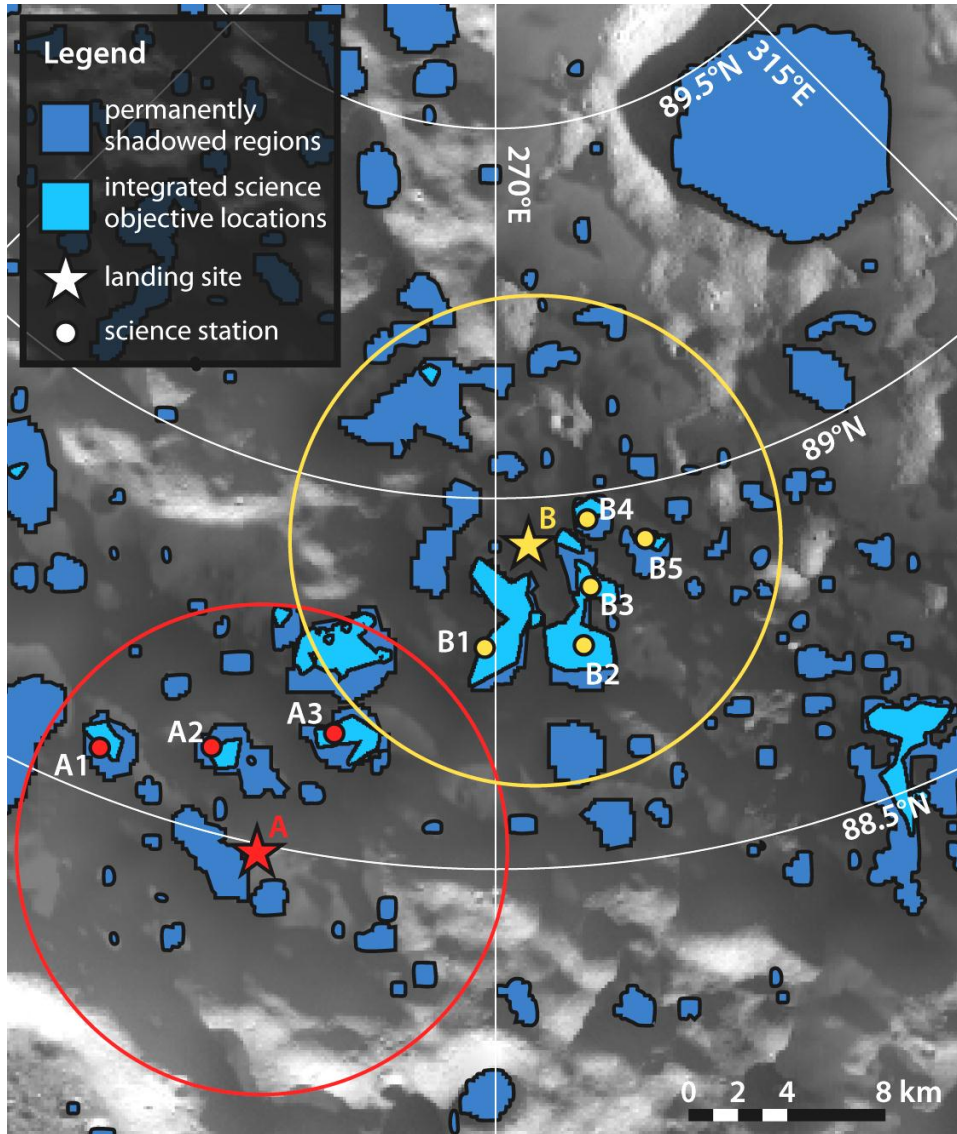


FIGURE 4.26 Case study for the IPH near the lunar North Pole, showing PSRs (dark blue), sites where all five Science Concept 4 Science Goal can be met (light blue), proposed landing sites (stars), and proposed science stations (circles). A 10-km exploration radius is shown around each landing site. Base map is LRO/WAC/LOLA shaded relief.

*Site A* (258°E, 88.5°N) consists of 3 science stations (Table 4.9). Station A1 never experiences temperatures >54 K, thus providing an opportunity to sample regolith that could contain volatile compounds with sublimation temperatures above 54 K (CO<sub>2</sub>, SO<sub>2</sub>, NH<sub>3</sub>, C<sub>5</sub>H<sub>12</sub>, HCN, C<sub>7</sub>H<sub>8</sub>, H<sub>2</sub>O, and S; [Zhang and Paige, 2010]). This station exhibits some of the highest hydrogen abundances in the IPH region (>155 ppm), further supporting the potential for hydrogen compounds within the regolith at this location. The low CPR values observed at Station A1 would permit ground truth for the global CPR dataset, which could prove to be immensely useful for locating subsurface ice in the future. At Station A2 there is an opportunity to sample volatiles with sublimation temperatures >50 K (like H<sub>2</sub>S and the

compounds listed for Station A1), as the maximum annual temperature is ~50 K at this location. Station A2 is located within a degraded simple crater and would enable access to deeper deposits from the crater floor. Enhanced hydrogen abundances (>154 ppm) are observed at Station A2, as well as high CPR values (suggestive of subsurface water ice). Station A3 is similar to Station A2 in that it has similar hydrogen abundances, and would provide an opportunity to sample volatiles that sublime above 50 K. On the other hand, Station A3 exhibits medium CPR values, in contrast with Station A2. The hills near the southern edge of Site A experience ~35–45% illumination over four full lunar cycles (Mazarico *et al.*, 2011) and have the greatest solar power collection potential for a mission to the IPH.

*Site B* (273°E, 89°N) stations (Table 4.9) exhibit hydrogen abundances of  $152 \pm 1$  ppm and temperatures (<49 K maximum annual) similar to stations in Site A, so they provide the same potential volatile sampling opportunities. All five Site B stations have minimum annual temperatures <20 K (with Stations B1 and B4 being <15 K) and could more completely address Science goals 4d and 4e. Station B4 is within a steep-walled (20°–35°) crater, enabling the sampling of the crater rim/wall material, and providing access to deeper deposits from the crater floor (similar to Station A2). As with Site A stations, Site B stations sample a range of CPR values.

TABLE 4.8 Inter crater Polar Highlands landing sites and science stations.

| Site | Station | Lat   | Long    | Science Goals addressed | Description/reasoning   |
|------|---------|-------|---------|-------------------------|---|
| A    | 1       | 88.56 | -111.73 | 4a, 4b, 4c, 4d, 4e      | slopes <5°, pre-Nectarian   |
|      | 2       | 88.61 | -106.03 | 4a, 4b, 4c, 4d, 4e      | slopes <10°, pre-Nectarian, bottom of a crater, access to deeper material   |
|      | 3       | 88.66 | -99.36  | 4a, 4b, 4c, 4d, 4e      | slopes <5°, Nectarian and pre-Nectarian, close proximity to T <sub>min</sub> material <23K                        |
| B    | 1       | 88.80 | -90.55  | 4a, 4b, 4c, 4d, 4e      | slopes <10°, Nectarian and pre-Nectarian  |
|      | 2       | 88.80 | -84.29  | 4a, 4b, 4c, 4d, 4e      | slopes <10°, Nectarian and pre-Nectarian  |
|      | 3       | 88.87 | -83.46  | 4a, 4b, 4c, 4d, 4e      | slopes <5°, Nectarian and pre-Nectarian   |
|      | 4       | 88.97 | -83.22  | 4a, 4b, 4c, 4d, 4e      | slopes <10°, Nectarian and pre-Nectarian, bottom of a crater, access to different lithologies and deeper material |
|      | 5       | 88.93 | -79.14  | 4a, 4b, 4c, 4d, 4e      | slopes <10°, Nectarian and pre-Nectarian, at outside edge of PSR  |

### Conclusions

The IPH is an ideal location to study lunar polar volatiles due to the prevalence of PSRs, consistent low temperatures, high hydrogen abundances, and very old terrain. Two landing sites within the IPH provide access to stations that can address all of the NRC objectives for the study of polar volatiles. Mission logistics will likely be challenging because of illumination conditions (*i.e.*, access to solar power) and extremely cold temperatures. The small size and patchy distribution of PSRs, however, provide an opportunity to base operations in sunlit areas and limit exploration of the PSRs to short-duration traverses.

